nature portfolio

Peer Review File

Spatial dynamics of brain development and neuroinflammation

Corresponding Author: Professor Rong Fan

Any redactions in this file are there to maintain patient confidentiality, the confidentiality of unpublished data, or to remove third-party material.

This file contains all reviewer reports in order by version, followed by all author rebuttals in order by version.

Version 0:

Reviewer comments:

Referee #1

(Remarks to the Author)
Transcriptomics, from single-molecule to bulk-level analysis, plays a critical role in advancing our understanding of biological processes. Multi-modality approaches, which integrate RNA, protein expression, morphology, functional studies, and chromatin architecture, have the potential to extend insights gained from transcriptomics to other biological modalities. This multi dimensional view enables the identification of novel mechanisms and the aiming better for most effective therapeutic strategies.

In this context, Zhang et al. introduce two DBiT-based spatial tri-omic technologies that provide valuable insights into the dynamics of transcription factors involved in both myelination and cortical layer specification during development and injury. The manuscript highlights both technological innovations and biological insights, offering significant & original contributions to the field.

They show that myelination-related genes show coordinated patterns of transcription and chromatin accessibility, with chromatin priming evident in early postnatal stages (P0-P5) before RNA expression appears at later stages (P10). By P21, even though some myelin genes continue to be transcribed, their chromatin accessibility has already started to decrease. This contrasts with cortical layer-specific transcription factors, which are primed during embryonic development but show reduced RNA expression in the postnatal period, while their chromatin accessibility remains high. These findings suggest distinct regulatory mechanisms: myelination involves early chromatin priming followed by RNA expression, whereas cortical layer specification maintains chromatin accessibility despite decreased RNA levels. The use of a multi-modal approach in this study is particularly valuable, as it uncovers complex details that would be missed if only one type of data were considered. By utilizing both RNA-seq and ATAC-seq enhanced with spatiotemporal resolution, the study provides a technology for a view for how gene regulation unfolds during development and injury.

Major:

- While the manuscript effectively highlights the tri-omic approach, it lacks specific examples of how protein sequencing enhances insights. Given that this is a key novelty of the study, this section needs to be strengthened to better demonstrate the added value of protein sequencing in the tri-omic analysis.
- Additionally, it is sometimes unclear which observations are derived from which specific analyses. Clarifying the source of each observation will improve the overall clarity and understanding of the findings.

- The use of a negative binomial generalized additive model (NB-GAM) to identify patterns based on gene expression, spatial location, time points, and their interactions is of particular interest. The parameters are well-thought-out and aptly suited for capturing variation along the spatio-temporal axis. However, while the methods section provides a detailed description of the computational framework for the spatiotemporal regression model, the corresponding code is not available on the GitHub page. Given the novelty and importance of this framework in the study's data analysis pipeline, providing the code is crucial for ensuring reproducibility and transparency. Additionally, including spatial pattern annotations for the replicates (not shown in the main figures) at each time point in an extended data figure would enhance the presentation.

This addition would help demonstrate the consistency of the findings, similar to the approach taken with other results in the study.

- The authors report observing an activated microglia population distal to the lesion site. Investigating the transcriptional and epigenetic programs that differ between the distal microglia and those in close proximity to the lesion could be particularly enlightening. Given the multi-modal technique the authors have developed, such an analysis could significantly enhance the paper's impact by elucidating biological mechanisms relevant to neurodegenerative states. Adding this mechanistic layer would complement the extensive descriptive developmental findings detailed throughout the paper.

-The effects of LPC-induced demyelination have been previously characterized using spatial transcriptomics (Androvic et al., 2023), showing that DAM-like state, likely CD11c+ (Itgax) microglia, are localized near the lesions. How does the diffuse activation observed in this study differ from previous findings? Additionally, how do the epigenetic and protein data from this study enhance or refine the existing understanding of microglial activation near LPC-induced lesions? It would be insightful to discuss these points.

- It is not clear how adjacent sections are cut, registered or aligned. How far apart are these adjacent sections? How well aligned? Please clarify whether this approach could lead to redundancy or potentially enhance the protein signal.

-In the supplementary figures, some columns and rows are positive for signal, suggesting leakage in one direction of the microfluidics. Are these issues related to microfluidic valve performance? Additionally, why is this leakage not observed in all analyses, and how widespread is this issue?

- The study could provide more in-depth analysis of the sparse immune cells, particularly the CD169+ cells shown in the supplementary figure2, which appear to be developmentally regulated. However, the resolution of the images is too low to assess this accurately. The tri-omic approaches should ideally offer better resolution for these cells, or it should be clarified if this is an artifact of CODEX.

-Additionally, it would be valuable to understand how the different detection approaches (CODEX, CITE-seq, and RNA-seq) were used to validate the strengths or weaknesses of the measurements. Where did these methods disagree, and how were discrepancies between CODEX, CITE-seq, and RNA-seq addressed?

- Legends should include sample size and stats. It is not clear statements are based on any stats.

- While the human data provide a valuable demonstration of the technology’s applicability, the insights are somewhat limited compared to the mouse findings. It would be beneficial to link the human data to a specific disease or developmental stage, which could offer a clearer context for comparison and highlight the relevance of the findings beyond validation in human tissue.
Minor:
- Typo in Page 38, Line 31, “RunUMA” should be “RunUMAP”
- Page 9, Line 1-3 refers to Ext Data Fig 3e,f but there is no f panel.
- Description of regional partitions of corpus callosum in Fig3a comes later in the text than descriptive results from the same figure. The sections can be re-ordered for better flow.
- To maintain consistency and accuracy, the authors should revert to using "spatial CITE sequencing" throughout the manuscript unless a clear distinction between the methods is being intentionally made. A brief explanation of the differences, if applicable, would also help clarify this for the reader.
- The sentence on Page 13, Line 31: 'Interestingly, R3-A2 and R5-A2 presented GO terms of glial migration were classified (Extended Data Figs. 16, 17); this needs revision to improve readability and ensure the message is conveyed accurately.
- Extended Fig. 5a, the bottom-left panel y-axis is not in log scale.
- Page 23, Fig 2.a, Under the schematic representation “Spatial Struture Isolation” should be Spatial Structure Isolation.

Referee #2

(Remarks to the Author)
Zhang et. al performed the spatial omic profiling from human and mouse brains using cutting-edge tri-omic technologies DBiT ARP-seq and DBiT CTRP-seq. Combined with multiplexed immunofluorescence, the authors characterized the spatially and temporally dynamic patterns of transcriptome and chromatin accessibility of the mouse cortex from neonates to juveniles. They observed a lateral to medial myelination progression in the corpus callosum in the developing brains. Using the lysolecithin injection inflammation model, they found two microglia subtypes activated at both the core and distal locations of the lesion.

It is an innovative approach to apply new technologies to samples from different species and disease models. The biological conclusions are intriguing. However, the authors have not convincingly demonstrated the suitability or advantage of their technologies in either the disease study or the neurodevelopmental study. Moreover, I found it hard to evaluate whether these technologies have the required dynamic range and sensitivity to quantify subtle differences in the disease models – and whether the observed changes, most of which were quite surprising, could be due to technical artifacts – more validation and replicates will strengthen this work. Most conclusions could be drawn simply by using simpler tools such as immunohistology and single-cell omics, which dampened my enthusiasm.

Major points:
1. The application on human tissues (Fig 1c) is great, but the data suggests the postmitotic neuron marker NeuN has a decreased expression throughout neurogenesis? This is shocking. The collective neuronal marker signals were barely detectable in the third trimester and infancy: is this an issue with the sample quality or just the variability of the technology?

2. In the current manuscript, transcript or protein abundance was shown visually, and it is hard to evaluate them quantitatively – and to what extent the measurement is consistent between batches and samples. In Fig 2d, neuronal markers Satb2 and Tbr1 were barely detectable in P21 – this is again surprising and raises the question of the sensitivity and reliability of DBiT. According to the works of many and the Allen ISH atlas, these genes have high and sustained expression in the cortex. I got more confused later seeing Satb2 does seem to be expressing in P21 in ExFig 2c - in sharp contrast to Fig 2d?

Strong conclusions were drawn from these visualizations: e.g., the authors claimed that there are decreased expressions of layer-specific TFs in development in mice and humans (Page 5, Line 10-12 and Line 38-40). These were inconsistent with the literature and potentially could be very interesting – but extraordinary claims require extraordinary evidence. Fig 1b: the P5 brain seems to have overall diminished signals compared to others – is this biological or technical? How many replicates are in each age, how are the data quantified to account for batch effects and technical biases, what are the internal controls, and have these been validated using alternative methods or datasets? Why does the GFAP signal closely resemble the meningeal lining (ExFig 2c), which is not its expected pattern - is this due to antibody artifacts?

The anatomical definition of a cortical column should be from pia to the white matter within a defined cortical region (SS or MO) – unlike the irregular boxes in Fig 2b or 2c. We know that TF expression varies greatly across cortical regions and any quantification should be done rigorously.

3. The same sentiment applied to Fig 3 related to the myelination pattern, forming laterally to medial corpus callosum in development. It is another surprising finding, but only from one replicate at P10. A quick check on the Allen ISH atlas also does not seem to support this claim – more replicates and validations are required.

4. The authors demonstrated that microglia were activated at the core and distal locations of the lesion. However, looking at the data in Fig 5e, the activation marker does not seem expressed at the ‘core’ of the lesion?

5. Quantitative data for chromatin, RNA, and protein mapping should be included in all figures. On page 17 Lines 13-16, the authors claim there is a divergence in chromatin accessibility and RNA expression for genes Itgax and Itgam based on data in ExFig 25. The qualitative images shown do not appear to support this conclusion.

6. How immune cells respond to brain injury is an important question. Given the unique spatial data, the authors may want to investigate microglia diversity within the lesion environment and benchmark the findings with existing single-cell studies (Hammond et al 2019 and many more). It would be critical to know if DBiT APR-seq recapitulates similar microglia subtypes in lesions as single-cell sequencing. Moreover, authors can capitalize the cell type-specific RNA and ATAC data, for example, to identify the different and shared RNA and ATAC patterns between disease-associated microglia (DAM) and axon tract-associated microglia (TAM) on how microglia respond to injury.

Minor
1. Consistency between CODEX versus ARP-seq readout: it was not clear to me how the CODEX data was quantified (or if this is quantifiable), because these are likely the multiplex immunofluorescence. Does the 150 antibody list from spatial proteomics (in the ARP-seq) overlap with the 23 antibodies in the CODEX? This could be a validation to gain more confidence about CODEX.
2. Readable multi-color images and cluster identity should be provided in the manuscript. Across almost all the main figures, it is hard to read out the genes displayed in the multiplexed images. For example, Fig 1b: CD169 is not visible and OLIG2/MOG are from similar colors; Fig 1c: only MBP stands out. Additionally, some annotations are confusing: Fig 4b, it is unclear if the authors were annotating brain regions or cell types.
3. Fig 1b typo “immunofluorescence”.
4. Fig 4a, CD11b has ‘b’ capitalized in one place and not in another.

Referee #3

(Remarks to the Author)
This manuscript integrates several technologies to interrogate transcriptome (RNA). proteome and chromatin states in terms of accessibility (ATAC) and genomic distribution of the H3K27me3 repressive histone mark (Cut&Tag), at a single cell resolution. The study relies on next generation sequencing technologies using Determinist Barcode In Tissue (DBiT) approaches and Co-detection by indexing (CODEX), using a panel of 23 antibodies for mouse tissue and 19 for human tissue, to create a spatial map of the developing murine brain at multiple time points (P0,P2,P5,P10,P21) and of the developing human visual cortex (at gestational week 13-23 , gestational weeks 27-34 and infancy up to 1 year of age), as well as of the mouse brain during the recovery period (at 5 and 21 days post lesion) from lysolecithin-induced demyelination. This technical and bioinformatic tour de force generated a wealth of information, which allows the analysis of "signal concordance " at a cellular level, with a spatial and temporal resolution. This is the major strength of the study, which provides a great resource , an atlas of the murine brain, which could be assessed by neurobiologists and

neuroepigeneticists.
On the conceptual level, however, the manuscript could benefit from deeper analysis.
Most of the Figures appear to provide a validation of previously reported phenomena, such as the concept of lateral to medial myelination of the corpus callosum (Sturrock 1980; Vincze et al., 2008). But adding a layer of molecular complexity. Other concepts, however, such as timing of myelination of corticofugal Pyramidal neurons followed by myelination of the CPN tracts would need lineage tracing experiments to be validated.
Overall a very nice resource paper

Version 1:

Reviewer comments:

Referee #1

(Remarks to the Author)
The authors have systematically addressed the raised concerns by substantial new experimental work, including the generation of new datasets and the addition of new experimental models. The revised manuscript exemplifies how an ideal resource and new method should be presented, as it not only introduces methodological advances but also uncovers new biological insights. Importantly, all of the reviewer's specific questions have been directly and convincingly addressed. We carefully checked each of our previously raised points (see below) and found that the authors have made a genuine effort to provide rigorous new analyses and meaningful biological new conclusions.
The authors convincingly demonstrate that the integration of spatial proteomics with transcriptomic and epigenomic profiling yields insights that could not be achieved with immunohistology together with single-cell omics alone.
I thank the authors for their thorough and thoughtful revisions and recommend publication of the manuscript in its current form.

Point 1: Added Value of Protein Sequencing
• Initial Point: The manuscript needed to provide specific examples of how protein sequencing enhanced the tri-omic analysis.
• Author Response and Sufficiency: This point was addressed by adding a focused analysis of the lysolecithin (LPC) mouse model. The authors now utilize the spatial ARP-seq protein data to suggest differentially phased immune responses between primary and distal lesion compartments. They identify distinct protein expression patterns for markers such as the laminin receptor CD49f and the inhibitory receptor PD-1 (CD279) across different lesion clusters (LC1-LC5). This new analysis provides an example of how the proteomic data offers distinct biological insights into immune cell dynamics.

Reviewer's Point 2: Reproducibility, Code Availability, and Data Consistency
• Initial Point: The code for the spatiotemporal regression model was not publicly available, and the consistency of the findings across replicates was not demonstrated.
• Author Response and Sufficiency: This point has been fully addressed. The authors have made their negative binomial generalized additive model (NB-GAM) code publicly accessible on GitHub. They also generated a new, higher-resolution dataset (S2) using newly designed DBiT chips with 220x220 barcodes and a 15 μm pixel size. An additional developmental time point (P7) was also included. The provided correlation analysis shows high concordance between the original (S1) and new (S2) datasets for RNA (Pearson $r > 0.95$ for both corpus callosum and cortex genes) and moderate concordance for ATAC data (Pearson $r \approx 0.60$). The inclusion of figures illustrating consistent spatiotemporal patterns across both datasets effectively demonstrates the reproducibility of their model and findings.

Reviewer's Point 3: Mechanistic Insights into Microglial Dynamics
• Initial Point: A deeper investigation into the transcriptional and epigenetic differences between microglial populations at the lesion core versus distal sites was requested, including comparison with existing literature.
• Author Response and Sufficiency: The authors expanded this section by adding a new time point (10 DPL) to the LPC model. They performed sub-clustering on microglia-specific pixels and benchmarked their findings against published single-cell datasets from Androvic et al. and Hammond et al.. This analysis revealed that specific microglial states, such as disease-associated and injury-responsive microglia, are spatially organized between the primary lesion and distal white matter compartments. The investigation is further supported by protein analysis and CellChat modeling to explore cellular interactions.

Reviewer's Point 4: Clarification on Tissue Sectioning and Alignment
• Initial Point: The methodology for cutting and aligning adjacent tissue sections for multi-modal analysis was not clearly described.
• Author Response and Sufficiency: The authors have clarified their procedure, stating that sections were cut at 10 μm thickness. They specified that sections for spatial ARP-seq and CODEX were either adjacent or from anatomically matched regions. Detailed sample information, including section-to-section distances, has been provided in new supplementary tables (Extended Data Tables 7-9). They also state that the sequencing and imaging data were analyzed independently for the purpose of cross-validation.

Reviewer's Point 5: Potential Microfluidic Leakage
• Initial Point: The issue of potential microfluidic leakage was raised, based on observations of column and row artifacts in

supplementary figures, along with questions about its cause and prevalence.
• Author Response and Sufficiency: The authors adequately address this point by clarifying that the observed effect is not leakage. They cite a previous publication (Cell, 2020, 183(6): 1665-1681) where they demonstrated that DNA diffusion is negligible. They explain that the row/column patterns are analogous to bead-to-bead variations common in single-cell sequencing, arising from slight differences in capture efficiency across microfluidic flow lanes. They state that these variations are correctable with standard normalization and do not affect downstream analyses, and that the phenomenon was not widespread in the current study.

Reviewer's Point 6: Analysis of Sparse CD169+ Immune Cells
• Initial Point: The need for a higher-resolution analysis of sparse CD169+ immune cells was identified, with a question as to whether the observed signal was biological or a technical artifact.
• Author Response and Sufficiency: This point has been thoroughly addressed. The authors provided new, high-resolution CODEX images for CD169 at single-cell resolution across all developmental time points (P0 to P21). To validate that the sparse signal is not an artifact, they compared their protein data with in situ hybridization (ISH) data for the corresponding gene (Siglec1) from the Allen Brain Atlas, which showed a similarly limited expression pattern. The response effectively demonstrates that the observation is biological.

Reviewer's Point 7: Cross-Validation of Different Detection Methods
• Initial Point: The manuscript needed to clarify how the different detection approaches (CODEX, CITE-seq, RNA-seq) were used to validate one another and how any discrepancies were addressed.
• Author Response and Sufficiency: The authors acknowledge that a direct comparison is challenging due to technical differences and incomplete marker overlap between panels. However, they state that they observed good general concordance with no substantial discrepancies. They provide visual evidence showing consistent spatial patterns for several key markers (Mbp, Olig2, Itgam (CD11b), etc.) across RNA, ATAC, Protein (ADT), and CODEX, which sufficiently demonstrates the cross-platform consistency of their findings.

Reviewer's Point 8: Inclusion of Sample Size and Statistics in Legends
• Initial Point: The absence of sample sizes and statistical details in the figure legends was noted as an issue to be addressed.
• Author Response and Sufficiency: This point has been comprehensively addressed. The authors have revised figure legends to include sample sizes and added new Extended Data Tables (7, 8, 9) with detailed information for all samples. They also provide a clear and detailed explanation of the statistical framework underpinning their analysis, clarifying that it relies on model-derived statistics from negative binomial generalized additive models (NB-GAMs) rather than traditional groupwise comparisons. They specify the use of likelihood ratio tests and stringent filtering criteria (FDR < 0.01, adjusted R^2 > 0.025) to identify significant spatiotemporal patterns.

Reviewer's Point 9: Limited Insights from Human Data
• Initial Point: The biological insights from the human data could be strengthened by a direct comparison with the mouse findings to provide better context.
• Author Response and Sufficiency: The authors responded directly to this by conducting a new comparative analysis between the human and mouse data to highlight conserved and divergent spatiotemporal dynamics in cortical development and oligodendrogenesis. This new analysis is presented in new figure panels (Fig. 2k,l) and a new manuscript section titled "Spatial dynamics of human visual cortical development," which sufficiently addresses the need for deeper contextualization.

Minor Points: All minor points raised by the reviewer have been addressed, including corrections to typos , figure references , logical flow , terminology , and figure axes.

Referee #2

(Remarks to the Author)
I appreciate the authors' comprehensive responses as well as the efforts in revising the manuscript. While the authors have strengthened the work by including additional data and time points, introducing new sample sets and performing a new AAV experiment, several key issues remain to be addressed. Additionally, I encourage the authors to compare their data with several recently published spatial technology studies such as SPACE-Seq (Huang et al., PNAS 2025) and ExIGS (Labade et al., Science 2025) to better highlight the advantages of their technology as the field moving forward.

Major:
1. The robustness and reliability of their technology need to be further addressed. There are various instances within the manuscript that raise concerns about data quality:
a. The correlation of RNA and ATAC data across timepoints is similar or sometimes higher than the correlation across technical replicates within a time point, indicating the measurements somehow capture more sample-to-sample noise than robust developmental changes (rebuttal pg 4). For example, in the ATAC analysis, the majority of samples across different time points appear highly correlated. Additionally, the P2_S1 is more correlated with P0_S1 than P2_S2 in the RNA data. The authors should explain why their technology generates homogenous measurement but fails to capture meaningful developing signatures.
b. Protein signal is occasionally not correlated with RNA and ATAC data, particularly with immune cell markers. Fig 5c protein data do not support the distal activation claim which was only observed in the ATAC and RNA data. The authors

should explain why protein accumulation at the distal sites of Cd11b, CD11c, and Cd68 is not detected at the protein level, despite being observed at RNA and ATAC levels. Similar inconsistencies are observed in Fig 5h with CD45 and CD115. The authors should elaborate on why these discrepancies may exist.
c. Poor detection quality in the human sample should be discussed or repeated with higher quality replicates. Although working with human tissue is challenging, this issue will greatly limit the applicability of this technology in more relevant tissue types and therefore dampen enthusiasm for this technique. In Fig 2k, BCL11B and TBR1 show different expression patterns compared to Fig 1c. In Fig 2l, many key marker gene expressions in the human cortical layer appear undetected, as indicated by missing data in the heatmap. Additionally, Fig 1c data failed to detect layer makers (CUX1/2, CTIP2, and TBR1) and glia maker (PDGFRa), which should be abundantly expressed and been used as positive references (Qian et al., Nature 2025) The authors should include high-magnification images with clear cortical layer annotations to substantiate their claim that the technology can actually be used forhuman samples.
Additionally, the authors made several interpretations and statements that are not well supported by their data. For instance, they stated that high ATAC activity precedes RNA expression for all myelin-associated genes in human samples, but this is not true for MOBP and BCAS1 in Fig 2l.
Moreover, several conclusions are based on one single human sample, with no accompanying quality control and replicates. The authors should increase the number of sample sizes, replicates and provide quantification and statistics to strengthen these conclusions and findings.

2. Immunofluorescence or ISH validations are needed for several main statements.
a. In Fig 3c, the cell proportion analysis shows there is no OPC population at P10 and P21. Additionally, the Fig 3h shows a similar reduction of OPC maker along the development. As shown by many studies, OPCs populate the brain throughout life and continue to reside in the corpus callosum throughout (Dawson, 2003, Allen Atlas, 2011, Bergles and Richarson, 2016). This lack of OPC at juvenile brain is controversial and likely wrong – the authors should provide IF results of OPC markers throughout the development to validate their findings.
b. The author demonstrated that the lateral CC shows stronger MBP colocalization with AAV-labeled neuronal projections. However, the MBP signal in Fig 3j actually shows a flat distribution from lateral to medial CC – contradictory to the claim. The results in Fig 3m and 3n could just reflect the intensity differences of neuronal projections but not myelination itself. To validate this result quantitatively, authors may just stain a panel of well known myelination markers throughout the developmental ages and quantify the spatial distribution in lateral and medial CC, which is a standard validation experiment.
c. The authors deduce in Fig 5 that there is distal activation of immune cells as an effect of LPC injection. The authors should provide IF/ISH staining alongside the CODEX images to validate their findings.

3. A more rigorous and systematically controlled experimental design using the LPC mouse model is necessary to support the study's conclusions. The distal activation of microglia in white matter is an interesting finding but lack several critical controls and therefore cannot be interpreted. A bilateral sham injection should be used as a control. This control would validate that the distal microglial activation was a product of the lesion and not of mechanical damage to the brain by intracranial injection. Additionally, the LPC injections should be performed with a fluorescent marker so that they are able to show that leakage of the injection is not the cause of the distal activation.
a. The authors should define the criteria used for identifying "distal lesioned areas." It would also strengthen the manuscript if they could provide quantitative data showing how the phenotype changes at varying distances from the lesion and at various temporal stages of the lesion.
b. The authors should include a control non-lesioned / mock injected animal in their analysis of cell proportion and microglial clusters in Fig 6.
c. The authors should compare their microglial subclusters to previous literature identifying activated microglial populations as an effect of demyelination of white matter areas. This would help confirm their findings and reliability of their technology.

Minor
1. In their rebuttal on page 29, the authors claimed to show P5 replicates next to each other to show consistency of the codex images. They did not provide this image.
2. In Fig 4h, the authors should align the 10DPL-S1 images so they are not sideways.
3. In Fig 5h, the slice chosen for 5DPL is posterior to the images in 10DPL and 21DPL. Authors should choose slices taken from the same region of the brain.

Referee #3

(Remarks to the Author)
The authors have adequately responded to previous concerns, by including additional references and new data convincingly showing the differential distribution of thalamo-cortical and cortico-cortical axons.
The only minor issue that remains for me is panel c in figure 3, is truly difficult to interpret and the figure legend is not very helpful

Version 3:

Reviewer comments:

Referee #1

(Remarks to the Author)

Overall, the authors' responses are acceptable. Only the reviewer2's concern about the human data is still valid. Authors should limit human comparisons and add the following clarification: "These human data serve as exploratory benchmarks to demonstrate human-tissue applicability of DBiT-based spatial ARP-seq. Analyses establish technical feasibility and cross-species consistency of epigenome-transcriptome-protein mapping in situ, rather than delivering definitive biological conclusions." With these revisions, the primary concern would be addressed. I think rest of the issues are well addressed and can be published.

We would like to thank the reviewers for their insightful and constructive feedback, which has greatly improved the quality of our manuscript. In response to the comments and suggestions from all three reviewers, we have conducted a substantial number of additional experiments, increasing the total experimental dataset by ~50%, including:

(i) a new set of developing mouse brains data (P0-P21) with newly designed DBiT chips featuring 220 × 220 barcodes and 15 μm pixel size;
(ii) the addition of a new time point for the LPC demyelination mouse model;
(iii) the generation of a new set of CODEX experiments for all samples;
(iv) retrograde-AAV-eGFP tracing experiments to map the projection of neuronal axons and myelination along the corpus callosum.

We have also performed new analyses to comprehensively address each comment. Below, we provide a detailed point-by-point response to all reviewer comments, which have further refined and strengthened our manuscript. All revisions have been highlighted in yellow in the manuscript.

Referees' comments:

Referee #1 (Remarks to the Author):

Transcriptomics, from single-molecule to bulk-level analysis, plays a critical role in advancing our understanding of biological processes. Multi-modality approaches, which integrate RNA, protein expression, morphology, functional studies, and chromatin architecture, have the potential to extend insights gained from transcriptomics to other biological modalities. This multi dimensional view enables the identification of novel mechanisms and the aiming better for most effective therapeutic strategies.

In this context, Zhang et al. introduce two DBiT-based spatial tri-omic technologies that provide valuable insights into the dynamics of transcription factors involved in both myelination and cortical layer specification during development and injury. The manuscript highlights both technological innovations and biological insights, offering significant & original contributions to the field.

They show that myelination-related genes show coordinated patterns of transcription and chromatin accessibility, with chromatin priming evident in early postnatal stages (P0-P5) before RNA expression appears at later stages (P10). By P21, even though some myelin genes continue to be transcribed, their chromatin accessibility has already started to decrease. This contrasts with cortical layer-specific transcription factors, which are primed during embryonic development but show reduced RNA expression in the postnatal period, while their chromatin accessibility remains high. These findings suggest distinct regulatory mechanisms: myelination involves early chromatin priming followed by RNA expression, whereas cortical layer specification maintains chromatin accessibility despite decreased RNA levels. The use of a multi-modal approach in this study is particularly valuable, as it uncovers complex details that would be missed if only one type of data were considered. By utilizing both RNA-seq and ATAC-seq enhanced with spatiotemporal resolution, the study provides a technology for a view for how gene regulation unfolds during development and injury.

Response: We would like to thank the reviewer for considering that our manuscript provides both technological innovations and biological insights, and that it offers valuable, significant, and original contributions to the field.

Major:

- While the manuscript effectively highlights the tri-omic approach, it lacks specific examples of how protein sequencing enhances insights. Given that this is a key novelty of the study, this section needs to be strengthened to better demonstrate the added value of protein sequencing in the tri-omic analysis.

Response: We thank the reviewer for the comments. Following the reviewer's suggestion, we have now strengthened the protein sequencing part in our revised manuscript to better demonstrate its added value in the tri-omic analysis. Apart from the use of the spatial ARP-seq to confirm myelination dynamics and the protein expression of cortical transcription factors, we focused on the lysolecithin (LPC) mouse model and the characterization of the distinct microglial dynamics in the primary focal and distal LPC lesion-like compartments, given that our protein panel was mainly targeting immune-related genes**.** We found that an array of proteins in our spatial ARP-seq had differential expression in the 5 compartments identified in both primary lesions and distal lesion-like compartments (**Fig. 6g**, below). While all the lesion compartments (except LC1) were identified to have microglia (with presence of CD68, CD11b, CX3CR1, and CD169 protein), the overall expression in LC5 was decreased (**Fig. 6g**). Instead, LC5 had expression of oligodendrocyte protein markers (OLIG2 and MBP) and was the compartment with the highest expression of CD279 or PD-1 (**Fig. 6g**), an inhibitory receptor of T-cells, B-cells and myeloid cells. While LC1-4 were positive for CD49f protein (highest in LC2), this laminin receptor that has costimulatory effects, was absent from LC5. Taken together, our protein spatial ARP-seq based analysis suggests differentially phased immune responses in the primary lesions site when compared to the distal white matter (WM) site.

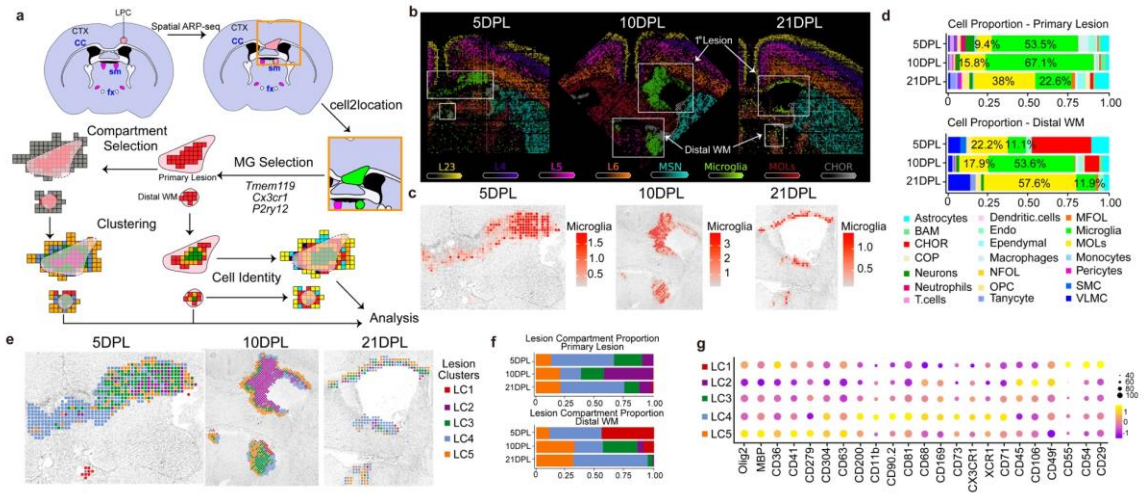

Fig. 6: a, Schematic illustration of the analysis workflow. **b,** Cell type predicted by cell2location from 5 DPL, 10 DPL, and 21 DPL. **c,** Predicted spatial abundance of microglia by cell2location in lesion-like compartments. **d,** Proportions of different cell types within lesion-like compartments in the primary lesion and distal white matter, as shown in **c**. **e,** Unsupervised clustering of the lesion-like compartments in **c**. **f,** Proportions of different clusters from primary lesion and distal white matter in **e**. **g,** The expression level and the percentage of pixels from clusters LC1-LC5 for ADT protein data in spatial ARP-seq.

- Additionally, it is sometimes unclear which observations are derived from which specific analyses. Clarifying the source of each observation will improve the overall clarity and understanding of the findings.

Response: Thank the reviewer for the comments. We have now clarified the source of each observation by indicating the specific analyses from which they were derived throughout the manuscript.

- The use of a negative binomial generalized additive model (NB-GAM) to identify patterns based on gene expression, spatial location, time points, and their interactions is of particular interest. The parameters are well-thought-out and aptly suited for capturing variation along the spatio-temporal axis. However, while the methods section provides a detailed description of the computational framework for the spatiotemporal regression model, the corresponding code is not available on the GitHub page. Given the novelty and importance of this framework in the study's data analysis pipeline, providing the code is crucial for ensuring reproducibility and transparency. Additionally, including spatial pattern annotations for the replicates (not shown in the main figures) at each time point in an extended data figure would enhance the presentation. This addition would help demonstrate the consistency of the findings, similar to the approach taken with other results in the study.

Response: We thank the reviewer for the comments. We have made the code for the spatiotemporal regression model publicly accessible via GitHub (https://github.com/di-0579/spatial_tri-omics/tree/main/Data_analysis).

In the original manuscript, we generated two spatial ARP-seq (renamed from DBiT ARP-seq per Reviewer 1's suggestion in the "Minor" section) replicates per time point (P0, P2, P5, P10, and P21) using a 100×100 barcode device with 20 μm pixel size. However, due to differences in the regions of interest (ROI) captured between replicates, such as limited cortical layer coverage in one of the P5 samples, we included only one replicate per time point in the spatiotemporal regression model analysis. Following the reviewer's suggestion, we have now generated a new set of spatial ARP-seq datasets covering developmental mouse brains from P0 to P21 (P0, P2, P5, P7, P10, and P21), the sample information was provided in **Extended Data Table 7**). These datasets were generated using newly designed high-resolution DBiT chips featuring 220×220 barcodes (BC 220) and 15 μm pixel size. The application of the new chips allowed us to capture almost the entire hemisphere of the mouse brain. In addition, an additional developmental time point (P7) was included during the revision to improve temporal resolution. The new BC220 dataset is referred to as the S2 dataset in the revised version of the manuscript.

Following the reviewer's suggestion, we first conducted a correlation analysis of raw RNA and ATAC data. The results showed high concordance within replicates and across time points, in particular for samples with similar ages (r ranges from 0.69 to 0.97, with most values above 0.92 for RNA; r typically > 0.90 for ATAC; r stands for Pearson correlation coefficient, please also see below). This metric reflects global similarity without accounting for spatial structure.

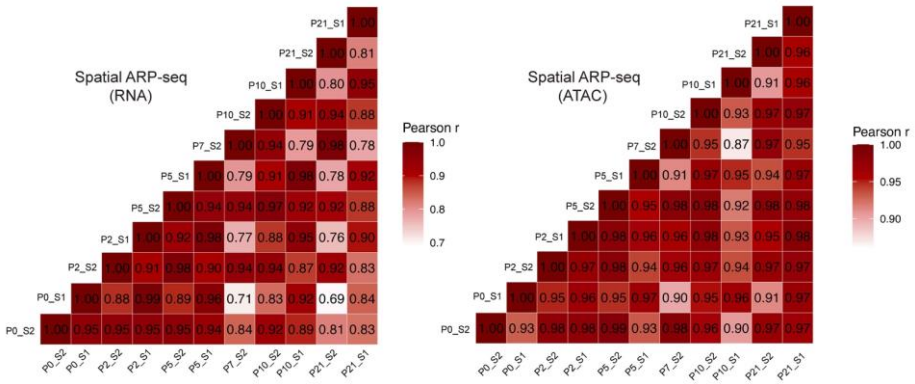

We then followed the reviewer's suggestion to model the spatiotemporal dynamics of gene expression and chromatin accessibility, we employed our generalized additive model (GAM) with negative binomial distribution, formulated as follows: gam_fit <- gam(y ~ library_id + ti(time) + ti(spatial) + ti(time, spatial), family = nb()). This framework enables smooth modeling over developmental time (time), spatial domains (spatial), and their interaction (ti(time, spatial)), capturing complex trends across both dimensions. Each gene or ATAC peak is independently fitted using this model to generate predicted response values across all sampled spatiotemporal points. One important point to note is that although high global correlation in raw data confirms technical reproducibility, it does not ensure that the spatiotemporal trends estimated by GAM models will be identical across datasets, since these outputs capture biological patterns after incorporating spatial complexity.

For the corpus callosum, following the reviewer's suggestion, we applied our spatiotemporal regression model separately to the S1(barcodes 100, BC100) and the newly generated S2 (barcodes 220, BC220) dataset. As shown below, both datasets independently revealed broadly concordant spatial and temporal expression patterns in the corpus callosum, confirming consistency across replicates.

Spatial patterns for S1 (without integration):

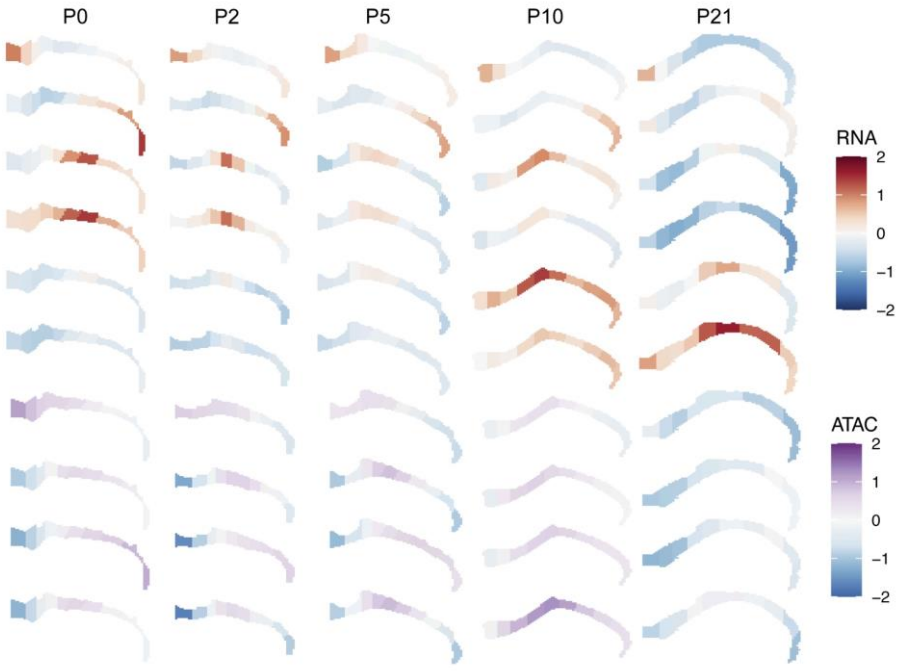

Spatial patterns for S2 (without integration):

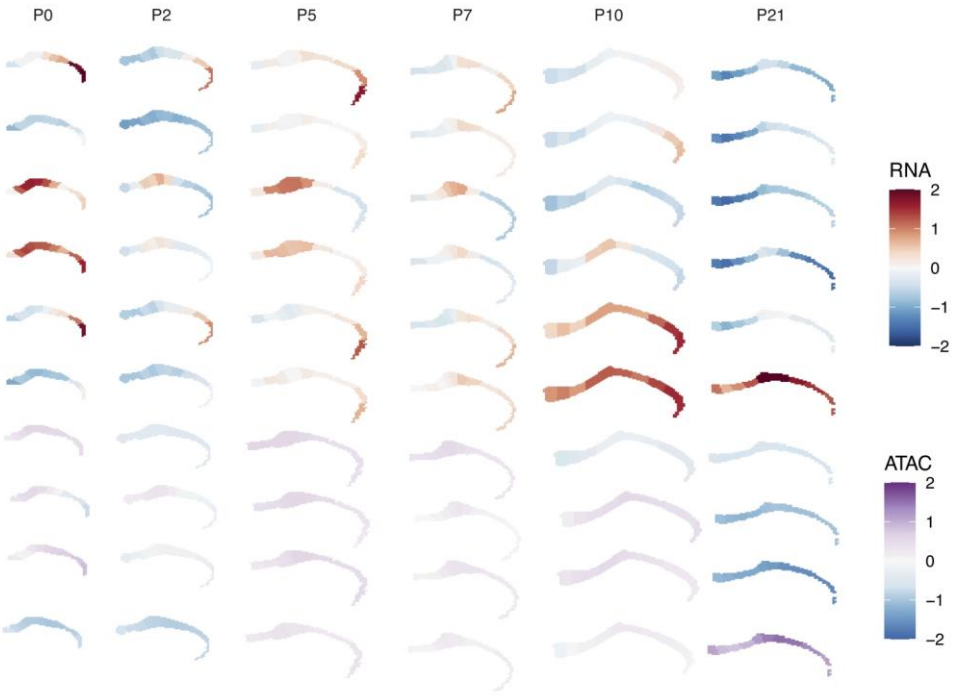

We further applied the spatiotemporal regression model to fit the integrated S1 and S2 dataset, as the corpus callosum region covered a relatively small spatial area with fewer total pixels, making joint modeling computationally feasible and potentially more robust. The results are shown in **Fig. 3e-h** and **Extended Data Figs. 39 and 40** (please also see below). The spatial and temporal trends were similar to those observed in the separate fits above.

Spatial patterns for S1 (Extended Data Fig. 40) (After integration):

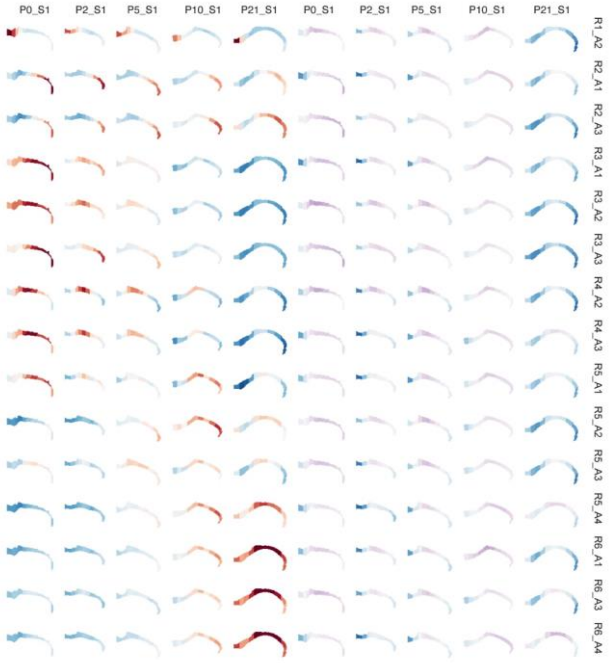

Spatial patterns for S2 (Extended Data Fig. 39) (After integration):

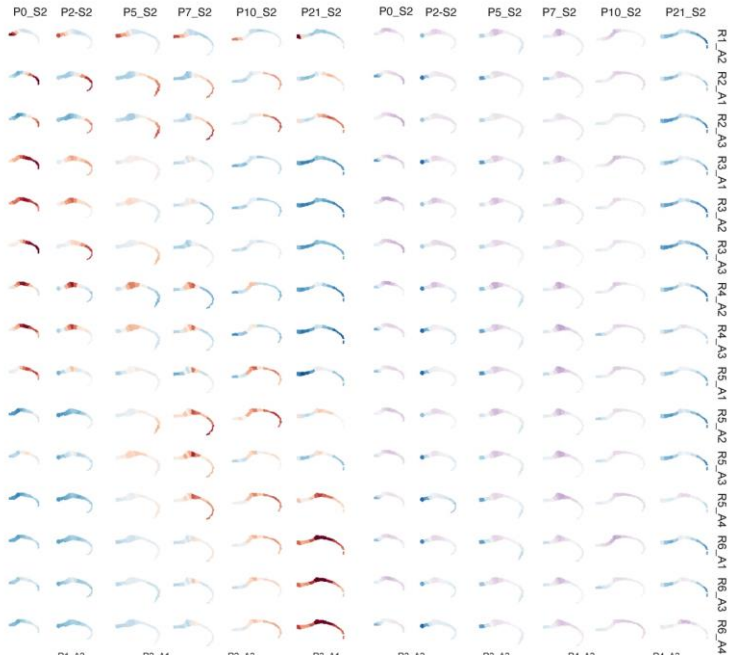

Besides, following the reviewer's suggestion, and for easier comparison, we computed the correlation between the resulting GAM-predicted profiles. The GAM-predicted RNA expression matrix from the S2 dataset exhibits a high correlation with the S1 dataset (Pearson r = 0.967, please see below, **Extended Data Fig. 18**), indicating strong consistency and robustness of the spatiotemporal modeling.

The GAM-predicted chromatin accessibility (ATAC) profiles from the two datasets exhibited moderate concordance (Pearson $r \approx 0.60$, please see below, **Extended Data Fig. 18**), which may reflect the inherently sparse nature of ATAC-seq data, as well as differences in biological context, modeling structure, and technical resolution, as elaborated in the subsequent discussion.

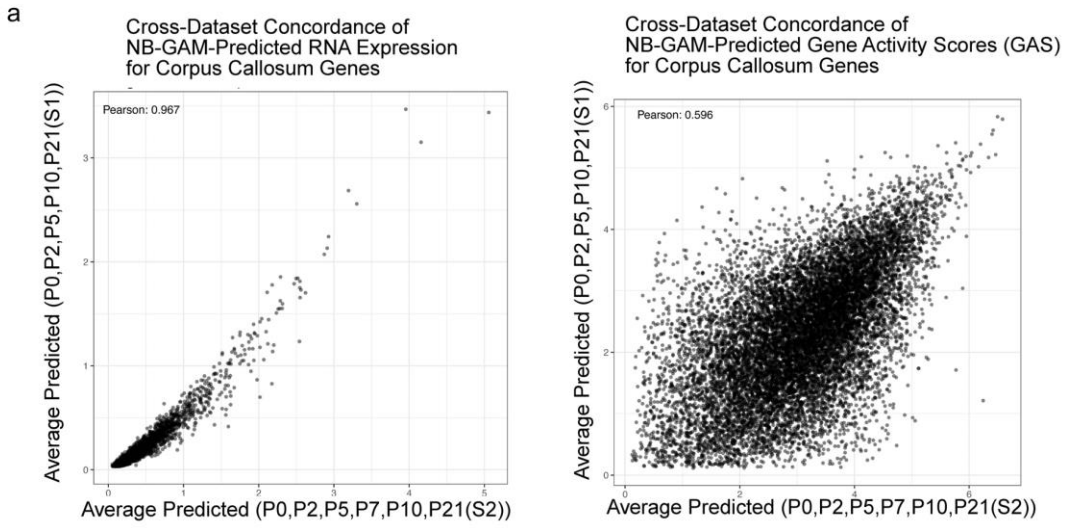

Similarly, following the reviewer's suggestion, we have also applied the spatiotemporal regression model to the newly generated replicate dataset (S2) to investigate the cortical layers during postnatal

development. The results are shown below (**Extended Data Figs. 26 and 27**). Due to the large number of gene x time x space combinations in the cortical layers, we did not integrate S1 and S2 for joint GAM fitting (which was performed for the corpus callosum), as the associated memory and computational demands exceeded feasible limits. Compared to the results of the regression model from the S1 dataset (Extended Data Fig. 27c-f), the GAM-predicted RNA expression matrix from the S2 dataset exhibits a high correlation (Pearson r = 0.956, please see below), indicating strong consistency and robustness of the spatiotemporal modeling. Moreover, the S2 dataset revealed more RNA patterns, likely due to the inclusion of an additional developmental time point (P7). To facilitate direct comparison, we are providing the spatial patterns generated from the regression model for both S1 and S2 datasets below and are also providing all the cortical RNA and ATAC patterns generated (Extended Data Figs. 26 and 27)

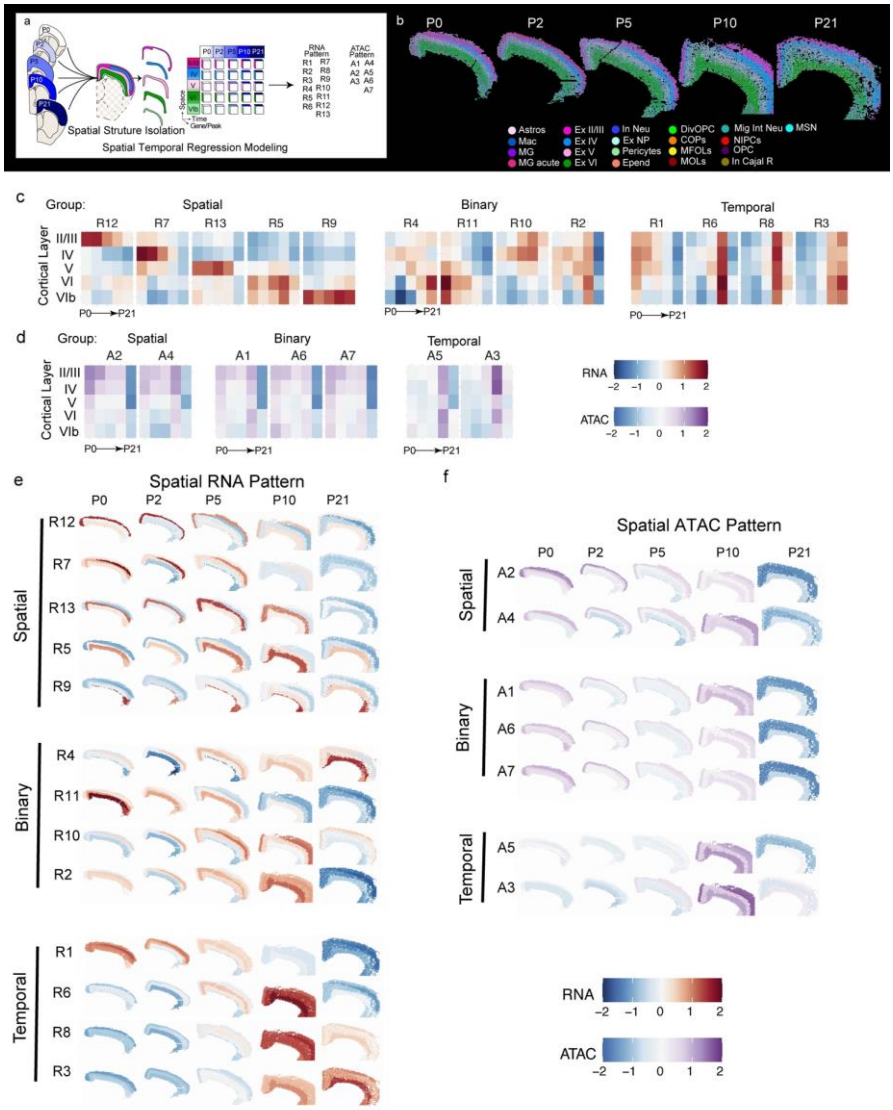

Extended Data Fig. 27 Further analysis of developing mouse brain cortical layers (S1). a, Schematic representation of spatial temporal regression model on mouse brain cortical layers. **b,** Decomposition and pie chart visualization of different cell types in cortical layers (S1) from the spatial RNA data. **c,** Heatmaps of the 13 RNA clusters generated from the regression model (S1). **d,** Heatmaps of the 7 ATAC clusters generated from the regression model (S1). **e-f,** Spatial RNA (**e**) and ATAC (**f**) patterns generated from the regression model (S1).

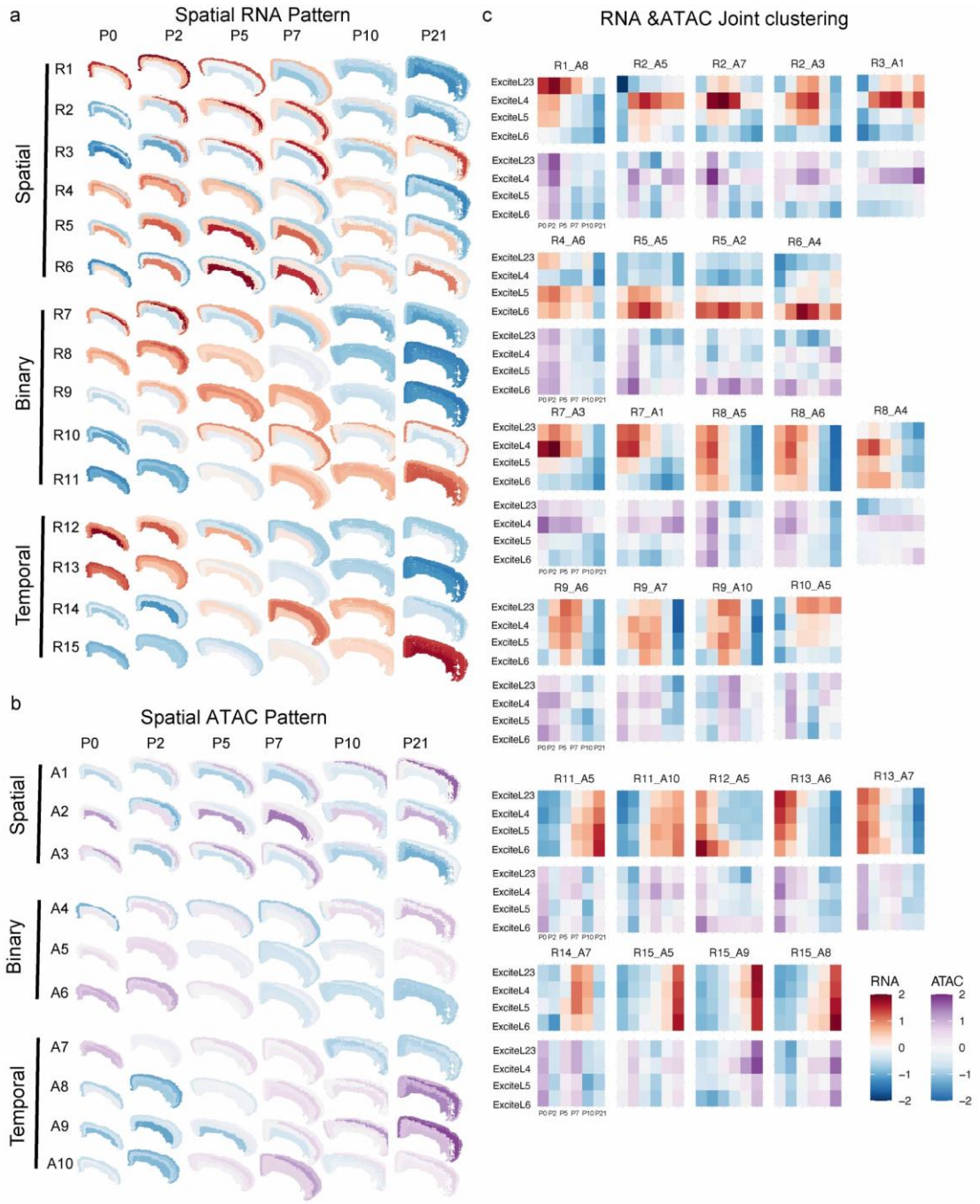

Extended Data Fig. 26 Further analysis of developing mouse brain cortical layers (S2). Spatial RNA (**a**) and ATAC (**b**) patterns generated from the regression model (S2). **c,** Heatmap for each of the 27 clusters from the RNA & ATAC joint clustering analysis (S2).

For the GAM-predicted ATAC profiles, as in the corpus callosum analysis, the correlation (r = 0.55, please see below) was not as strong as for the RNA. This is expected, as chromatin accessibility is inherently more variable and less spatially confined than transcriptomic profiles, particularly in developing mouse brain samples, which may reflect multiple underlying factors, as discussed below. Importantly, we plotted all genes discussed in the manuscript in Extended Data Figs. 28-34, and most of these genes exhibited similar temporal and spatial trends across datasets.

b

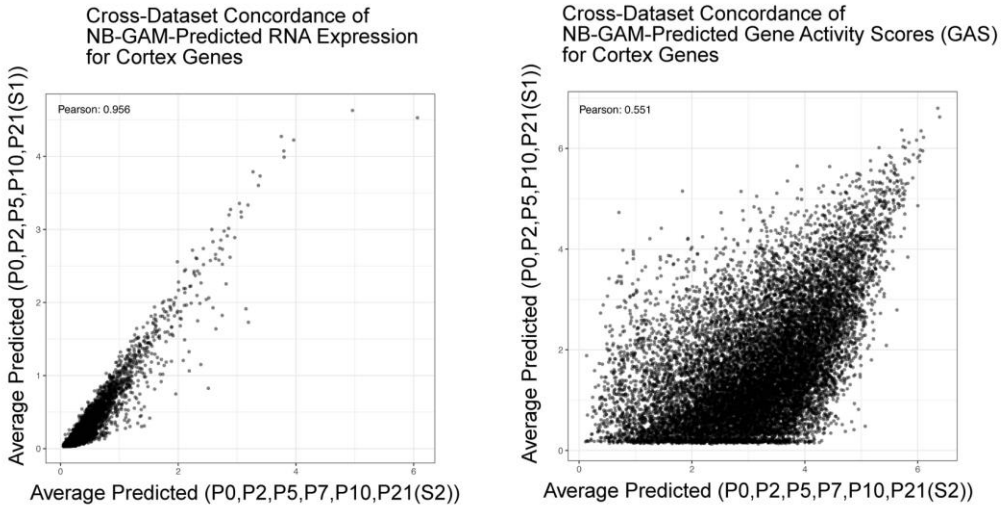

Given the sparsity of ATAC-seq data, the minor variations in spatiotemporal sampling structures between datasets might contribute to the moderate correlation observed in the ATAC analysis.

For the corpus callosum (CC), this region has been delineated manually due to its highly dynamic developmental trajectory. During early postnatal stages (P0-P10), RNA expression profiles do not consistently delineate the CC boundary, which becomes anatomically distinguishable only around P21. To address this variability, we manually selected spatial domains corresponding to the CC anatomical region in each sample. Subsequently, we subdivided each selected CC region into 10 equally spaced bins along the medial-lateral axis to enable trend fitting. Given inter-sample minor variations in CC size and morphology, these bins do not always align precisely across replicates. While biologically relevant, this manual delineation, coupled with temporal and anatomical variability, might introduce slight spatial misalignments of local accessibility signals, affecting the correlation of GAM-fitted chromatin accessibility trajectories across samples.

For cortical layers, spatial domains were defined using a multimodal integration approach implemented by SpatialGlue (Long *et al.*, *Nat. Methods*, 2024), jointly leveraging RNA and ATAC modalities. Given the clear laminar delineation of RNA expression patterns, the spatial structures were mainly defined based on RNA-derived region boundaries. This RNA-guided segmentation ensures strong biological interpretability, as RNA signals are fitted within well-aligned anatomical boundaries, whereas ATAC signals exhibit inherently broader and less spatially confined distributions. This loss of laminar resolution limits the ability of the GAM to capture precise regional trends from ATAC signals and might contribute to the slightly reduced cross-replicate concordance. Furthermore, while S1 and S2 datasets were processed under similar pipelines, the difference in spatial resolution (15 μm in S2 vs. 20 μm in S1) likely affects nuclear capture efficiency per pixel, leading to subtle differences in chromatin accessibility profiles.

In general, our GAM framework demonstrates robust performance on RNA data, as evidenced by its strong concordance and biological interpretability. Although the raw ATAC-seq data showed high

reproducibility, the correlation of GAM-derived profiles was not as strong as RNA, which is also expected given the inherent nature of ATAC data sparsity. This may also reflect the biological complexity of chromatin accessibility (e.g., less spatially confined, particularly in developing samples) and suggests that additional considerations might be necessary when modeling their spatiotemporal dynamics to further unveil additional epigenetic mechanisms. Currently, spatial ATAC-seq datasets remain limited, and to the best of our knowledge, there are no fully established or widely used computational methods specifically designed to model chromatin accessibility jointly across space and time. This lack of established approaches points to the potential benefit of developing strategies better suited to the dynamic nature of spatial epigenomic regulation. Further investigation may help elucidate the dynamic regulatory processes underlying chromatin accessibility.

- The authors report observing an activated microglia population distal to the lesion site. Investigating the transcriptional and epigenetic programs that differ between the distal microglia and those in close proximity to the lesion could be particularly enlightening. Given the multi-modal technique the authors have developed, such an analysis could significantly enhance the paper's impact by elucidating biological mechanisms relevant to neurodegenerative states. Adding this mechanistic layer would complement the extensive descriptive developmental findings detailed throughout the paper.

-The effects of LPC-induced demyelination have been previously characterized using spatial transcriptomics (Androvic et al., 2023), showing that DAM-like state, likely CD11c+ (Itgax) microglia, are localized near the lesions. How does the diffuse activation observed in this study differ from previous findings? Additionally, how do the epigenetic and protein data from this study enhance or refine the existing understanding of microglial activation near LPC-induced lesions? It would be insightful to discuss these points.

Response: We thank the reviewer for these comments. To address them, we have added additional time points of the lysolecithin (LPC) mouse model, in particular 10 days post-lesion (n=2, coronal sections), resulting in 3 stages of demyelination/remyelination process (5 DPL, 10 DPL, and 21 DPL), all profiled with both spatial ARP-seq and CODEX. To understand the distal microglia/macrophage properties in the context of lesional microglia responses to demyelination, we employed a stepwise strategy to (1) dissect the primary lesion and distal general compartments; (2) selection of microglia specific pixels, positive for *P2ry12, Tmem119,* and *Cx3cr*1; and (3) perform a deeper investigation into the microglia occupying these different compartments (**Fig. 6a-c**, please also see below for **Fig. 6**). We performed unsupervised clustering with joint ATAC and RNA data on the lesion-like compartments and segregated 5 distinct compartments (**Fig. 6e,f**). Protein analysis and GO analysis for the RNA and ATAC components suggested differentially phased immune responses in the primary lesions site when compared to the distal WM site. To further investigate the primary lesion and distal WM inflammation, we performed microglia subclustering on microglia-specific pixels (positive for *P2ry12, Tmem119*, and *Cx3cr*1), and for the remaining pixels, we assigned cell identities across the primary lesion and distal WM (**Fig. 6h** and **Extended Data Fig. 54b**). We also determined with their likely identity using module scoring comparing geneset from previously published data by Androvic and colleagues, as mentioned by the reviewer, and also another microglia dataset by Hammond and colleagues. We found that all the

Androvic microglia clusters (foamy, interferon-responsive, and disease-associated microglia) and Hammond microglia (axon tract-associated, disease-associated, and injury-responsive) were predicted in our RNA data set to a higher extent in the primary lesion at 10 DPL, with reduced prediction in the distal WM (**Fig. 6i** and **Extended Data Figs. 53g,h, 54c,d and 55a**). However, in one of the replicates (S1), the ATAC module prediction was higher in the distal WM, while in the other (S2) the differences in both RNA and ATAC between primary lesion and distal WM were not as striking, suggesting that the inflammation in this area is still evolving. Moreover, the Hammond injury-responsive module was predicted to be enriched in the distal WM lesion-like compartment rather than in the primary lesion core (**Extended Data Figs. 54c,d and 55a**). Our data suggested that differential signaling and cellular interactions might occur specifically in primary and distal lesions at 5 DPL and 10 DPL. To investigate this possibility, we performed CellChat analysis, predicting the overall cellular interactions that were happening across these time points to determine which cells were communicating with our differential microglia clusters (**Fig. 6l and Extended Data Fig. 56a-c**). Taken together, our new analysis indicates that LPC lesions can induce lesion-like compartments in distal WM tracks, displaying a delay in microglial activation when compared to the primary WM lesion.

All the above discussions have been added in the revised manuscript in the newly added section “Distinct microglial dynamics in the primary focal and distal LPC lesion-like compartments” according to the reviewer’s insightful suggestions.

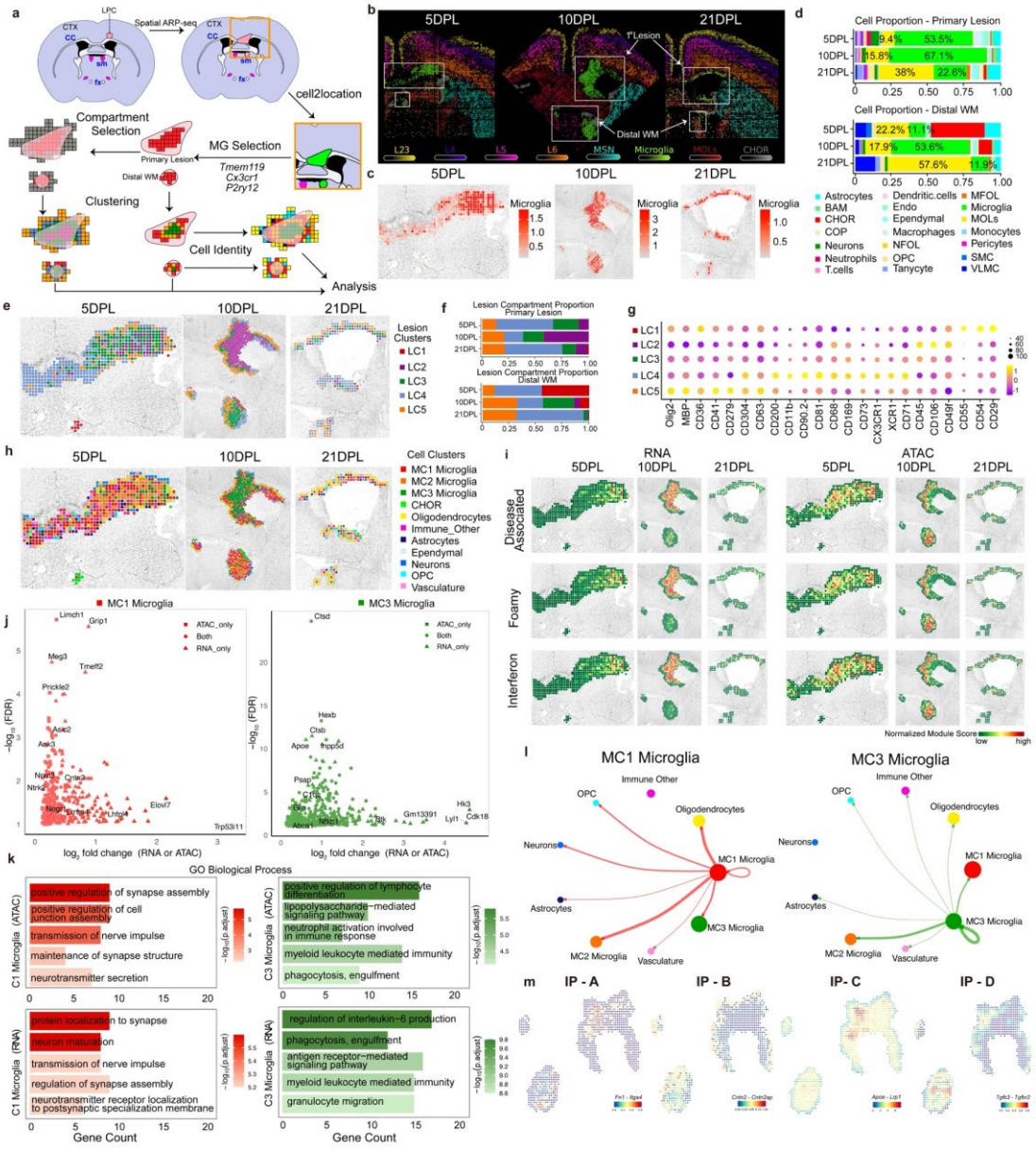

Fig. 6: Microglial dynamics in the primary focal and distal lesion-like compartments. a, Schematic illustration of the analysis workflow. **b,** Cell type predicted by cell2location from 5 DPL, 10 DPL, and 21 DPL. **c,** Predicted spatial abundance of microglia by cell2location in lesion-like compartments. **d,** Proportions of different cell types within lesion-like compartments in the primary lesion and distal white matter, as shown in **c**. **e,** Unsupervised clustering of the lesion-like compartments in **c**. **f,** Proportions of different clusters from primary lesion and distal white matter in **e**. **g,** The expression level and the percentage of pixels from clusters LC1-LC5 for ADT protein data in spatial ARP-seq. **h,** Cell types and subclusters of microglia (MC1-MC3) in **e**. **i,** Spatial module scores of disease-associated, foamy, and interferon microglial states based on RNA and ATAC data at 5DPL, 10DPL, and 21DPL in lesion-like compartments. Gene sets were based on Andrović et al., 2023. **j,** Volcano plots showing differential gene expression or GAS for MC1 (left, red) and MC3 (right, green) microglia subclusters. **k,** GO analysis of microglia subclusters (MC1, left; MC3, right) (One-sided version of Fisher's exact test, p-value was adjusted for multiple comparisons by Benjamini & Hochberg method). **l,** Communication networks of MC1 (left) and MC3 (right) microglia with other microglial subtypes and brain cell types, based on CellChat analysis. **m,** Representative spatial maps of ligand–receptor interaction strength for *Fn1–Itga4* (A), *Cntn2–Cntnap2* (B), *Apoe–Lrp1* (C), and *Tgfb3–Tgfbr2* (D), showing regional enrichment within lesion-like compartments at 10 DPL.

- It is not clear how adjacent sections are cut, registered or aligned. How far apart are these adjacent sections? How well aligned? Please clarify whether this approach could lead to redundancy or potentially enhance the protein signal.

Response: We thank the reviewer for the comments. Tissue sections for both spatial ARP-seq, spatial CTRP-seq (renamed from DBiT ARP-seq and DBiT CTRP-seq per the reviewer's suggestion in the "Minor" section), and CODEX were cut at a thickness of 10 µm using the same embedding and cryosectioning protocols. Spatial ARP-seq and CODEX sections were generally obtained from the same tissue block, though not always from immediately adjacent sections. We have now included **Extended Data Tables 7-9** (also provided below), which summarize the sample information, including section-to-section distances between spatial tri-omic sequencing and CODEX across developmental and disease stages of the mouse and human brain. All sections were cut at closely analogous positions with consistent orientation. In the original manuscript, we broadly used the term "adjacent" to describe the relationship between spatial ARP-seq and CODEX sections. However, for some mouse developmental time points, spatial ARP-seq sections were not always paired with directly adjacent CODEX sections. The adjacency status is also clearly indicated in the Extended Data Tables 7-9. We now clarify that the sections processed with spatial ARP-seq and CODEX were obtained either from adjacent serial sections or from anatomically matched regions at the same developmental stages. The sentence previously stating "*To investigate the spatial dynamics of mammalian cortical and white matter development at the molecular level, we utilized spatial ARP-seq on adjacent tissue sections processed with CODEX*." has been revised to "*To investigate the spatial dynamics of mammalian cortical and white matter development at the molecular level, we utilized spatial ARP-seq on tissue sections that were either adjacent to or from anatomically matched regions at the same developmental stages as those processed with CODEX*." in the revised manuscript.

Extended Data Table 7. Summary of mouse sample information for spatial ARP-seq and CODEX.

Samples		Spatial ARP-seq		CODEX	Sex	Spatial adjacency between spatial ARP-seq and CODEX	
		Sample name	# of barcodes	Sample name		Yes/No	Section distance
P0	Rep 1	P0_S1	100x100	P0_S1	N/A	No	N/A
	Rep 2	P0_S2	220x220	P0_S2	N/A	Yes	0 µm
	Rep 3	P0_S3	100x100		N/A		
	Rep 4	P0_S4	100x100		N/A		
P2	Rep 1	P2_S1	100x100	P2_S1	N/A	Yes	10 µm
	Rep 2	P2_S2	220x220	P2_S2	N/A	Yes	0 µm
	Rep 3	P2_S3	100x100		N/A		
P5	Rep 1	P5_S1	100x100	P5_S1	N/A	Yes	10 µm
	Rep 2	P5_S2	220x220	P5_S2	N/A	No	N/A
	Rep 3	P5_S3	100x100		N/A		
P7		P7_S2	220x220	P7	N/A	No	N/A
P10	Rep 1	P10_S1	100x100	P10_S1	N/A	Yes	20 µm
	Rep 2	P10_S2	220x220	P10_S2	N/A	No	N/A

	Rep 3	P10_S3	100x100		N/A	No	N/A
P21	Rep 1	P21_S1	100x100	P21_S1	M	No	N/A
	Rep 2	P21_S2	220x220	P21_S2	M	Yes	20 μm
	Rep 3	P22_S3	100x100		M		
5DPL	Rep 1	5DPL_S1	100x100	5DPL_S1	F	Yes	10 μm
	Rep 2	5DPL_S2	100x100	5DPL_S2	F	Yes	10 μm
10DPL	Rep 1	10DPL_S1	100x100	10DPL_S1	F	Yes	0 μm
	Rep 2	10DPL_S2	100x100	10DPL_S2	F	Yes	0 μm
21DPL	Rep 1	21DPL_S1	100x100	21DPL_S1	F	Yes	10 μm
	Rep 2	21DPL_S2	100x100	21DPL_S2	M	Yes	10 μm

Extended Data Table 8. Summary of mouse sample information for spatial CTRP-seq and CODEX.

Samples		Spatial ARP-seq		CODEX	Sex	Spatial adjacency between spatial ARP-seq and CODEX	
		Sample name	# of barcodes	Sample name		Yes/No	Section distance
5DPL	Rep 1	5DPL_S1	100x100	5DPL_S1	F	Yes	0 μm
	Rep 2	5DPL_S2	100x100	5DPL_S2	F	Yes	0 μm
21DPL	Rep 1	21DPL_S1	100x100	21DPL_S1	F	Yes	0 μm
	Rep 2	21DPL_S2	100x100	21DPL_S2	M	Yes	0 μm

Extended Data Table 9. Summary of human sample information for spatial ARP-seq and CODEX.

Samples	Spatial ARP-seq	Sex	Spatial adjacency between spatial ARP-seq and CODEX	
	# of barcodes		Yes/No	Section distance
Second trimester	100x100	N/A	Yes	30 μm
Third trimester	100x100	F	Yes	20 μm
Infancy	100x100	F	Yes	N/A

We did not perform image registration or algorithmic alignment between spatial sequencing and CODEX sections. Spatial sequencing data capture robust and interpretable regional patterns across the brain at the epigenomic, transcriptomic, and protein levels, while CODEX imaging provides an orthogonal modality to validate protein expression patterns in corresponding anatomical regions. The sequencing and imaging data were analyzed independently and were not merged for quantification. We do not consider the use of both spatial tri-omic sequencing and CODEX to be redundant. Applying both approaches enables cross-validation of biological findings without artificially enhancing protein signals. For example, we observed the expression of *Mbp* (MBP) in the lateral part of the corpus callosum at P10 using chromatin accessibility (ATAC), RNA, and protein (ADT, antibody-derived DNA tag) signals from spatial ARP-seq. CODEX imaging independently confirmed MBP localization in the same region (The results were shown in Fig. 1j-l and Extended Data Fig. 6, please also see below). These convergent results from sequencing- and imaging-based approaches strengthen confidence in spatial

protein expression patterns without inflating signal levels. The spatial tri-omic and CODEX datasets may serve as useful resources for future investigations involving sequencing and imaging modalities.

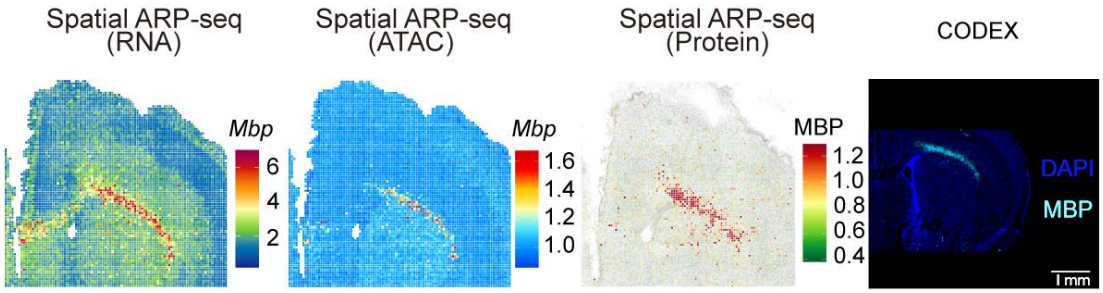

- In the supplementary figures, some columns and rows are positive for signal, suggesting leakage in one direction of the microfluidics. Are these issues related to microfluidic valve performance? Additionally, why is this leakage not observed in all analyses, and how widespread is this issue?

Response: We thank the reviewer for the comments. The possibility of DNA diffusion has been evaluated by analyzing a 3D confocal fluorescence image in our previous study (Cell, 2020, 183(6): 1665-1681), which demonstrated negligible leakage signal throughout the tissue section thickness (please see the figure below). It was found to be 4.5 ± 1 μm for 50 μm channels and 0.9 ± 0.2 μm for 10 μm channels, which confirmed spatially confined delivery and binding of DNA barcodes in tissue with our microfluidic device.

[REDACTED FIGURE]

Regarding the positive signals, they are analogous to bead-to-bead intensity variation commonly observed in single-cell sequencing. In our system, the pixels are physically aligned in rows and columns, which can result in row-to-row or column-to-column variation in signal due to slight differences in capture efficiency across the microfluidic flow lanes. These variations can be corrected with standard data normalization, similar to that used in single-cell RNA-seq workflows, and do not affect downstream analyses. This was clarified in our *Cell* paper (2020, 183(6): 1665-1681). In our current manuscript, we did not observe a prominent occurrence of this phenomenon, indicating that the effect is not widespread.

- The study could provide more in-depth analysis of the sparse immune cells, particularly the CD169+ cells shown in the supplementary figure2, which appear to be developmentally regulated. However, the resolution of the images is too low to assess this accurately. The tri-omic approaches should ideally offer better resolution for these cells, or it should be clarified if this is an artifact of CODEX.

Response: We thank the reviewer for the comments. We have now provided high-resolution CODEX images for CD169 from P0 to P21 mouse brains (**Extended Data Figs. 2-7**), which were captured at single-cell resolution. The cell density of CD169+ cells is quite low in developing mouse brains, consistent with the sparse distribution. Here we include higher magnification images to show that it is highly specific at labeling cells in the meningeal comparted as shown by the segregation between the layer of subpial GFAP and PDGFRα labeling meningeal pericytes (see image on the right).

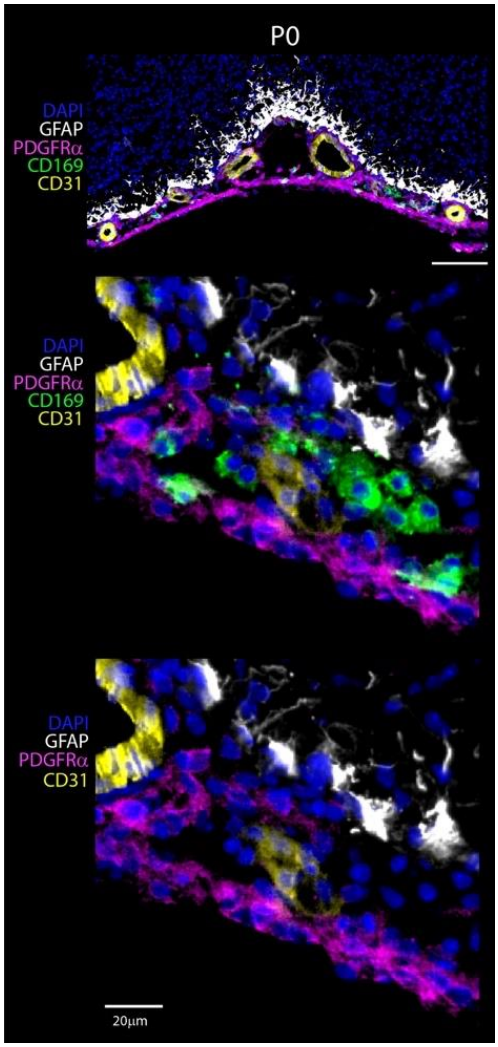

We also checked the Allen brain atlas ISH data for the gene *Siglec1* (CD169) from P56 mouse brain sagittal sections (the only available time point for this gene, please see the images below). The gene expression pattern overlaps with the regions labeled by CODEX in the developing mouse brains, and the signal is similarly limited. This consistency supports that the CD169 signals we observed are not artifacts of the CODEX imaging. Based on these results, we have improved the description in our manuscript to: "*CD169, however, was abundant in the meninges and present in the choroid plexus, identifying a developmental border associated macrophage counterpart to CNS resident CD169+ cells that increase after ischemia*." in our manuscript.

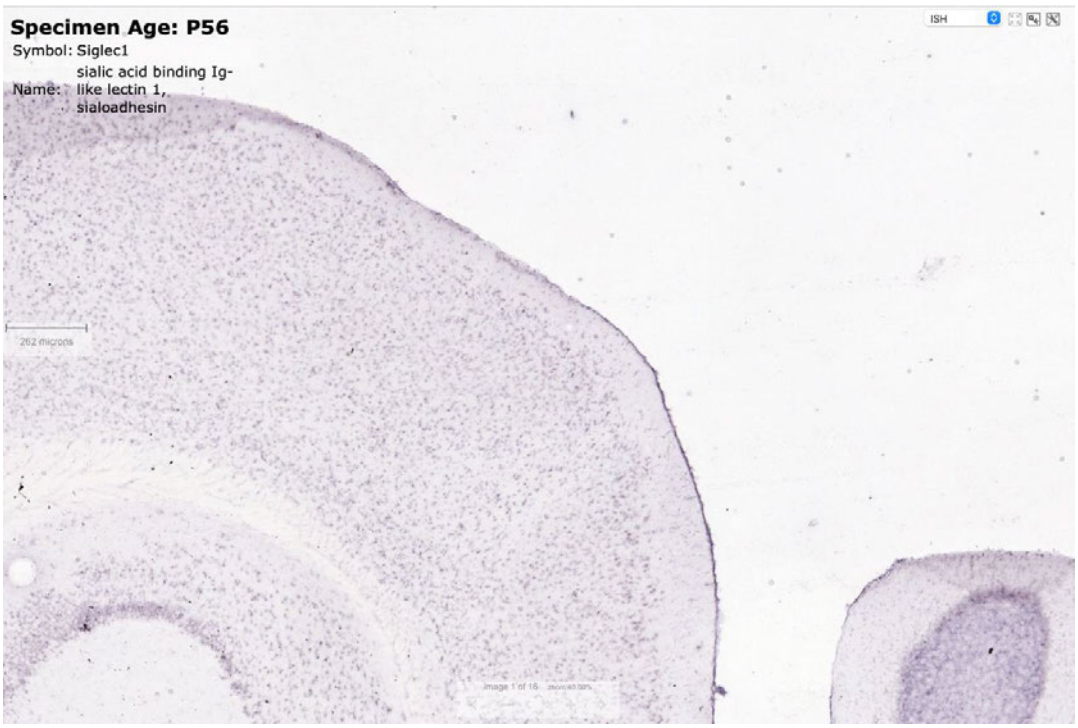

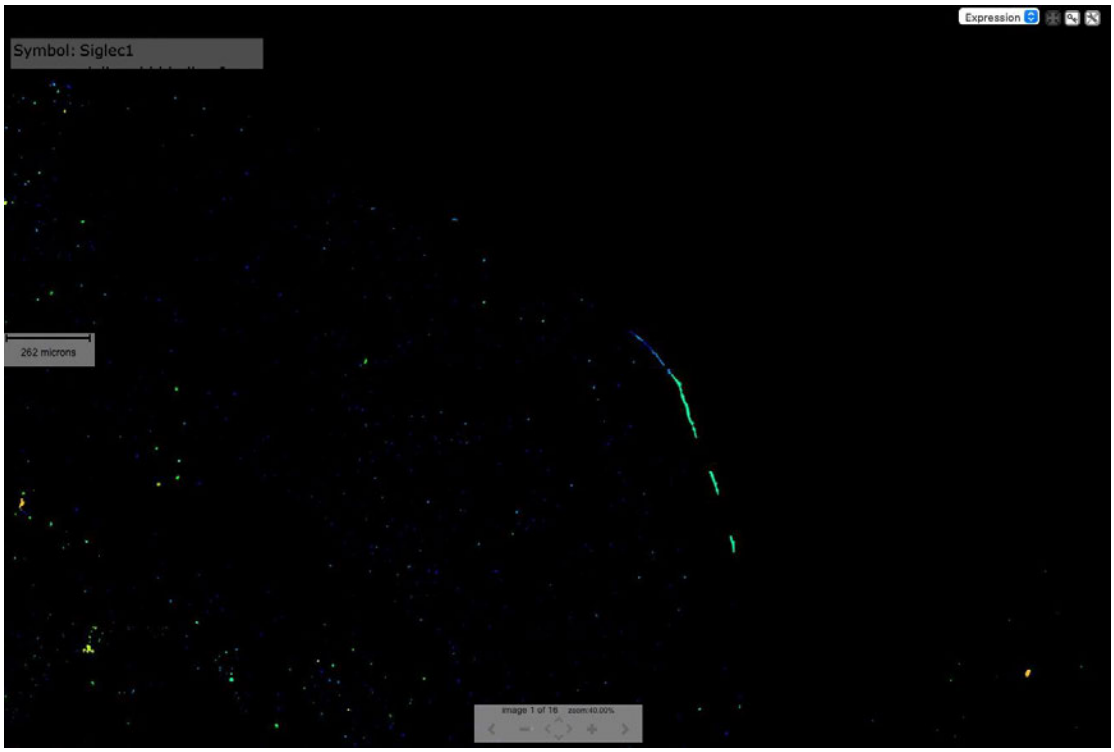

- Additionally, it would be valuable to understand how the different detection approaches (CODEX, CITE-seq, and RNA-seq) were used to validate the strengths or weaknesses of the measurements. Where did these methods disagree, and how were discrepancies between CODEX, CITE-seq, and RNA-seq addressed?

Response: We agree with the reviewer that this is an interesting question, but challenging to address, as potential discrepancies could be of technical origin or biological, and unique for each individual protein/RNA. Another challenge for comparing the CODEX and the CITE-seq data in our datasets is that they are not obtained from the same section, and only a few markers in both panels are overlapping. Nevertheless, in general, despite the differences in resolution and modality, we observed good concordance with no substantial discrepancies, as exemplified with *Mbp, Olig2, Mog, Itgam* (CD11b), and *Itgax* (CD11c) below.

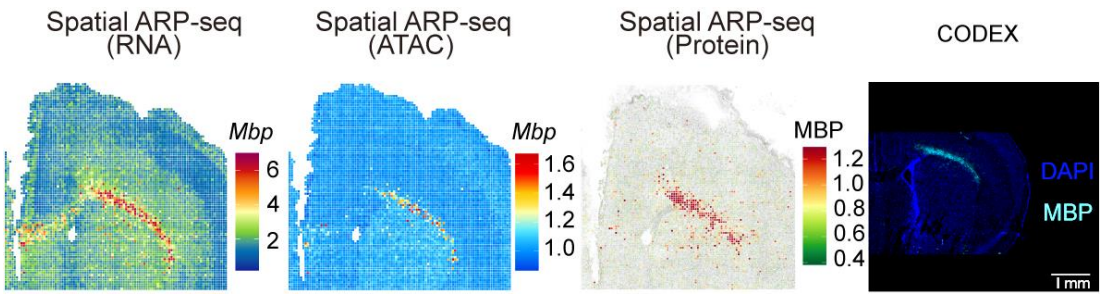

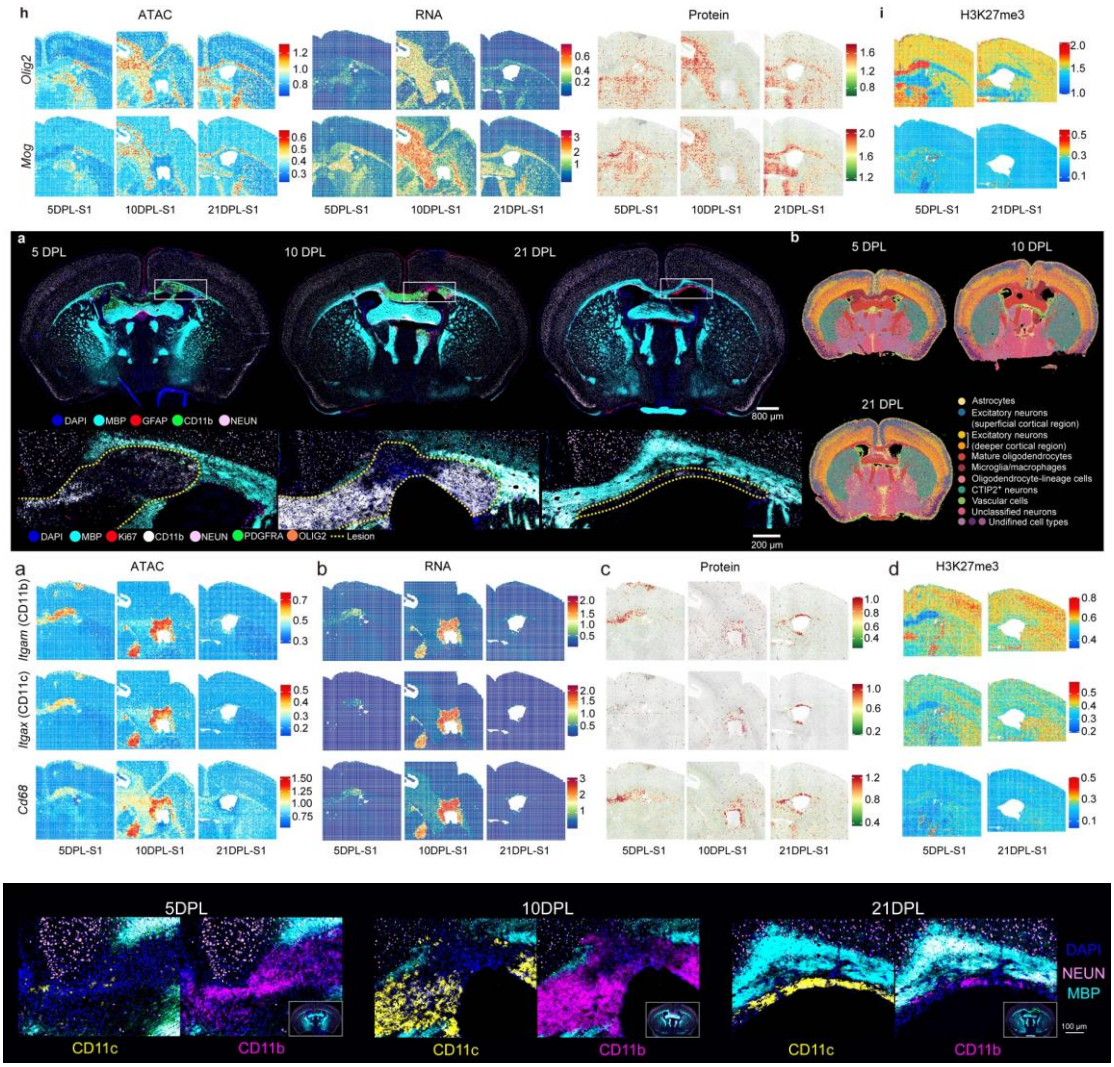

- Legends should include sample size and stats. It is not clear statements are based on any stats.

Response: We thank the reviewer for the suggestions. We have revised the figure legends for both the main and extended data figures to clearly indicate the sample size used for each modality and timepoint, specifying whether data were derived from a single developmental series or represent integrated results from two independent datasets. To further improve transparency, we have added Extended Data Tables (Extended Data Tables 7,8,9, also provided in our response to the reviewer's previous comment) that provide detailed information on all samples processed in this manuscript.

In addition, we would like to clarify the statistical analyses used in our study. While our work does not involve traditional groupwise statistical comparisons (e.g., differential expression testing between biological replicates or timepoints), we apply multiple layers of model-derived statistical evaluation to identify genes and features with significant spatiotemporal dynamics. Specifically, we fit negative binomial generalized additive models (NB-GAMs) to each gene or peak, incorporating temporal, spatial, and spatiotemporal smooth terms. We perform likelihood ratio tests (LRTs) comparing the full model to a null model containing only batch effects, and we extract p-values for each smooth term to assess the statistical significance of dynamic patterns. P-values are adjusted for multiple testing using the

Benjamini–Hochberg method, and only genes or peaks with significant smooth terms (adjusted p < 0.01), significant LRT p-values (FDR < 0.01), and sufficient model fit (adjusted R^2 > 0.025) are retained for downstream analyses.

- While the human data provide a valuable demonstration of the technology's applicability, the insights are somewhat limited compared to the mouse findings. It would be beneficial to link the human data to a specific disease or developmental stage, which could offer a clearer context for comparison and highlight the relevance of the findings beyond validation in human tissue.

Response: We thank the reviewer for the comments. Following the reviewer's suggestion, we have now conducted comparison between the human and mouse data, highlighting conserved and divergent spatial-temporal dynamics, both for cortical development and oligodendrogenesis. Additional results have now been added in **Fig. 2k,l** (below) and **Extended Data Figs. 35-38**. We have also included a new section "Spatial dynamics of human visual cortical development" to provide a more detailed discussion of the results.

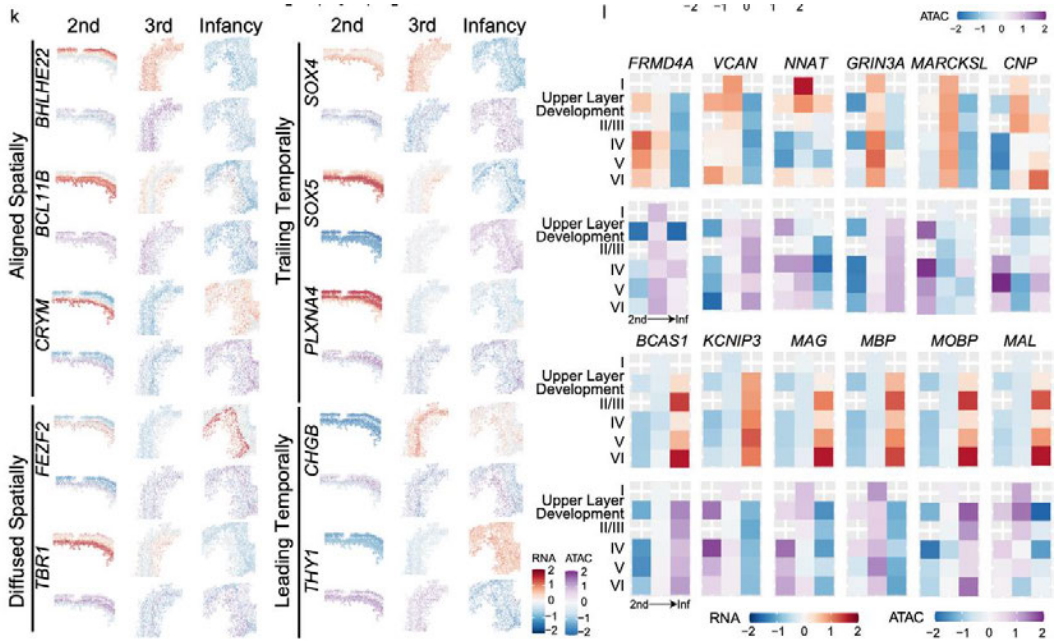

Fig. 2: k, Representative gene expression (top) and ATAC GAS (bottom) for human brains (2nd: second trimester; 3rd: third trimester), segregated into groups based on variance of ATAC gene activity score in comparison to RNA expression. **l,** Heatmaps of representative RNA gene expression (top) and ATAC GAS (bottom) for oligodendrocyte lineage associated and myelination associated genes through human V1 cortical development.

Minor:

- Typo in Page 38, Line 31, "RunUMA" should be "RunUMAP"

Response: We thank the reviewer for pointing this out. We have now revised this typo to "RunUMAP" in the "Data clustering and visualization" section of the Methods.

- Page 9, Line 1-3 refers to Ext Data Fig 3e,f but there is no f panel.

Response: Thank you for pointing this out. The figure panel was originally mislabeled in the text as

Extended Data Fig. 3e,f, but it should have referred to Extended Data Fig. 3d,e. During revision, this figure has been moved and is now labeled as Extended Data Fig. 25b,c. We have updated the main text accordingly.

- Description of regional partitions of corpus callosum in Fig3a comes later in the text than descriptive results from the same figure. The sections can be re-ordered for better flow.

Response: We thank the reviewer for the helpful suggestions. We have re-organized Fig. 3 to match the flow of the manuscript.

- To maintain consistency and accuracy, the authors should revert to using "spatial CITE sequencing" throughout the manuscript unless a clear distinction between the methods is being intentionally made. A brief explanation of the differences, if applicable, would also help clarify this for the reader.

Response: We thank the reviewer for this helpful comment. We fully agree that consistency in terminology is important for clarity. In this manuscript, we describe two newly developed technologies for the simultaneous profiling of genome-wide chromatin accessibility or histone modifications, along with transcriptome and proteome, within the same tissue section. While these methods could technically be referred to as “spatial ATAC–CITE-seq” and “spatial CUT&Tag–CITE-seq”, respectively, we found these names to be somewhat long and less intuitive. To improve readability and ease of communication, we introduced the terms **DBiT ARP-seq** (spatial ATAC–RNA–Protein-seq) and **DBiT CTRP-seq** (spatial CUT&Tag–RNA–Protein-seq), which more directly reflect the modalities profiled. In light of the reviewer’s helpful suggestion, we have revised the terminology to **spatial ARP-seq** (spatial ATAC–RNA–Protein-seq) and **spatial CTRP-seq** (spatial CUT&Tag–RNA–Protein-seq), which we believe strike a better balance between clarity and brevity. A brief explanation has been included in the opening section of our manuscript.

- The sentence on Page 13, Line 31: 'Interestingly, R3-A2 and R5-A2 presented GO terms of glial migration were classified (Extended Data Figs. 16, 17); this needs revision to improve readability and ensure the message is conveyed accurately.

Response: We thank the reviewer for the comments. We have now revised this section combining the integrated regression model data which has shifted the text.

- Extended Fig. 5a, the bottom-left panel y-axis is not in log scale.

Response: We thank the reviewer for pointing this out. We have corrected the y-axis of the bottom-left panel to display in log scale.

- Page 23, Fig 2.a, Under the schematic representation “Spatial Struture Isolation” should be Spatial Structure Isolation.

Response: We thank the reviewer for pointing out the typo. The label has been corrected from “Spatial Struture Isolation” to “Spatial Structure Isolation.”

Referee #2 (Remarks to the Author):

Zhang et. al performed the spatial omic profiling from human and mouse brains using cutting-edge tri-omic technologies DBiT ARP-seq and DBiT CTRP-seq. Combined with multiplexed immunofluorescence, the authors characterized the spatially and temporally dynamic patterns of transcriptome and chromatin accessibility of the mouse cortex from neonates to juveniles. They observed a lateral to medial myelination progression in the corpus callosum in the developing brains. Using the lysolecithin injection inflammation model, they found two microglia subtypes activated at both the core and distal locations of the lesion.

It is an innovative approach to apply new technologies to samples from different species and disease models. The biological conclusions are intriguing. However, the authors have not convincingly demonstrated the suitability or advantage of their technologies in either the disease study or the neurodevelopmental study. Moreover, I found it hard to evaluate whether these technologies have the required dynamic range and sensitivity to quantify subtle differences in the disease models – and whether the observed changes, most of which were quite surprising, could be due to technical artifacts – more validation and replicates will strengthen this work. Most conclusions could be drawn simply by using simpler tools such as immunohistology and single-cell omics, which dampened my enthusiasm.

Response: We would like to thank the reviewer for considering our approach innovative and the biological conclusions intriguing. To address the reviewer's concerns regarding dynamic range and sensitivity, we have considerably increased the number of biological ns and expanded our analysis. In response to the comments and suggestions from all three reviewers, we have conducted a substantial number of additional experiments, increasing the total experimental dataset by ~50%, including:

(i) a new set of developing mouse brains data (P0-P21) with newly designed DBiT chips featuring 220 × 220 barcodes and 15 μm pixel size;
(ii) the addition of a new time point for the LPC demyelination mouse model;
(iii) the generation of a new set of CODEX experiments for all samples;
(iv) retrograde-AAV-eGFP tracing experiments to map the projection of neuronal axons and myelination along the corpus callosum.

These new datasets enabled us to perform deeper analyses, specifically, we (i) included further analysis for the developing human brain data, and conducted a comparison between human and mouse to highlight conserved and divergent spatial-temporal programs in cortical development, (ii) deciphered the dynamics of neuroinflammation from epigenome, transcriptome, and protein levels during the progression from demyelination to remyelination in LPC mouse model, (iii) demonstrated the microglial states at lesion core and distal white matter compartments with distinct epigenomic and transcriptional features, (iv) uncovered spatially distinct myelination dynamics of different cortical projection neuron subtypes.

This improvement led to the addition of two new sections "*Spatial dynamics of human visual cortical development*", and "*Distinct microglial dynamics in the primary focal and distal LPC lesion-like compartments*", and improvement in sections "*Layer-specific projection neuron axonogenesis and*

synaptogenesis time may orchestrate myelination", "*Spatial tri-omic mapping of neuroinflammation and remyelination using a focal lesion mouse model of MS*", "*A transient population of microglia arise during myelination in development and remyelination in the LPC models of MS*", "*Distal microglia associated with WM tracks are observed far from the LPC lesion*", as well as new and improved figures (Fig. 2k-l, Fig. 3i-n, Fig. 4a,e,h, Fig. 5f-h, and Fig. 6). We consider the revised manuscript better highlights the power of the spatial tri-omic technologies to dissect not only cell types or states but also the mechanisms controlling cell fate dynamics.

Major points:

1. The application on human tissues (Fig 1c) is great, but the data suggests the postmitotic neuron marker NeuN has a decreased expression throughout neurogenesis? This is shocking. The collective neuronal marker signals were barely detectable in the third trimester and infancy: is this an issue with the sample quality or just the variability of the technology?

Response: We thank the reviewer for the comments. The NeuN signal shown in Fig. 1c was derived from CODEX multiplexed immunofluorescence staining. This was performed on the commercial CODEX platform (Akoya Biosciences), which is coupled to a Keyence BZ-X800 epifluorescence microscope for image acquisition. All CODEX experiments across samples were performed under identical protocols, including tissue processing, antibody incubation, and imaging parameters. The observed decrease in signal intensity over developmental stages may be influenced by changes in cell density and spatial organization during human brain development, rather than reflecting a downregulation of NeuN expression. To further support visualization, we have now also included enlarged panels in extended data figures with zoomed-in views of these markers (**Extended Data Figs. 12-14**).

To further investigate this, we conducted a quantitative analysis of NeuN. We applied the SPACEc pipeline (https://github.com/yuqiyuqitan/SPACEc) with Cellpose (cyto model) for nuclear segmentation using the DAPI channel. Raw DAPI channel images (please see the figure below, left) were fed into Cellpose. Predicted segmentation masks (below, right) outlined every detected nucleus. This process generated binary masks with unique IDs assigned to each nucleus. For each segmented cell, we computed the mean intensity of NeuN and other neuronal markers using *extract_features()*. This yielded a cell-by-marker matrix for downstream statistical analysis, with spatial coordinates and morphological metadata retained per cell.

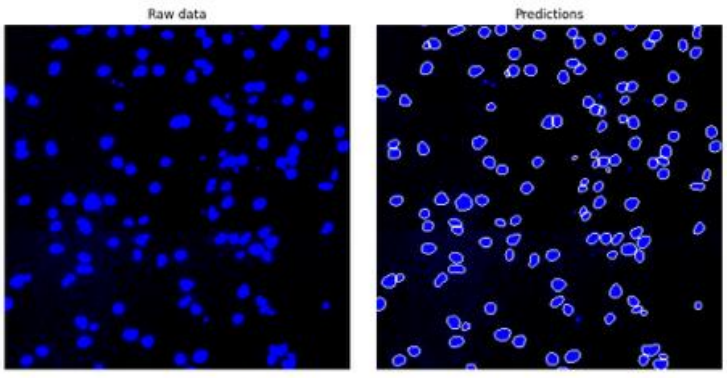

To mitigate nonspecific background signal and reduce noise, we filtered out the bottom 25% of NeuN-

intensity cells in each sample. These typically corresponded to poorly stained, out-of-focus, or non-neuronal regions. This thresholding preserves the meaningful NeuN+ signal distribution without distorting quantitative relationships. We then directly computed the density of segmented nuclei in each tissue section using:

Cell_density = number_of_segmented_cells / tissue_area_in_mm²

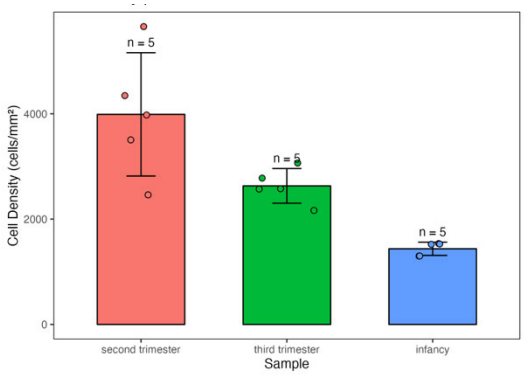

As shown below, the second trimester had ~1-2 times higher cell density than the third trimester and infancy. This was consistent across computational replicates and anatomical subregions.

To evaluate whether NeuN expression truly decreases, we plotted violin plots of single-cell NeuN intensities (log-transformed) across developmental stages (please see the results below, left). These analyses did not reveal a clear reduction in median NeuN intensity per cell over time. NeuN intensity remained relatively stable or slightly increased over time, without evidence of systematic decline. In addition, we also visualized the spatial distribution of NeuN using z-score normalized expression (please see the figure below, right), which showed preserved spatial patterns of NeuN across stages. As the z-score normalization highlights within-sample spatial variation, it is not suited for assessing global expression loss. However, the raw intensity distributions confirm no reduction in absolute signal.

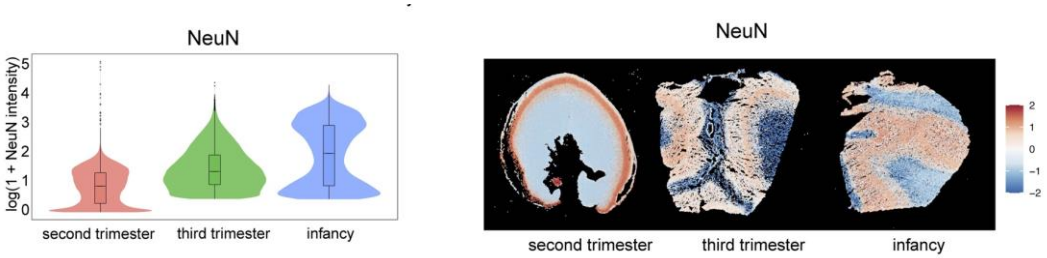

All staining and imaging steps were conducted under identical protocols to minimize variability of the technology. The visually weaker signals of other neuronal markers (SATB2 and CTIP2 in the original Extended Data Fig. 3) are not readily attributable to sample quality or variability of the technology, and instead reflect factors such as tissue architecture, cell density, and the large field of view (4–5 mm per side), all of which may influence image-level visualization. We also plotted violin distributions of per-cell intensity (log-transformed) across developmental stages (please see the figures below, left). SATB2 and CTIP2 showed relatively stable median expression levels across the second trimester, third trimester, and infancy. We also visualized the spatial distribution of SATB2 and CTIP2 using z-score

normalized expression maps, which confirmed the preservation of expected spatial patterns.

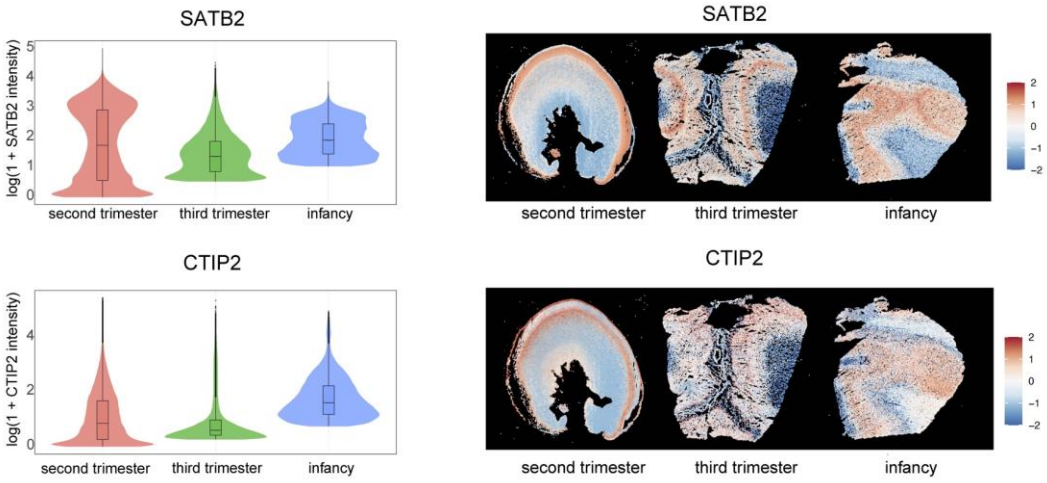

In sum, these results suggest that the apparent reduction in NeuN, CTIP2, and SATB2 signal in Fig. 1c reflects tissue-level structural changes rather than decreased expression per cell. We appreciate the reviewer's careful observation. We have now revised the main text accordingly by adding the following clarification: "*Nevertheless, correcting for the cellular density between the different time points indicates that there might in contrast an expansion of these domains, consistent with an increase in brain volume during these stages in development*." We also included this analysis in Extended Data Fig. 15.

2. In the current manuscript, transcript or protein abundance was shown visually, and it is hard to evaluate them quantitatively – and to what extent the measurement is consistent between batches and samples. In Fig 2d, neuronal markers Satb2 and Tbr1 were barely detectable in P21 – this is again surprising and raises the question of the sensitivity and reliability of DBiT. According to the works of many and the Allen ISH atlas, these genes have high and sustained expression in the cortex. I got more confused later seeing Satb2 does seem to be expressing in P21 in ExFig 2c - in sharp contrast to Fig 2d? Strong conclusions were drawn from these visualizations: e.g., the authors claimed that there are decreased expressions of layer-specific TFs in development in mice and humans (Page 5, Line 10-12 and Line 38-40). These were inconsistent with the literature and potentially could be very interesting – but extraordinary claims require extraordinary evidence.

Response: We thank the reviewer for the comment. For consistency between batches and samples, we first conducted a correlation analysis of raw RNA and ATAC data. The results showed high reproducibility, in particular for samples with similar ages (r ranges from 0.69 to 0.97, with most values above 0.92 for RNA; r typically > 0.90 for ATAC; r stands for Pearson correlation coefficient, please also see below). These results confirm the robustness and technical consistency of our spatial sequencing data, supporting the reliability of the spatial patterns shown in the manuscript. CODEX experiments were performed using the commercial CODEX platform (Akoya Biosciences), following the manufacturer's standardized protocols for staining and imaging. All samples were processed using identical antibodies, and imaging was performed with consistent exposure settings across all timepoints, ensuring comparability across samples.

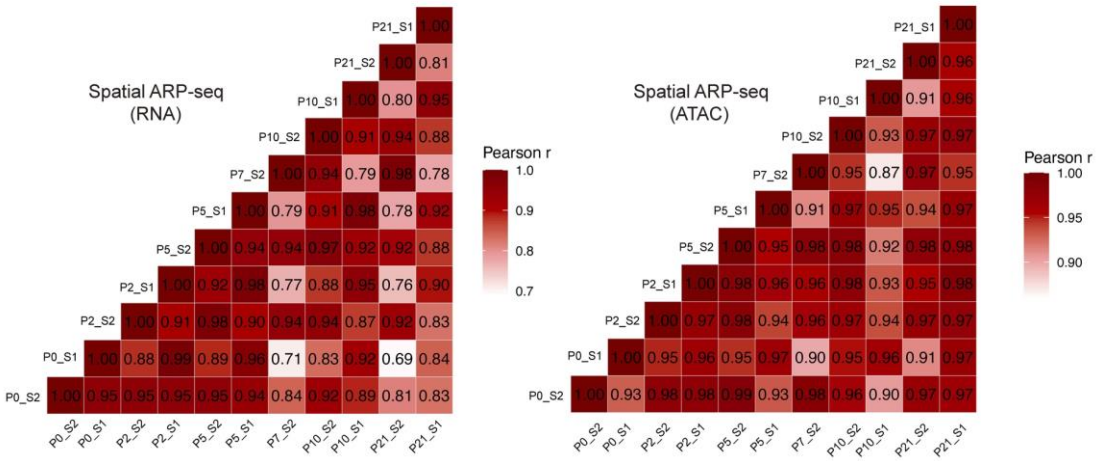

Regarding SATB2 and TBR1, the images shown in Fig. 2d (now **Fig. 2b**) were derived from CODEX multiplexed immunofluorescence protein imaging, rather than from DBiT sequencing. To validate the observed differences, we provided multiple complementary lines of evidence: (1) updated CODEX images across developmental stages; (2) systematic quantification of per-cell protein intensity and marker-positive cell density; (3) reproducibility of observations across independent experiments; (4) cross-validation using spatial transcriptomic (DBiT) data; (5) consistency with *in situ* hybridization (ISH) data from the Allen Brain Atlas; and (6) spatiotemporal NB-GAM modeling of sequencing data capturing the dynamic patterns.

The images shown in Fig. 2d (now Fig. 2b) correspond to selected regions of interest outlined by dashed rectangles in Fig. 2b (now Fig. 2a). We have now revised the figure legend to more clearly indicate the data source and adjusted the placement of the rectangles in Fig. 2b (now Fig. 2a), following the reviewer's helpful suggestion below. The SATB2 has robust expression in cortical layers as shown in Extended Data Fig. 2c (now Extended Data Figs. 2-7).

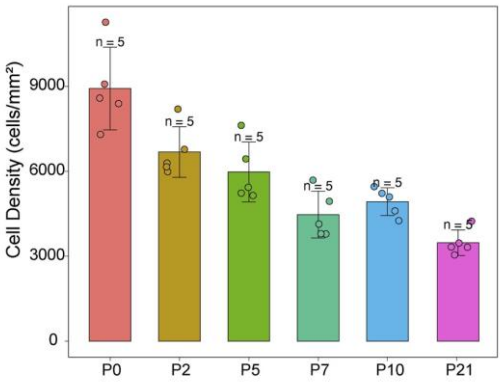

The relatively reduction of the signals of SATB2 and TBR1 in Fig. 2d (now Fig. 2b) for P21 may due to the use of uniform fluorescence intensity scaling across all developmental timepoints, which facilitates consistent visual comparison across ages. However, this visualization approach may underrepresent expression in later stages such as P21. This might because the brain volume becomes substantially larger and less densely packed during postnatal development (please see the cell density on the right), resulting in a lower local concentration of marker-positive cells. As a result, the overall visual signal appears weaker in the context of reduced cellular density.

Also for SATB2 in Fig 2d (now Fig. 2b), besides the reasons we mentioned above, the quality and size of the image might have also contributed to the weaker visualization. We have now improved the image quality to show the SATB2 and TBR1 in Fig. 2b (also provided below), with both showing sustained expression. This is consistent with the visualization of single-marker images (Extended Data Figs. 2-7). All raw CODEX data will be submitted to the public repository upon publication.

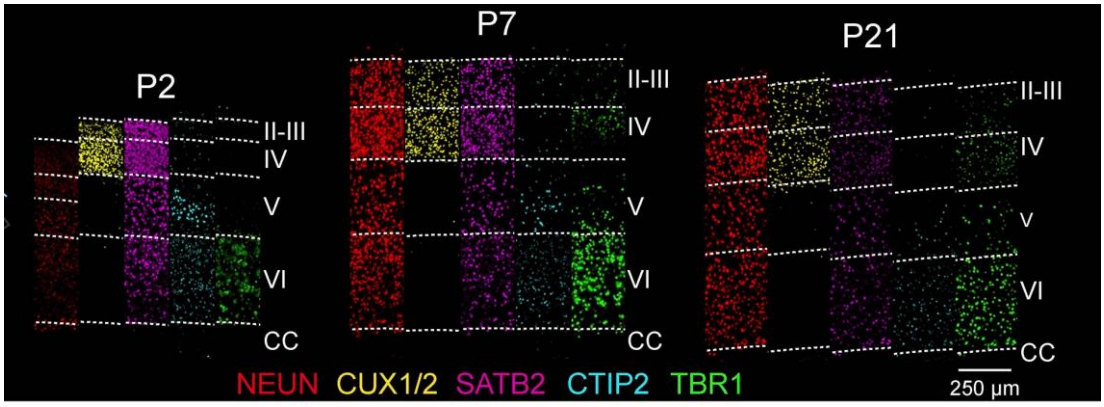

In addition, we examined the Allen Brain Atlas for RNA *in situ* hybridization (ISH) and processed expression data for *Satb2, Tbr1, Bcl11b* (CTIP2), and *Cux2* (also provided below). While comparisons between protein imaging and RNA ISH represent distinct modalities, they are generally expected to exhibit consistent developmental trends. Although the timepoints available in the Allen Brain Atlas do not precisely match ours, we observed similar patterns of decreased expression at P28, supporting the consistency of our findings. We did not include ISH data for *Rbfox3* (NEUN), as it is not available in the Allen Brain Atlas. We have now included the Allen Brain Atlas images below as Extended Data Fig. 11c.

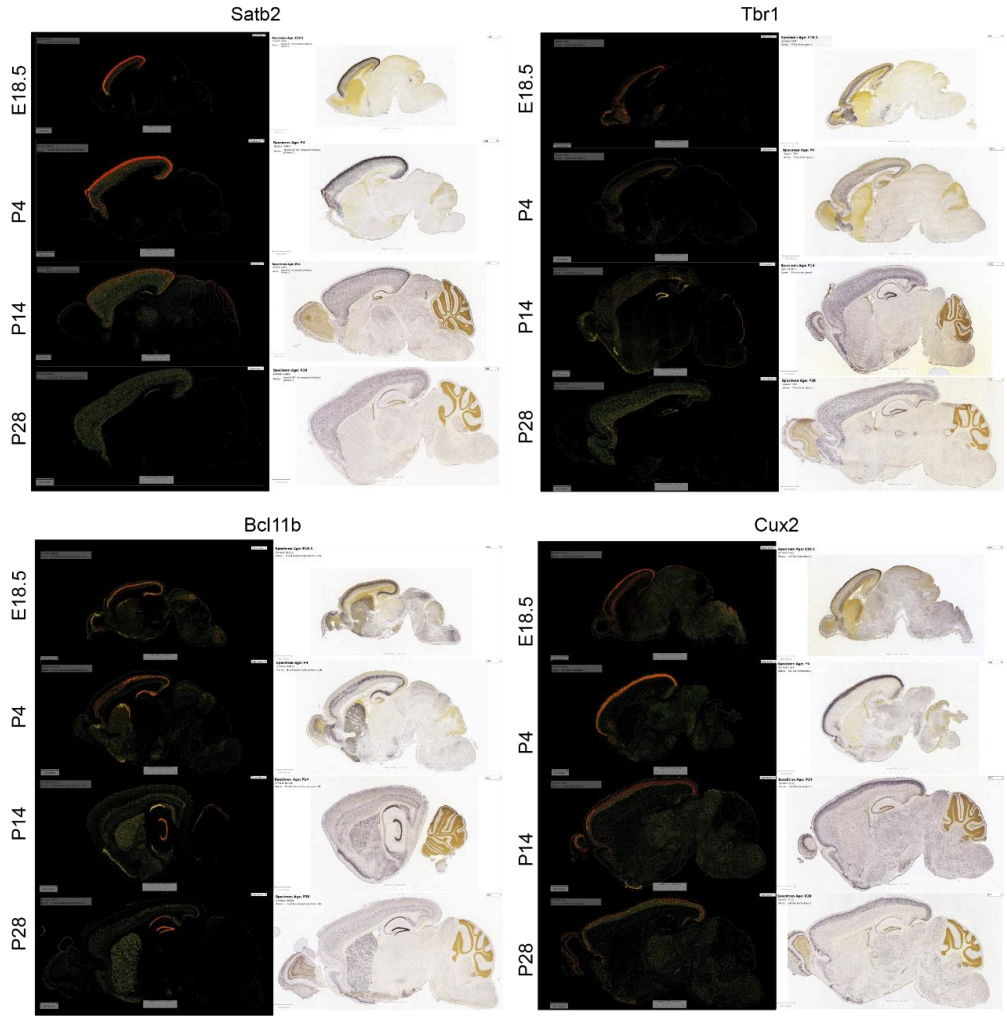

To check the CODEX results quantitatively, we also measured the per-cell fluorescence intensity across all developmental stages for the relevant neuronal markers from our mouse CODEX data (Extended Data Fig. 11a,b, please also see below) using the same methods as we described in our response to reviewer's previous comment. In general, this analysis revealed that while NEUN (*Rbfox3*) expression remained stable with a slight increase over development, other markers, including SATB2, CTIP2 (*Bcl11b*), TBR1, and CUX1/2, exhibited temporal variation, all showing lower per-cell signal intensity at P21 compared to P0.

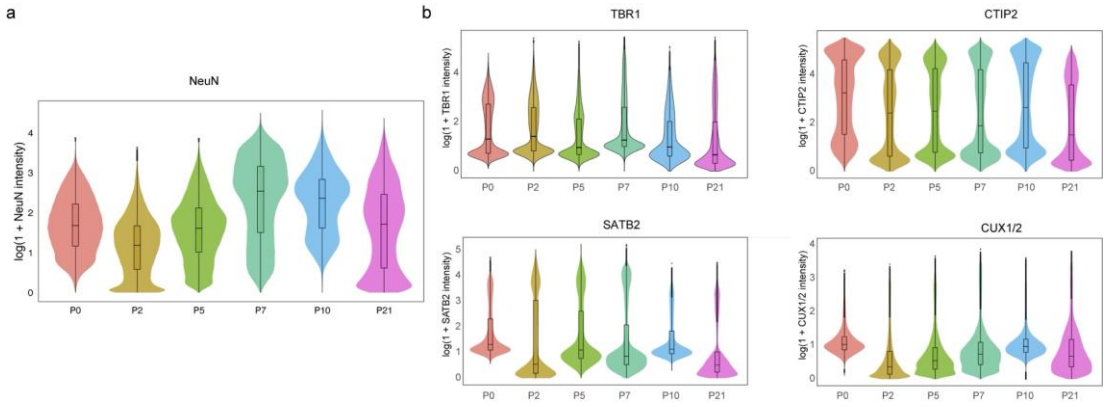

Furthermore, we also analyzed our spatial transcriptomic data from spatial ARP-seq, which provides an independent measure of gene expression across space and developmental time. The RNA-level trends for these TFs are consistent with the protein-level results, further supporting the biological validity of our observations (please see the results below).

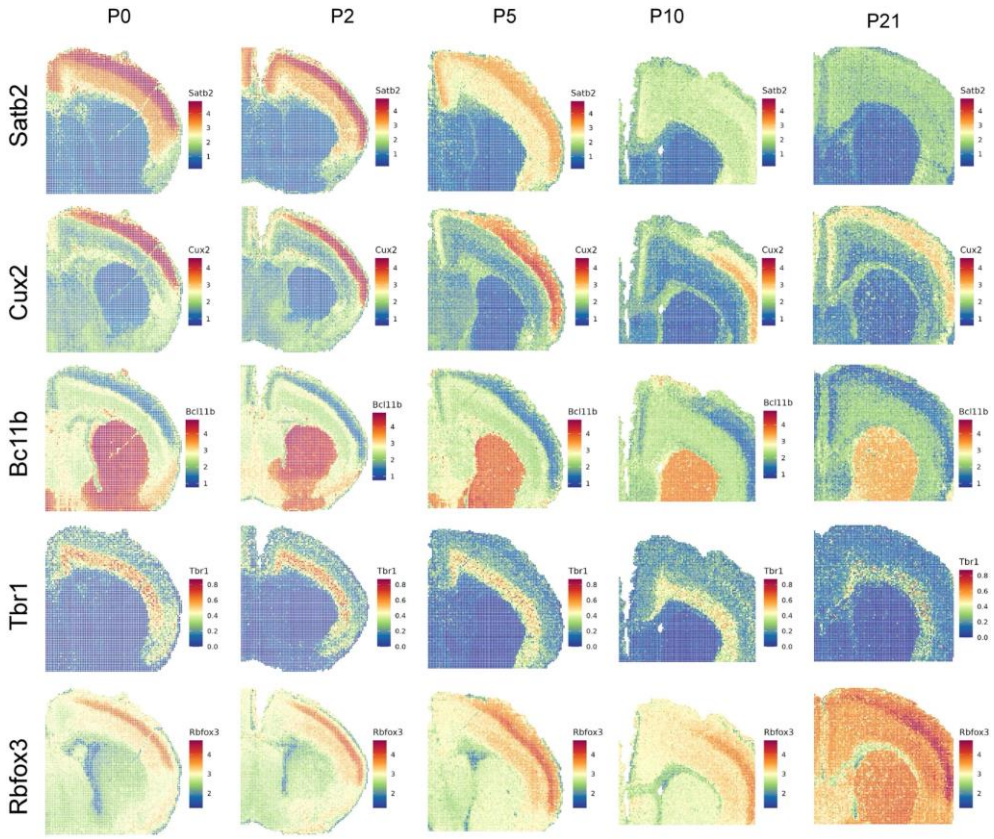

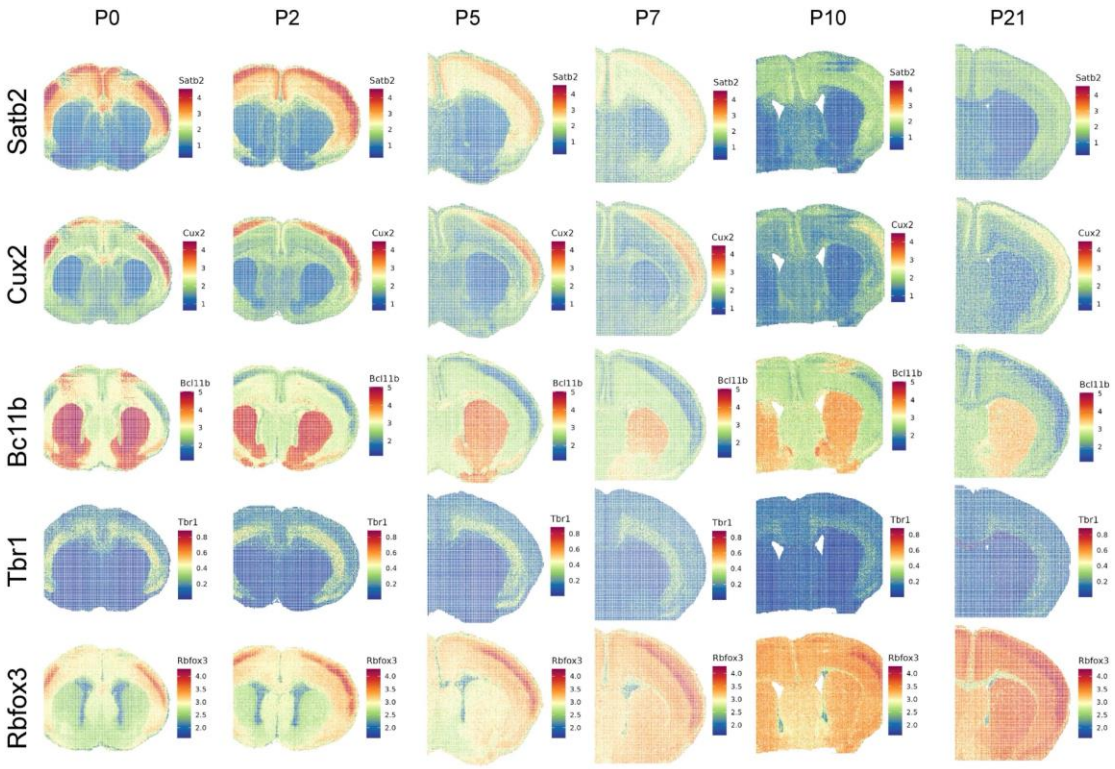

In addition to the gene expression, we also performed generalized additive model (GAM) fitting on the DBiT spatial transcriptomic data to quantify spatiotemporal expression trends of cortical layer-defining transcription factors. This analysis allowed us to decompose gene expression into smooth components associated with spatial delineation (across cortical layers II–VI), developmental time (P0–P21), and their interaction. The fitted models confirmed that these layer-specific markers (e.g., *Satb2*, *Cux2*, *Bcl11b*, and *Tbr1*) exhibit temporal decline in expression (please see the results below), while maintaining spatial localization to appropriate layers, consistent with our observations at the protein level.

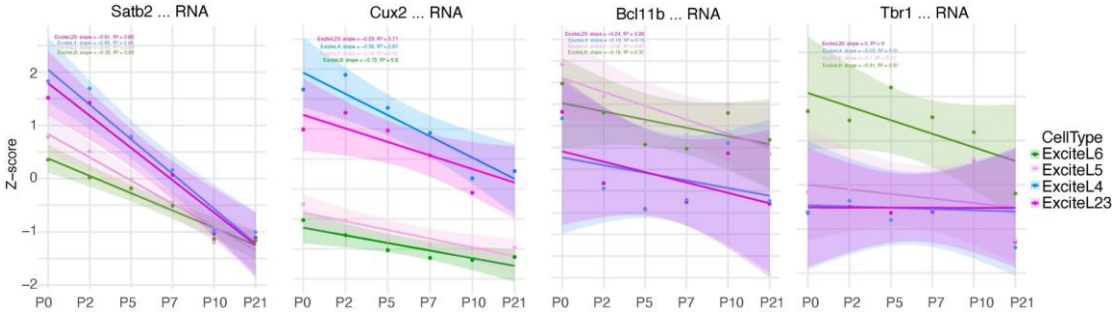

We have now also revised the main text (originally on Page 5, Line 10-12 and Line 38-40) in the manuscript and included the updated wording below. For the mouse brain lines, we now state "*While these layer-defining transcription factors (CUX1/2, CTIP2, and SATB2) were expressed at P21, their protein expression and cellular density of cells expressing these markers was reduced compared to early postnatal stages (Figs. 1b,2a,b and Extended Data Figs. 2-7 and 11), consistent to in situ hybridization staining in the Allen Brain Atlas*."

For the human brain lines, we have added "*Nevertheless, correcting for the cellular density between the different time points indicates that there might in contrast an expansion of these domains, consistent with an increase in brain volume during these stages in development*."

- Fig 1b: the P5 brain seems to have overall diminished signals compared to others – is this biological or technical?

Response: We thank the reviewer for the comment. The staining in Fig. 1b, including P5 mouse brain, was performed using the commercial CODEX platform (Akoya Biosciences), following the manufacturer's standard protocol. We have now increased the resolution of the image in Fig. 1b, which has improved the visualization of the P5 mouse brain. We have now also included a replicate for the P5 mouse brain in Fig. 1b, with two replicates presented side-by-side (please also see below). We did not observe a notable reduction in signal between the two replicates. To ease with visualization of CODEX images, we have provided higher magnification images in Extended Data Figs. 2-9.

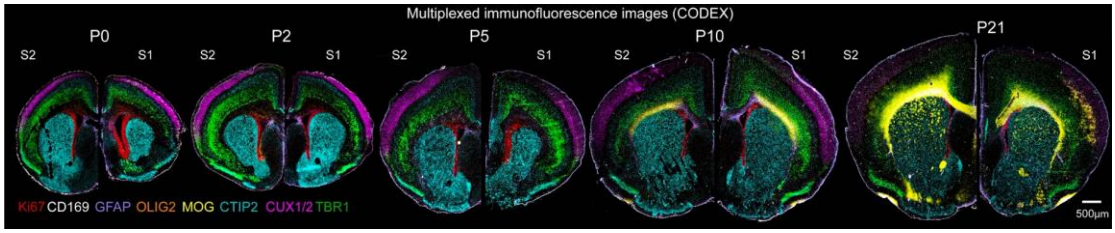

- How many replicates are in each age, how are the data quantified to account for batch effects and technical biases, what are the internal controls, and have these been validated using alternative methods or datasets?

Response: We thank the reviewer for the comments. In the original manuscript, we generated two spatial ARP-seq (renamed from DBiT ARP-seq per Reviewer 1 suggestion in the "Minor" section) replicates per time point (P0, P2, P5, P10, and P21) using a 100 × 100 barcode device with 20 μm pixel size. During the revision, we generated a new set of spatial ARP-seq datasets covering developmental mouse brains from P0 to P21 (P0, P2, P5, P7, P10, and P21). These datasets were generated using newly designed high-resolution DBiT chips featuring 220×220 barcodes and 15 μm pixel size. The application of the new chips allowed us to capture almost the entire hemisphere of the mouse brain. In addition, an additional developmental time point (P7) was included during the revision to improve temporal resolution. We have now included **Extended Data Tables 7,8,9** (also provided below), which summarizes the sample information, including section-to-section distances between spatial sequencing and CODEX across developmental and disease stages of the mouse and human brain.

Extended Data Table 7. Summary of mouse sample information for spatial ARP-seq and CODEX.

Samples		Spatial ARP-seq		CODEX	Sex	Spatial adjacency between spatial ARP-seq and CODEX	
		Sample name	# of barcodes	Sample name		Yes/No	Section distance
P0	Rep 1	P0_S1	100x100	P0_S1	N/A	No	N/A
	Rep 2	P0_S2	220x220	P0_S2	N/A	Yes	0 μm
	Rep 3	P0_S3	100x100		N/A		
	Rep 4	P0_S4	100x100		N/A		
P2	Rep 1	P2_S1	100x100	P2_S1	N/A	Yes	10 μm
	Rep 2	P2_S2	220x220	P2_S2	N/A	Yes	0 μm
	Rep 3	P2_S3	100x100		N/A		
P5	Rep 1	P5_S1	100x100	P5_S1	N/A	Yes	10 μm
	Rep 2	P5_S2	220x220	P5_S2	N/A	No	N/A
	Rep 3	P5_S3	100x100		N/A		
P7		P7_S2	220x220	P7	N/A	No	N/A
P10	Rep 1	P10_S1	100x100	P10_S1	N/A	Yes	20 μm
	Rep 2	P10_S2	220x220	P10_S2	N/A	No	N/A
	Rep 3	P10_S3	100x100		N/A	No	N/A
P21	Rep 1	P21_S1	100x100	P21_S1	M	No	N/A
	Rep 2	P21_S2	220x220	P21_S2	M	Yes	20 μm
	Rep 3	P22_S3	100x100		M		
5DPL	Rep 1	5DPL_S1	100x100	5DPL_S1	F	Yes	10 μm
	Rep 2	5DPL_S2	100x100	5DPL_S2	F	Yes	10 μm
10DPL	Rep 1	10DPL_S1	100x100	10DPL_S1	F	Yes	0 μm
	Rep 2	10DPL_S2	100x100	10DPL_S2	F	Yes	0 μm
21DPL	Rep 1	21DPL_S1	100x100	21DPL_S1	F	Yes	10 μm
	Rep 2	21DPL_S2	100x100	21DPL_S2	M	Yes	10 μm

Extended Data Table 8. Summary of mouse sample information for spatial CTRP-seq and CODEX.

Samples		Spatial ARP-seq		CODEX	Sex	Spatial adjacency between spatial ARP-seq and CODEX	
		Sample name	# of barcodes	Sample name		Yes/No	Section distance
5DPL	Rep 1	5DPL_S1	100x100	5DPL_S1	F	Yes	0 μm
	Rep 2	5DPL_S2	100x100	5DPL_S2	F	Yes	0 μm
21DPL	Rep 1	21DPL_S1	100x100	21DPL_S1	F	Yes	0 μm
	Rep 2	21DPL_S2	100x100	21DPL_S2	M	Yes	0 μm

Extended Data Table 9. Summary of human sample information for spatial ARP-seq and CODEX.

Samples	Spatial ARP-seq	Sex	Spatial adjacency between spatial ARP-seq and CODEX	
	# of barcodes		Yes/No	Section distance
Second trimester	100x100	N/A	Yes	30 μm
Third trimester	100x100	F	Yes	20 μm
Infancy	100x100	F	Yes	N/A

For consistency between batches and samples, we conducted reproducibility assessments across all biological replicates, please see the results mentioned above. In addition, to address potential technical variation and sample heterogeneity across developmental stages and experimental batches, we applied a series of robust data integration and normalization procedures at each analysis level. These steps were designed to ensure reliable spatial and temporal comparisons across all replicates and modalities.

For the spatial RNA data, raw count matrices were first processed using Seurat v4.1. We normalized gene expression data and performed scaling, followed by principal component analysis (PCA). To account for batch effects and regional heterogeneity between samples, we applied the Harmony algorithm for integration, using the top 50 PCs. This enabled joint analysis across multiple biological replicates while preserving developmental and spatial structure. Following this, we performed clustering and extracted spatial domain annotations to support downstream analyses.

For the spatial ATAC data, we constructed a unified peak set across samples using the GenomicRanges package. Fragment files from each sample were processed into peak-by-cell matrices, which were then merged. To integrate multiple datasets and correct for batch effects, we used latent semantic indexing (LSI) followed by the *FindIntegrationAnchors()* function (with LSI as the reduction method), facilitating cross-sample comparison.

For multi-modal integration, we used the SpatialGlue (Long *et al.*, *Nat. Methods*, 2024) pipeline to align ATAC and RNA data, deriving spatial domains consistent across modalities. These spatial domains were subsequently used to guide downstream integration in ArchR. For each modality (RNA, ATAC, and CUT&Tag), we performed using the *addImputeWeights()* function in ArchR, which improves signal robustness and facilitates consistent spatial registration across datasets.

To quantitatively evaluate the spatiotemporal patterns of gene expression and chromatin accessibility, we developed a customized negative binomial generalized additive model (NB-GAM) framework. Importantly, this modeling approach is implemented independently of the nearest-neighbor smoothing used in ArchR and is specifically designed to identify statistically significant spatial, temporal, and spatiotemporal effects in both RNA expression and ATAC-based gene activity scores. This framework allows us to rigorously assess regulatory dynamics beyond qualitative visualization. Notably, we did not limit our analysis to genes commonly present in both RNA and ATAC datasets. Instead, we first used FigR to identify peak-to-gene linkages, thereby selecting genes that are likely to be functionally associated with nearby regulatory regions. These genes were then subjected to NB-GAM fitting for downstream statistical analysis.

Together, these preprocessing, integration, and modeling steps mitigate batch effects and enhance the reproducibility of observed biological patterns across datasets. Details of these computational steps have been added to the Methods section. Our data also showed consistency with the Allen ISH Data as we provided in our previous response.

- Why does the GFAP signal closely resemble the meningeal lining (ExFig 2c), which is not its expected pattern - is this due to antibody artifacts?

Response: We thank the reviewer for this observation. The GFAP signal indeed appears enriched along the meningeal lining in the images that we have for CODEX when the entire tissue is shown (Fig. 1b). We have now included higher magnification images in extended data figures of all of the main CODEX figures to help with the ease of viewing and provide extra material for this multiplex protein panel (Extended Data Figs. 2-7). The observation is indeed correct that the GFAP signal is enriched along this border in the subpial parenchyma (see CODEX image on the right; P0 CTX, P0 HY, P14 CTX and P14 HY). Here we include images of the subpial area of the hypothalamus due to the invagination of the parenchymal tissue that preserves the meningeal barrier (Labeled HY) well in this region. Additional images (P0 CTX and P14 CTX) of the cortical meninges are also provided. Upon further investigation, we found that this localization is stable throughout our postnatal samples, so we have included images of P0 (left) and P14 (right; not included in manuscript) with additional stains to mark the meningeal border (PDGFRα), vasculature (CD31), and resident meningeal macrophages (CD169). It is notable that in the provided images, the GFAP signal is cellular and consistent with expected astrocyte morphology. GFAP+ astrocytes have recently been better characterized and have become an established component of the glial limitans (specifically the glial limitans superficialis), forming the end foot structure (Hasel et al. 2025. Cell Reports), in accordance with previous studies (Nakazawa and Ishikawa. 1998. J. Neurocytology, and Ramón y Cajal.

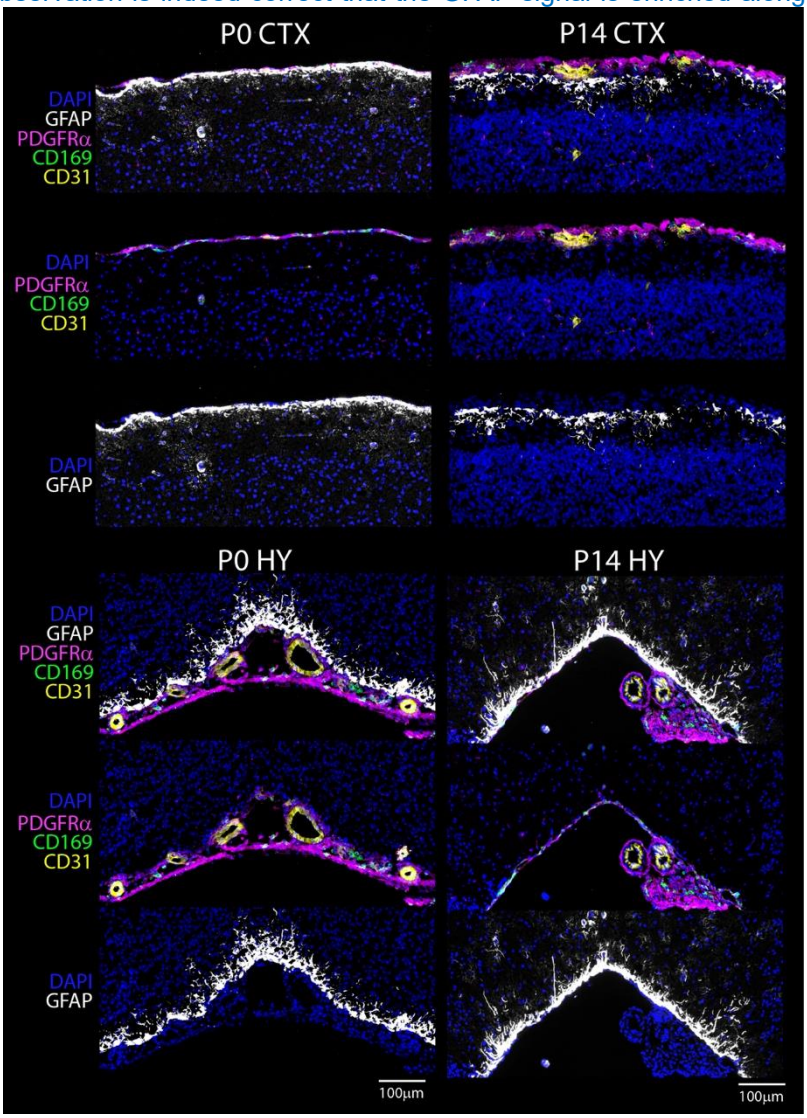

1904. Textura del Sistema Nervioso del Hombre y de los Vertebrados). Our CODEX staining for this structure is consistent with images and descriptions of this astrocyte subtype (See below Bottom figure panel D; Hasel et al. 2025). Finally, we have edited the manuscript to specify that the GFAP near the border is in the glial limitans.

[REDACTED FIGURE]

- The anatomical definition of a cortical column should be from pia to the white matter within a defined cortical region (SS or MO) – unlike the irregular boxes in Fig 2b or 2c. We know that TF expression varies greatly across cortical regions and any quantification should be done rigorously.

Response: We thank the reviewer for bringing this to our attention. We fully agree that rigorous anatomical definitions are essential. In the original manuscript, our aim was to provide zoomed-in views of cortical layers for visualization purposes, rather than conduct quantification from those regions. Following the reviewer's helpful suggestion, we have now revised Fig. 2a and 2b (now) accordingly. To better capture a cortical region with layer IV, we focused on the primary somatosensory area of the SSp-m region. Using the Allen Brain Atlas as a reference, we selected the entire region, as depicted in Fig. 2a, then rotated the region of interest and drew a vertical rectangle covering all of the layers (Fig. 2b, please also see below).

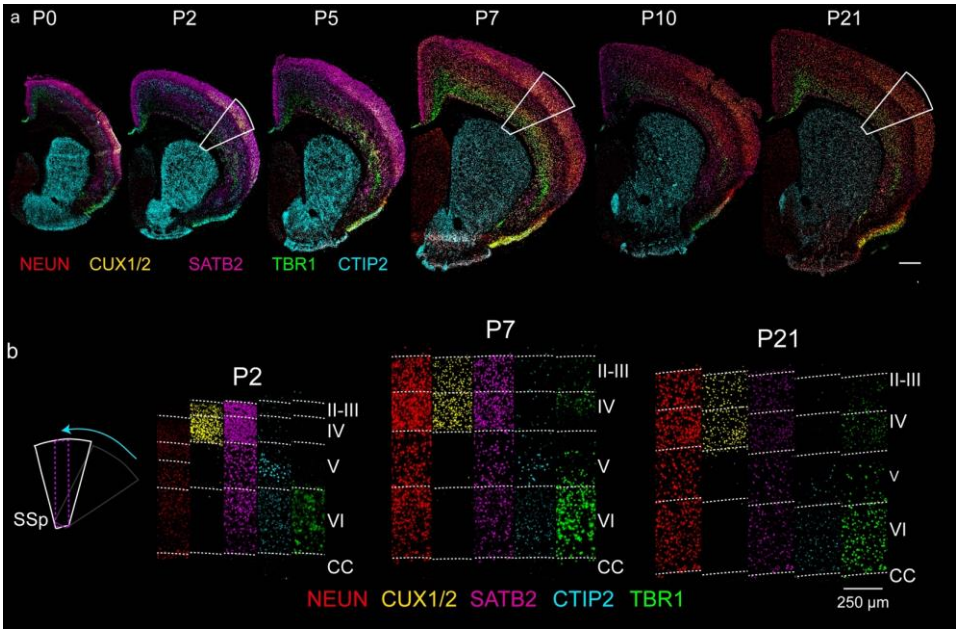

3. The same sentiment applied to Fig 3 related to the myelination pattern, forming laterally to medial corpus callosum in development. It is another surprising finding, but only from one replicate at P10. A quick check on the Allen ISH atlas also does not seem to support this claim – more replicates and validations are required.

Response: We thank the reviewer for the comments. Following the reviewer's suggestion, we have now generated an additional set of replicates, resulting in three biological replicates of spatial ARP-seq (Fig. 1e-i and Extended Data Figs.19-22) and two biological replicates of CODEX imaging (Fig. 1b and Extended Data Figs. 2-8). We first validated the expression for myelination markers *Mbp* and *Mog* on both sequencing and CODEX imaging data (please see figures below). The observation of lateral myelination pattern at P10 was consistent across all datasets.

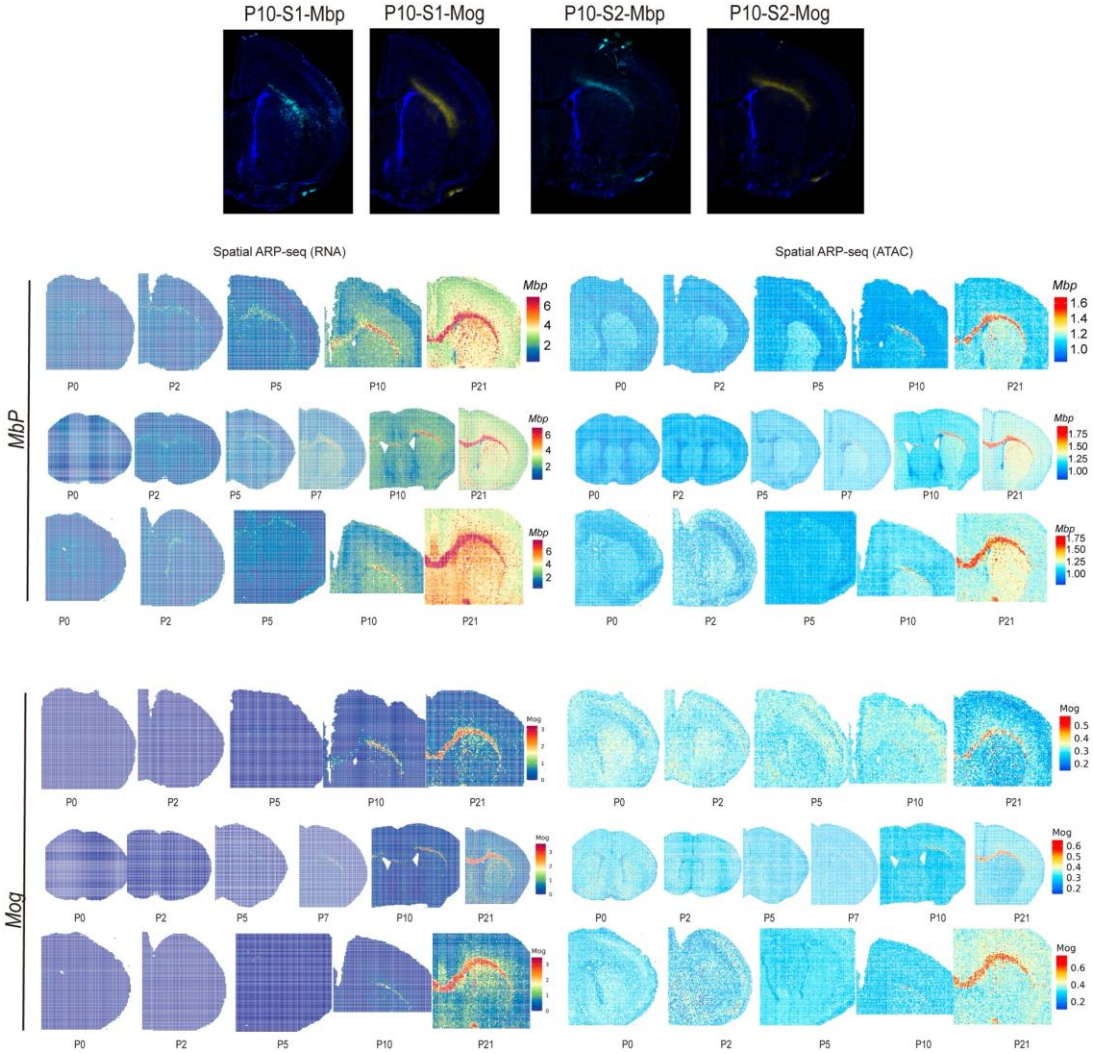

To systematically assess this spatial dynamic, we partitioned the corpus callosum into ten bins from medial to lateral and reconstructed regional RNA and ATAC signals across six developmental timepoints (P0-P21). This approach revealed that myelination-associated gene programs (R6-A4), including *Mbp*, *Mog*, *Mag*, and *Mobp*, first appeared at the lateral corpus callosum at P10 and expanded medially to cover the whole corpus callosum by P21 (Fig. 3g–h and Extended Data Figs. 39-43, please also see below).

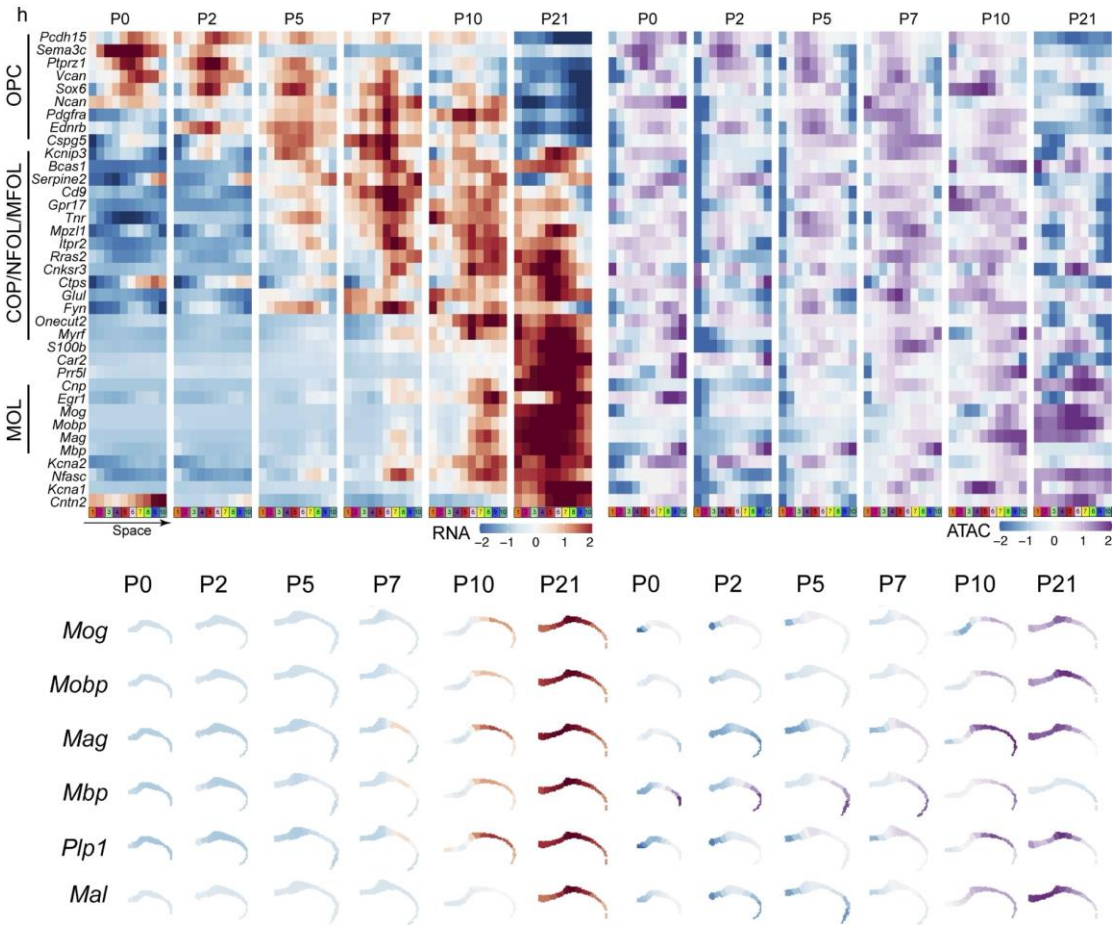

These results were further supported by spatial cell-type annotations from RNA data (please see image below).

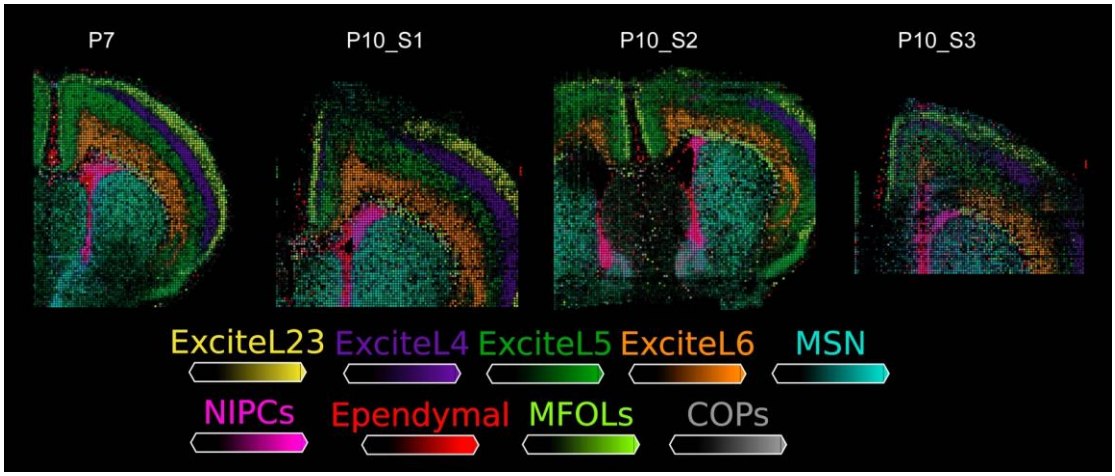

In addition, to provide orthogonal validation, we performed retrograde-AAV-eGFP tracing experiments to selectively label callosal projection neurons (CPNs) and corticothalamic projection neurons (CThPNs). We found that the CThPN tract, localized to the lateral corpus callosum (CC), showed strong co-localization with MBP staining at P10, whereas CPN axons in the medial CC showed little to no MBP signal at the same timepoint (new **Fig. 3i-k**, please also see below). This indicates that lateral tracts undergo earlier myelination, consistent with our spatial multi-omics data. Besides, we performed

quantitative analysis of MBP protein intensity across the medial–lateral axis of the CC, showing a steep increase in MBP signal around bin 6-8, corresponding to the cingulum bundle—precisely where the lateral tracts exit the corpus callosum and where we observed a transition zone in both gene and protein expression patterns (**Fig. 3l-n**).

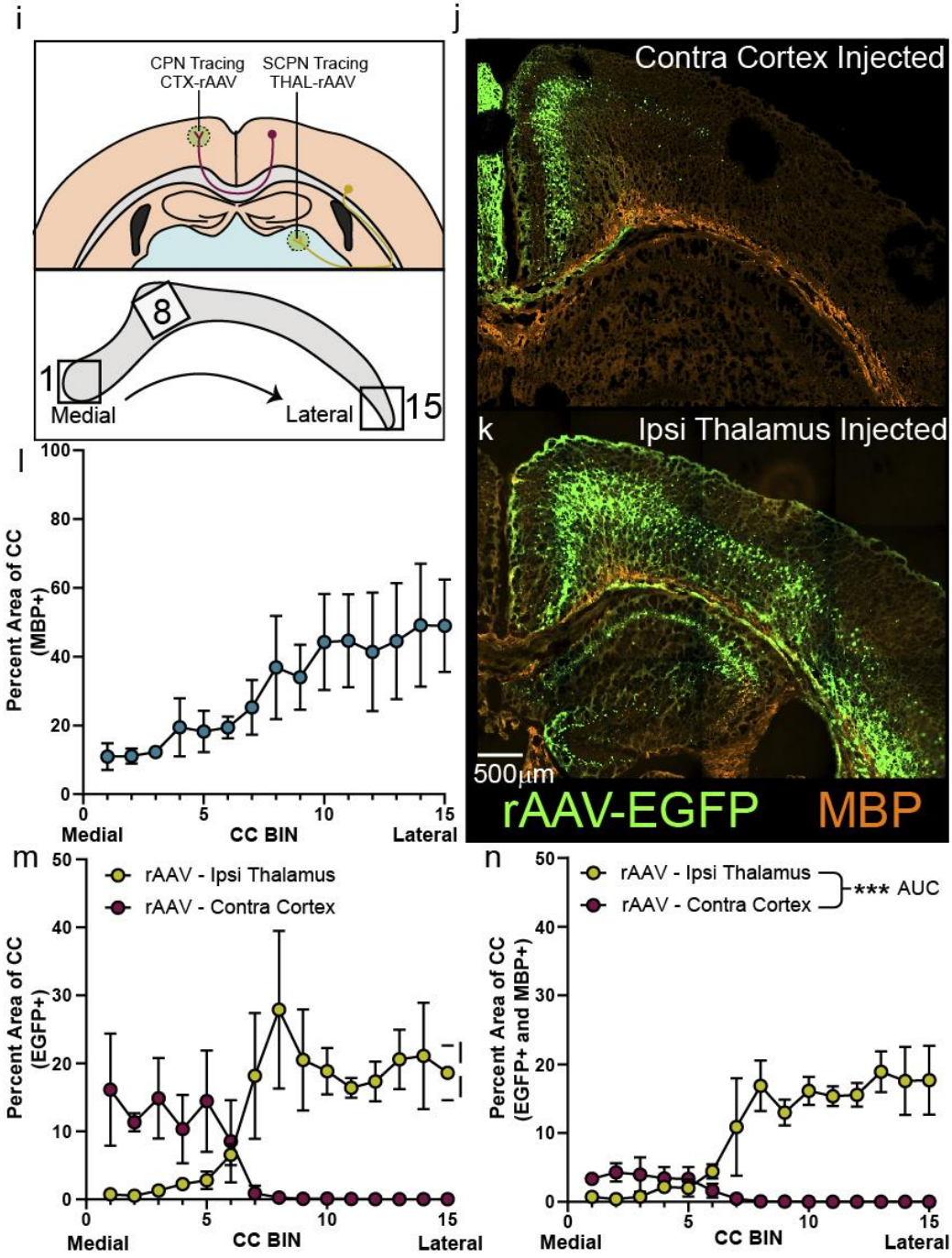

Regarding the Allen Brain Atlas reference, we appreciate that the ISH resource offers valuable spatial information. However, to the best of our knowledge, ISH data for *Mbp* and other myelin-associated genes are available at P56 (adult stage) for coronal sections, and at P4, P14, P28, P56, and later stages for sagittal sections. In our data, we showed the lateral part of myelination at P10 from coronal sections first occurring in the region of the corpus callosum that resides directly below the somatosensory cortex as early as P7 (MBP only) and P10 (MBP and MOG) (Fig. 3a and Extended Data Figs. 2-7). Interestingly,

the developmental progression shown in the Allen ISH data, such as sparse *Mbp* expression at P4 and strong expression by P14, appears generally consistent with our interpretation that P10 represents a transitional stage during myelination.

Moreover, as reviewer 3 mentions, the pattern of myelination in the developing mouse corpus callosum has been reported through histological methods, including MBP immunostaining, Luxol Fast Blue myelin staining, and electron microscopy (Sturrock 1980 and Vincze et al., 2008). Accordingly, we see an identical area of the corpus callosum (sub somatosensory to the cingulum) first being myelinated as what was reported previously at P10 (Vincze et al. 2008) (see images C and E below). We have now added this referenced observation to our manuscript.

[REDACTED FIGURE]

Nevertheless, our spatial data go beyond histology, with findings derived from chromatin accessibility, RNA, and protein. These data not only recapitulate the reported anatomical patterns of myelination but also uncover molecular features underlying this process. Specifically, transcriptional dynamics across spatial bins confirmed a lateral-to-medial progression of key myelination genes (e.g., *Mbp, Mog*), consistent with prior histological observations (Fig. 3, please also see below). Importantly, our spatial chromatin accessibility data revealed chromatin priming in oligodendrocyte-lineage cells prior to detectable RNA and protein expression, indicating that molecular commitment to myelination precedes

histological detection (Fig. 3). This regulatory insight, inaccessible by conventional histological methods, provides molecular-level validation and mechanistic context for the spatial progression of myelination, confirming that myelination is tightly regulated both spatially and temporally across modalities. We consider that the added molecular resolution provides novel insights into the regulatory architecture and temporal coordination of neurodevelopment, beyond what has previously been demonstrated. Our strategic analysis and our rich multimodal dataset enabled our model suggesting that the observed pattern might be related with the timing of myelination of neurons from different cortical layers.

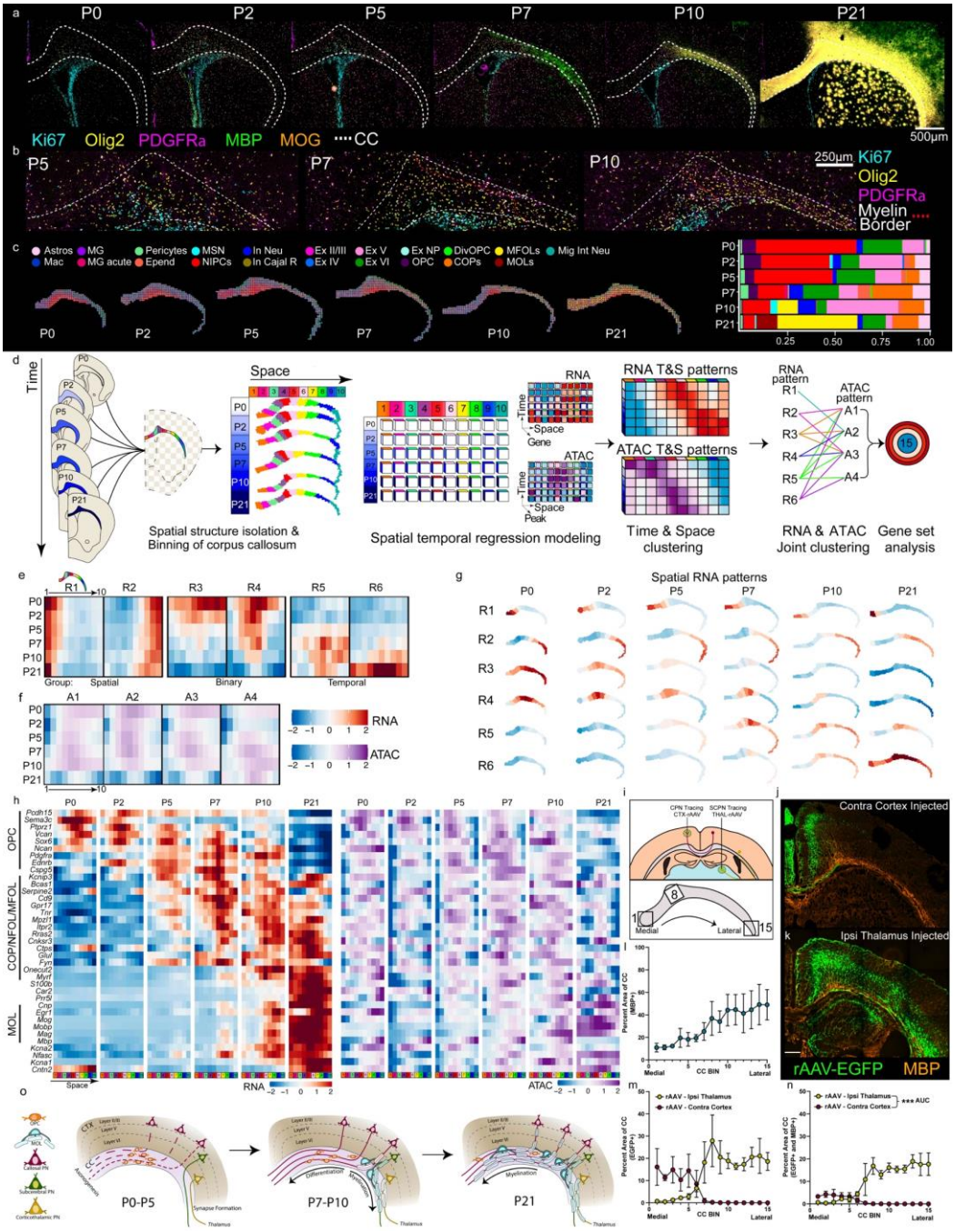

Fig. 3: Spatiotemporal dynamics of the mouse corpus callosum during development and myelination. da, CODEX images of the mouse brain corpus callosum from P0 to P21. Scale bar, 500 μm. **b,** Zoomed-in CODEX images of the medial corpus callosum regions in **a** from P5, P7, and P10, respectively, showing staining for OLIG2, PDGFRα, and Ki67. **c,** Decomposition and pie chart visualization of cell types in corpus callosum (S2) from the spatial RNA data. **,** Schematic representation of spatial

temporal regression model on mouse brain corpus callosum from P0 to P21. **e,** Heatmaps of the 6 RNA clusters generated from the regression model. **f,** Heatmaps of the 4 ATAC clusters generated from the regression model. **g,** Spatial RNA patterns for RNA clusters (R1-R6) from the regression model. **h,** The RNA gene expression calculated on the basis of the regression model for specific genes. **i,** Schematic illustration of the injection sites and tracing pathways for CPN and CThPN (top) using retro-AAV-eGFP at the terminal location for both tracts separately. Segmentation strategy using confocal imaging at high magnification (40x) for MBP staining and retro-AAV-eGFP labeling quantification throughout the corpus callosum (bottom). **j,** Confocal images (20x) stitched together to capture the corpus callosum and overlying cortex of one hemisphere for CPN tracing in P10 mouse after retro-AAV-eGFP injection at P1. Representative retro-AAV-eGFP tracing from the contralateral cortical layer II/III injected terminal. **k,** Representative Retro-AAV-eGFP tracing from the ipsilateral thalamic injected terminal. **l,** Percent area of MBP staining per bin across the defined corpus callosum in each image moving medial to lateral (n=6; 3 CPN traced + 3 CThPN traced). **m,** Percent area of retro-AAV-eGFP labeled axons of the area of corpus collosum defined per image. **n,** Percent area of co-labeled MBP and retro-AAV-eGFP labeled axons of the area of corpus collosum defined per image (n=3 CPN traced and n=3 CThPN traced). Significance was determined by calculating the area under the curve then running a two-tailed, unpaired t-test (P value = 0.0001) on the mean total area values (CTX: 18.79 and Thalamus: 143.2) with the standard error values (CTX: 2.770 and Thalamus: 7.942) that were derived from the area under the curve statistics. CTX: cortex, THAL: Thalamus. **o,** Descriptive model summarizing how myelination progresses in the corpus callosum and cerebral cortex.

We have now revised the main text and figure legend to clarify that these findings are supported by multiple biological replicates and different methods. We sincerely appreciate the reviewer's suggestion, which has helped us improve the clarity of this conclusion.

4. The authors demonstrated that microglia were activated at the core and distal locations of the lesion. However, looking at the data in Fig 5e, the activation marker does not seem expressed at the 'core' of the lesion?

Response: We thank the reviewer for the comments. The activation marker signal in the lesion core appears relatively weaker in the original Fig. 5e, which may be due to the limited spatial resolution of the original image. We have now provided high-resolution images of the same region in the revised Fig. 5i (Extended Data Fig. 53 and please also see below), which clearly shows the presence of activation marker within the core area. These higher-resolution images support our conclusion that microglial activation occurs both at the lesion core and in distal regions.

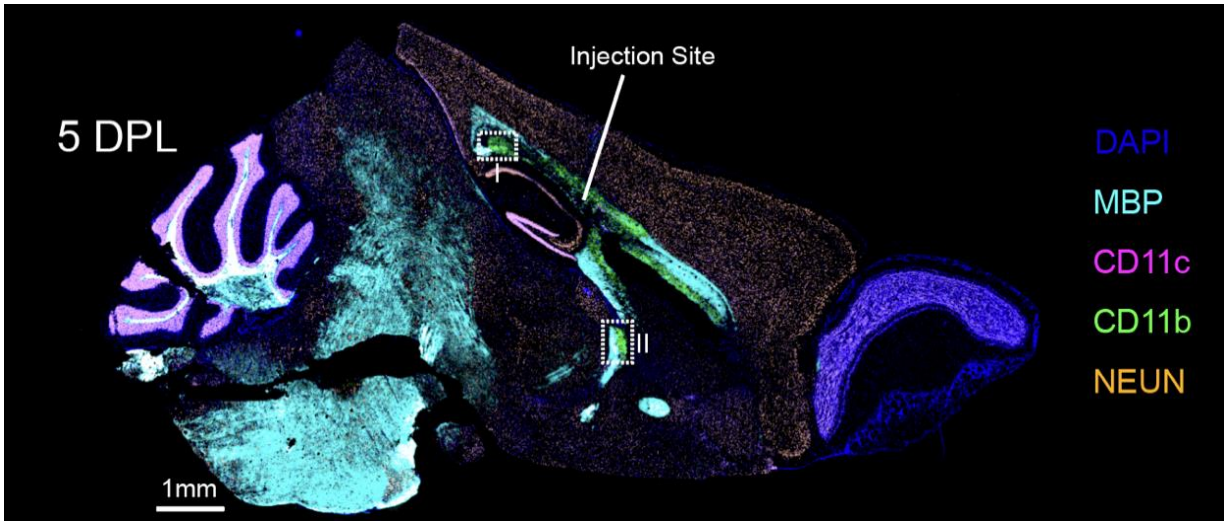

5. Quantitative data for chromatin, RNA, and protein mapping should be included in all figures. On page 17 Lines 13-16, the authors claim there is a divergence in chromatin accessibility and RNA expression for genes Itgax and Itgam based on data in ExFig 25. The qualitative images shown do not appear to support this conclusion.

Response: We thank the reviewer for the comments. We agree that quantitative representation is important. Following the reviewer's suggestion, we have now presented our data in a format that allows for quantitative interpretation, as detailed below. We have systematically updated all spatial expression and chromatin accessibility figures, both in the main and extended data figures (such as Extended Data Figs. 49-51), to include gene-specific scale bars. These scale bars reflect min–max normalized expression/accessibility values computed across the entire spatiotemporal dataset (i.e., all biological replicates and timepoints). This ensures that the visualized intensity corresponds to a consistent and quantitative range for each gene. These updates have now been applied to all genes presented, not only *Itgax* and *Itgam*, and allow for accurate cross-timepoint interpretation within each gene. These changes have been implemented in the revised figures.

In the original manuscript, we included a statement suggesting that *Itgax* and *Itgam* displayed divergent spatial patterns across RNA and ATAC modalities. This interpretation was initially based on preliminary spatial trends observed during exploratory analysis. To further evaluate this point, we performed a quantitative cross-modality correlation analysis by calculating pairwise Pearson correlation coefficients between RNA, ATAC, and protein signals across spatiotemporal samples. As shown in the figures below, the correlations among the three modalities for *Itgax* and *Itgam* were indeed low. Given the low signal intensity across samples, in the revised manuscript, we have removed the sentence that previously claimed a divergence in these genes' spatial dynamics in the revised manuscript.

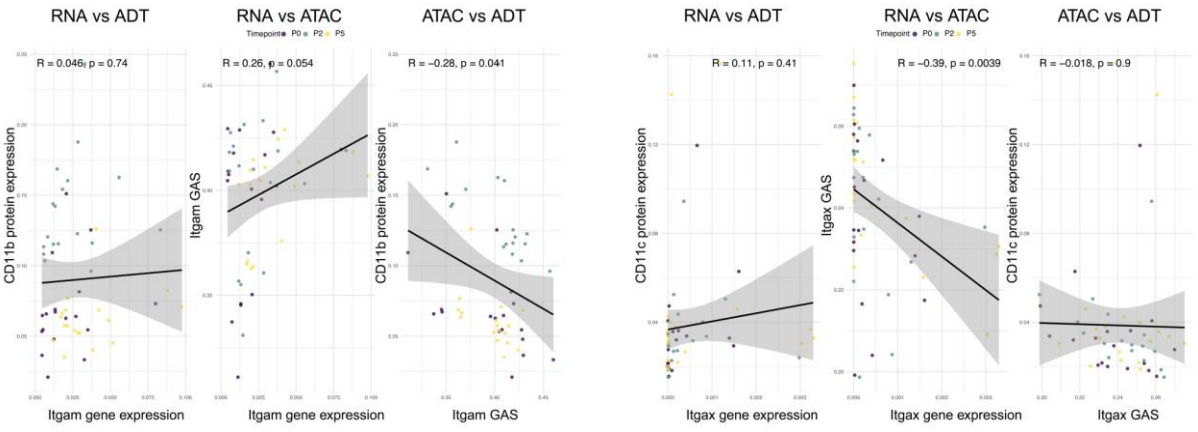

In addition to spatial maps for the genes, we also present heatmaps (e.g., Fig. 2e,f and similar panels) that depict gene expression or chromatin accessibility trends across cortical layers and corpus callosum at various developmental stages. These heatmaps are not based on raw values or direct measurements, but instead are derived from generalized additive model (GAM) that we use to model spatial and temporal expression dynamics. Specifically, each gene was modeled independently using a negative binomial generalized additive model (NB-GAM) incorporating temporal, spatial, and interaction smooth terms. Predicted values were extracted at each spatiotemporal bin (e.g., layer x timepoint) and either

displayed directly as model-predicted values or summarized as z-scores of the smooth terms. The heatmaps shown in Fig. 2h reflect these model outputs, which were normalized to ensure visual consistency across genes and conditions. These outputs were intended to illustrate general patterns of expression or accessibility over time and space, the genes included in the figures were selected based on stringent model criteria, with significant smooth terms (FDR < 0.01) and acceptable model fit (e.g., adjusted $R^2 > 0.025$), to ensure biological relevance and interpretability.

6. How immune cells respond to brain injury is an important question. Given the unique spatial data, the authors may want to investigate microglia diversity within the lesion environment and benchmark the findings with existing single-cell studies (Hammond et al 2019 and many more). It would be critical to know if DBiT APR-seq recapitulates similar microglia subtypes in lesions as single-cell sequencing. Moreover, authors can capitalize the cell type-specific RNA and ATAC data, for example, to identify the different and shared RNA and ATAC patterns between disease-associated microglia (DAM) and axon tract-associated microglia (TAM) on how microglia respond to injury.

Response: We thank the reviewer for these comments. To address them, we have added additional time points of the lysolecithin (LPC) mouse model, in particular 10 days post lesion (n=2, coronal sections), resulting in 3 stages of demyelination/remyelination process (5 DPL, 10 DPL, and 21 DPL), all profiled with both spatial ARP-seq and CODEX. To understand the distal microglia/macrophage properties in the context of lesional microglia responses to demyelination, we employed a stepwise strategy to (1) dissect the primary lesion and distal general compartments; (2) selection of microglia specific pixels, positive for *P2ry12, Tmem119,* and *Cx3cr*1; and (3) perform a deeper investigation into the microglia occupying these different compartments (new Fig. 6a-c, please see below **Fig. 6**). We performed unsupervised clustering with joint ATAC and RNA data on the lesion-like compartments and segregated 5 distinct compartments (new Fig. 6e). Protein analysis and GO analysis for the RNA and ATC component suggested differentially phased immune responses in the primary lesion site when compared to the distal white matter (WM) site. To further investigate the primary lesion and distal WM inflammation, we performed microglia subclustering on microglia-specific pixels (positive for *P2ry12, Tmem119*, and *Cx3cr*1), and for the remaining pixels, we assigned cell identities across the primary lesion and distal WM (new Fig. 6h and Extended Data Figs. 53 and 54). We also determined with their likely identity using module scoring comparing gene sets from previously published data by Androvic and colleagues and Hammond and colleagues. We found that all the Androvic microglia clusters (foamy, interferon-responsive, and disease-associated microglia) and Hammond microglia (axon tract-associated, disease-associated, and injury-responsive) were predicted in our RNA data set to a higher extent in the primary lesion at 10 DPL, with reduced prediction in the distal WM (new Fig. 6i and Extended Data Figs. 54c,d and 55a). However, in one of the replicates (S1), the ATAC module prediction was higher in the distal WM, while in the other (S2) the differences in both RNA and ATAC between primary lesion and distal WM were not as striking, suggesting that the inflammation in this area is still evolving. Moreover, the Hammond injury-responsive module was predicted to be enriched in the distal WM lesion-like compartment rather than in the primary lesion core (new Extended Data Fig. 54c,d and 55a). Our data suggested that differential signaling and cellular interactions might occur specifically in primary and distal lesions at 5 DPL and 10 DPL. To investigate this possibility, we performed CellChat

analysis, predicting the overall cellular interactions that were happening across these time points and determine which cells were communicating with our differential microglia clusters (new Fig. 6l and Extended Data Fig. 56a-c). Taken together, our new analysis indicates that LPC lesions can induce lesion-like compartments in distal WM tracks, displaying a delay in microglial activation when compared to the primary WM lesion.

All the above discussions have been added in the revised manuscript in the newly added section "Distinct microglial dynamics in the primary focal and distal LPC lesion-like compartments" according to reviewer's insightful suggestions.

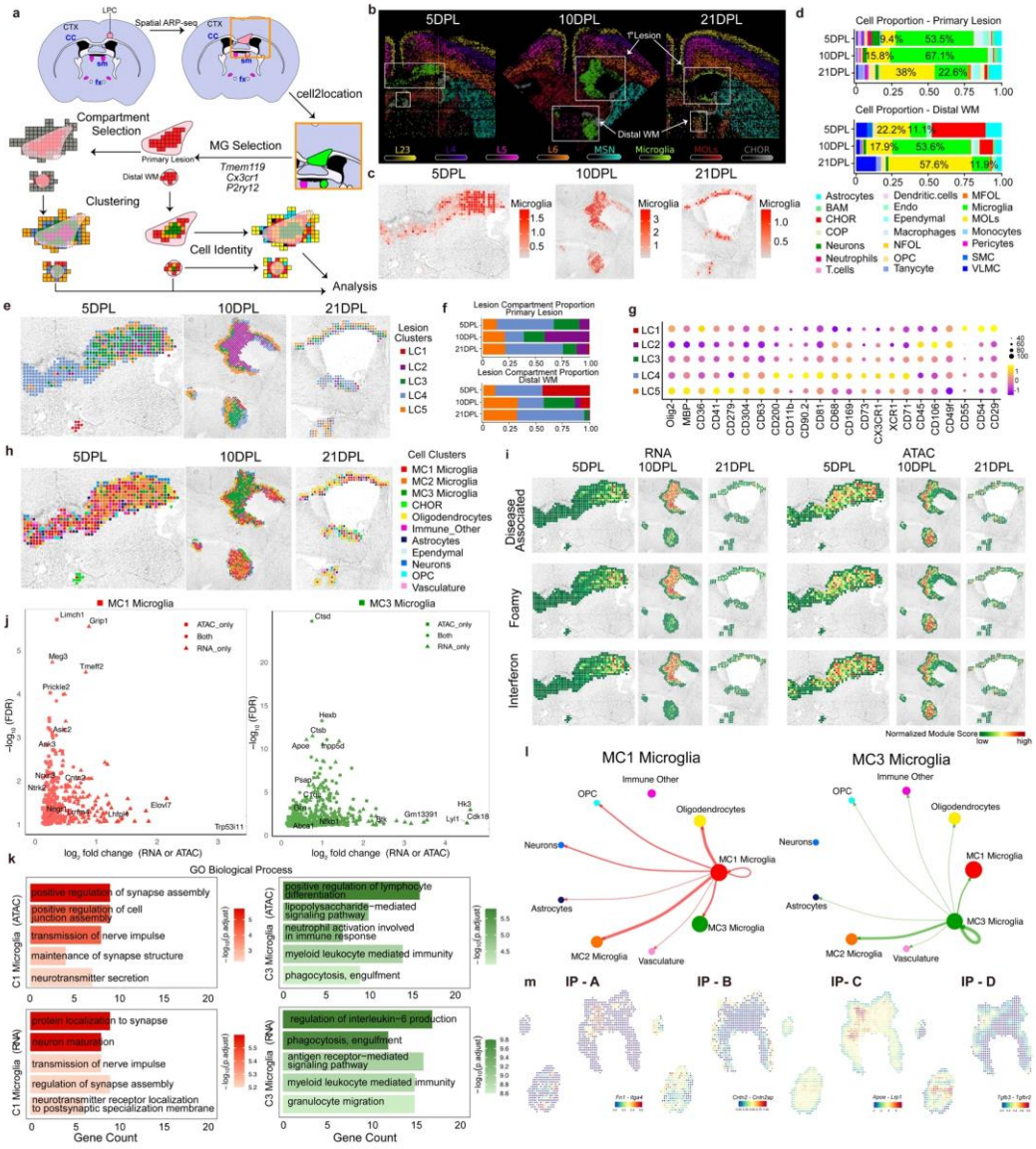

Fig. 6: Microglial dynamics in the primary focal and distal lesion-like compartments. a, Schematic illustration of the analysis workflow. **b,** Cell type predicted by cell2location from 5 DPL, 10 DPL, and 21 DPL. **c,** Predicted spatial abundance of microglia by cell2location in lesion-like compartments. **d,** Proportions of different cell types within lesion-like compartments in the primary lesion and distal white matter, as shown in **c**. **e,** Unsupervised clustering of the lesion-like compartments in **c**. **f,** Proportions of different clusters from primary lesion and distal white matter in **e**. **g,** The expression level and the percentage of pixels from

clusters LC1-LC5 for ADT protein data in spatial ARP-seq. **h,** Cell types and subclusters of microglia (MC1-MC3) in **e**. **i,** Spatial module scores of disease-associated, foamy, and interferon microglial states based on RNA and ATAC data at 5DPL, 10DPL, and 21DPL in lesion-like compartments. Gene sets were based on Androvic et al., 2023. **j,** Volcano plots showing differential gene expression or GAS for MC1 (left, red) and MC3 (right, green) microglia subclusters. **k,** GO analysis of microglia subclusters (MC1, left; MC3, right) (One-sided version of Fisher's exact test, p-value was adjusted for multiple comparisons by Benjamini & Hochberg method). **l,** Communication networks of MC1 (left) and MC3 (right) microglia with other microglial subtypes and brain cell types, based on CellChat analysis. **m,** Representative spatial maps of ligand–receptor interaction strength for *Fn1–Itga4* (A), *Cntn2–Cntnap2* (B), *Apoe–Lrp1* (C), and *Tgfb3–Tgfbr2* (D), showing regional enrichment within lesion-like compartments at 10 DPL.

Minor

1. Consistency between CODEX versus ARP-seq readout: it was not clear to me how the CODEX data was quantified (or if this is quantifiable), because these are likely the multiplex immunofluorescence. Does the 150 antibody list from spatial proteomics (in the ARP-seq) overlap with the 23 antibodies in the CODEX? This could be a validation to gain more confidence about CODEX.

Response: We thank the reviewer for the comments. CODEX is based on multiplexed immunofluorescence imaging and was used in our manuscript primarily for cell type identification and tissue architecture visualization; therefore, we did not include intensity-based quantification in the manuscript. The 23 antibodies included in the CODEX panel are canonical markers for major cell types and do not fully overlap with the antibody panel used in the ARP-seq experiments. The overlapped markers, such as CD11b and CD11c, exhibited consistent spatial patterns across both modalities (Figs. 4k and 5a-d, please also see below), providing cross-validation as suggested by the reviewer.

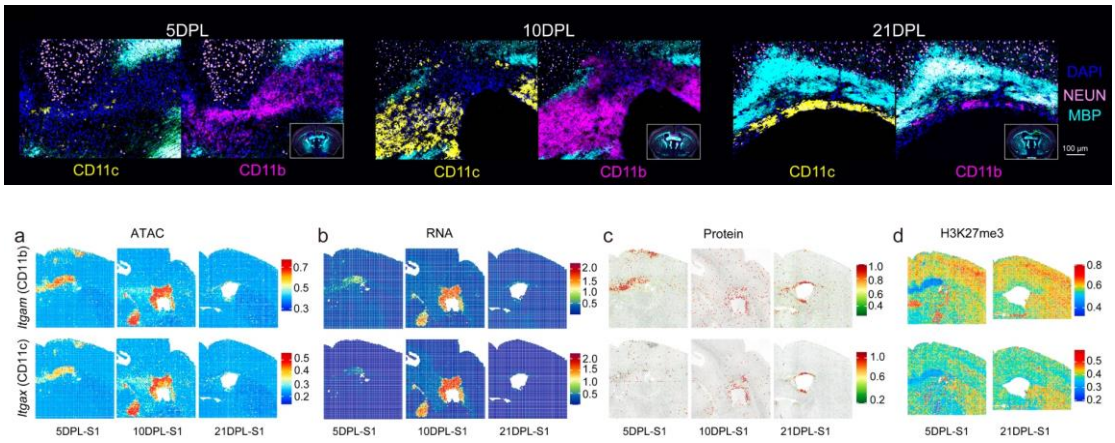

2. Readable multi-color images and cluster identity should be provided in the manuscript. Across almost all the main figures, it is hard to read out the genes displayed in the multiplexed images. For example, Fig 1b: CD169 is not visible and OLIG2/MOG are from similar colors; Fig 1c: only MBP stands out. Additionally, some annotations are confusing: Fig 4b, it is unclear if the authors were annotating brain regions or cell types.

Response: We thank the reviewer for the comments. We have regenerated all multiplexed images (including the newly generated replicates) in the main figures to improve readability according to the reviewer's suggestion. The updated images are now included in **Fig. 1b** and **Fig. 1c**. In Fig. 1b, the

abundance of CD169 is substantially lower than the other markers. This made it difficult to distinguish in whole-brain imaging. To better highlight its spatial distribution, CD169 has been shown separately in Extended Data Figs. 2-7 and 52 to highlight its spatial pattern more clearly. The expression of individual markers including OLIG2 and MOG has now been provided in Extended Data Figs. 2-9. In Fig. 1c, as we discussed in our responses to reviewer's previous comment, the visualization of certain markers may be influenced by tissue architecture, cell density, and the large field of view. To aid visualization, corresponding individual markers with zoomed-in images have now been provided in Extended Data Figs. 12-14). In addition, we also have reduced the number of overlaid markers in each multi-color image in Fig. 1c to enhance clarity. For Fig. 4b, we have revised the annotations by providing cell types. The revised version is now included in the updated Fig. 4b.

3. Fig 1b typo "immunofluorescence".

Response: We thank the reviewer for pointing out the typo in Fig. 1b. The term has been corrected to "immunofluorescence" in Fig. 1b in the revised manuscript.

4. Fig 4a, CD11b has 'b' capitalized in one place and not in another.

Response: We thank the reviewer for pointing out the inconsistency. We have corrected the capitalization to ensure it is consistently shown as "CD11b." in Fig. 4a in our revised manuscript.

Referee #3 (Remarks to the Author):

This manuscript integrates several technologies to interrogate transcriptome (RNA). proteome and chromatin states in terms of accessibility (ATAC) and genomic distribution of the H3K27me3 repressive histone mark (Cut&Tag), at a single cell resolution. The study relies on next generation sequencing technologies using Determinist Barcode In Tissue (DBiT) approaches and Co-detection by indexing (CODEX), using a panel of 23 antibodies for mouse tissue and 19 for human tissue, to create a spatial map of the developing murine brain at multiple time points (P0,P2,P5,P10,P21) and of the developing human visual cortex (at gestational week 13-23 , gestational weeks 27-34 and infancy up to 1 year of age), as well as of the mouse brain during the recovery period (at 5 and 21 days post lesion) from lysolecithin-induced demyelination.
This technical and bioinformatic tour de force generated a wealth of information, which allows the analysis of "signal concordance " at a cellular level, with a spatial and temporal resolution. This is the major strength of the study, which provides a great resource, an atlas of the murine brain, which could be assessed by neurobiologists and neuroepigeneticists.

Response: We thank the reviewer for the encouraging comments and considering our work a tour de force. We are especially grateful for the recognition of our technical and bioinformatic efforts in generating and analyzing spatiotemporal data. We are pleased that the resulting brain atlas is recognized as a valuable resource for the broader neuroscience community.

- On the conceptual level, however, the manuscript could benefit from deeper analysis.

Response: We thank the reviewer for the comment. In response to the reviewer's insightful suggestion, we have now strengthened the conceptual aspects of the manuscript by incorporating deeper analyses. We have performed a substantial number of additional experiments that increased the total experimental dataset by approximately 50%. These additions include: (i) a new set of developing mouse brains data (P0-P21) with newly designed DBiT chips featuring 220 × 220 barcodes and 15 μm pixel size; (ii) the addition of a new time point for the lysolecithin (LPC) demyelination mouse model; (iii) the generation of a new set of CODEX images for all samples; and (iv) retrograde-AAV-eGFP tracing experiments to map the projection of neuronal axons and myelination along the corpus callosum. These new datasets enabled us to perform deeper analyses, specifically, we (i) included further analysis for the developing human brain data, and conducted a comparison between human and mouse to highlight conserved and divergent spatial-temporal programs in cortical development, (ii) deciphered the dynamics of neuroinflammation from epigenome, transcriptome, and protein levels during the progression from demyelination to remyelination in LPC mouse model, (iii) demonstrated the microglial states at lesion core and distal white matter compartments with distinct epigenomic and transcriptional features, (iv) uncovered spatially distinct myelination dynamics of different cortical projection neuron subtypes.

This improvement led to the addition of two new sections "Spatial dynamics of human visual cortical development", and "Distinct microglial dynamics in the primary focal and distal LPC lesion-like compartments", and improvement in sections "Layer-specific projection neuron axonogenesis and synaptogenesis time may orchestrate myelination", "Spatial tri-omic mapping of neuroinflammation and

remyelination using a focal lesion mouse model of MS", "A transient population of microglia arise during myelination in development and remyelination in the LPC models of MS", "Distal microglia associated with WM tracks are observed far from the LPC lesion", as well as new and improved figures (Figs. 2k-l, Fig. 3i-n, 4a,e,h, 5f-h, and Fig. 6).

- Most of the Figures appear to provide a validation of previously reported phenomena, such as the concept of lateral to medial myelination of the corpus callosum (Sturrock 1980; Vincze et al., 2008). But adding a layer of molecular complexity.

- Other concepts, however, such as timing of myelination of corticofugal Pyramidal neurons followed by myelination of the CPN tracts would need lineage tracing experiments to be validated.

Response: We thank the reviewer for the comments. As the reviewer indicates, the pattern of myelination in the developing mouse corpus callosum has been reported through histological methods, including MBP immunostaining, Luxol Fast Blue myelin staining, and electron microscopy (Sturrock 1980 and Vincze et al., 2008). We have now added this referenced observation into the manuscript. Nevertheless, our spatial data go beyond histology, with findings derived from chromatin accessibility, RNA, and protein. These data not only recapitulate the reported anatomical patterns of myelination but also uncover molecular features underlying this process. Specifically, transcriptional dynamics across spatial bins confirmed a lateral-to-medial progression of key myelination genes (e.g., *Mbp, Mog*), consistent with prior histological observations (Fig. 3, please also see below).

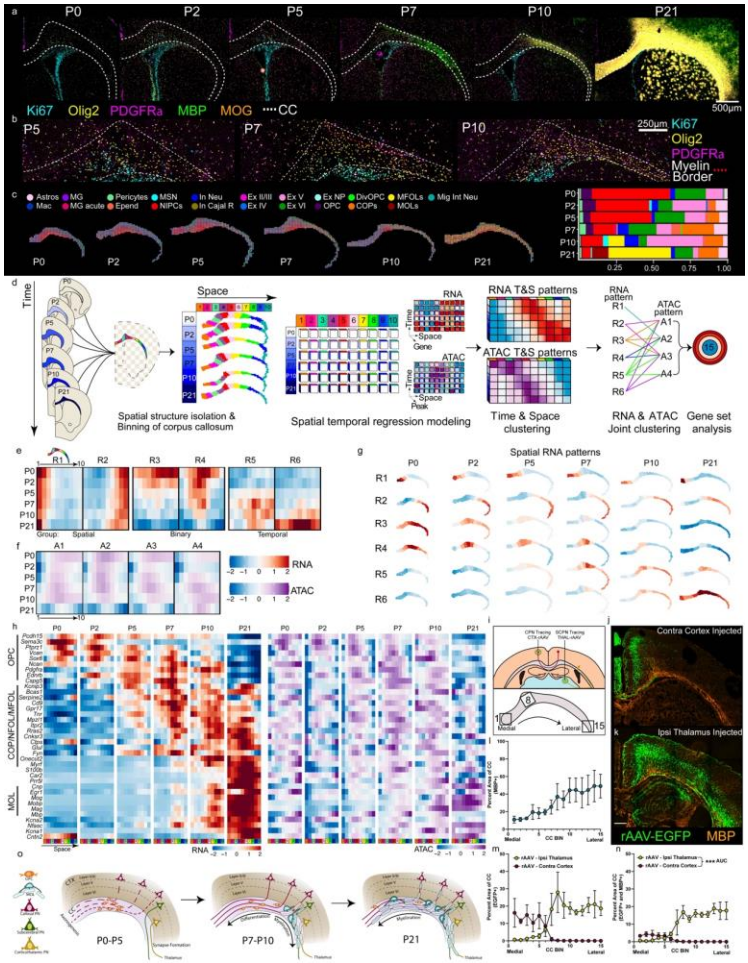

Fig. 3: Spatiotemporal dynamics of the mouse corpus callosum during development and myelination. a, CODEX images of the mouse brain corpus callosum from P0 to P21. Scale bar, 500 μm. **b,** Zoomed-in CODEX images of the medial corpus callosum regions in **a** from P5, P7, and P10, respectively, showing staining for OLIG2, PDGFRα, and Ki67. **c,** Decomposition and pie chart visualization of cell types in corpus callosum (S2) from the spatial RNA data. **d,** Schematic representation of spatial temporal regression model on mouse brain corpus callosum from P0 to P21. **e,** Heatmaps of the 6 RNA clusters generated from the regression model. **f,** Heatmaps of the 4 ATAC clusters generated from the regression model. **g,** Spatial RNA patterns for RNA clusters (R1-R6) from the regression model. **h,** The RNA gene expression calculated on the basis of the regression model for specific genes. **i,** Schematic illustration of the injection sites and tracing pathways for CPN and CThPN (top) using retro-AAV-eGFP at the terminal location for both tracts separately. Segmentation strategy using confocal imaging at high magnification (40x) for MBP staining and retro-AAV-eGFP labeling quantification throughout the corpus callosum (bottom). **j,** Confocal images (20x) stitched together to capture the corpus callosum and overlying cortex of one hemisphere for CPN tracing in P10 mouse after retro-AAV-eGFP injection at P1. Representative retro-AAV-eGFP tracing from the contralateral cortical layer II/III injected terminal. **k,** Representative Retro-AAV-eGFP tracing from the ipsilateral thalamic injected terminal. **l,** Percent area of MBP staining per bin across the defined corpus callosum in each image moving medial to lateral (n=6; 3 CPN traced + 3 CThPN traced)**. m,** Percent area of retro-AAV-eGFP labeled axons of the area of corpus collosum defined per image**. n,** Percent area of co-labeled MBP and retro-AAV-eGFP labeled axons of the area of corpus collosum defined per image (n=3 CPN traced and n=3 CThPN traced). Significance was determined by calculating the area under the curve then running a two-tailed, unpaired t-test (P value = 0.0001) on the mean total area values (CTX: 18.79 and Thalamus: 143.2) with the standard error values (CTX: 2.770 and Thalamus: 7.942) that were derived from the area under the curve statistics. CTX: cortex, THAL: Thalamus. **o,** Descriptive model summarizing how myelination progresses in the corpus callosum and cerebral cortex.

Importantly, our spatial chromatin accessibility data revealed chromatin priming in oligodendrocyte-lineage cells prior to detectable RNA and protein expression, indicating that molecular commitment to myelination precedes histological detection (Fig. 3). This regulatory insight, inaccessible by conventional histological methods, provides molecular-level validation and mechanistic context for the spatial progression of myelination, confirming that myelination is tightly regulated both spatially and temporally across modalities. We consider that the added molecular resolution provides novel insights into the regulatory architecture and temporal coordination of neurodevelopment, beyond what has previously been demonstrated. Our strategic analysis and our rich multimodal dataset enabled our model suggesting that the observed pattern might be related with the timing of myelination of neurons from different cortical layers, which we now elaborate on by performing tracing experiments, considering the reviewer's constructive comment.

We investigated preferential myelination of projection neuronal tracts by utilizing a retrograde AAV tracing approach. In order to achieve this, segregation of projection neuron tracts and the corpus callosum was required. Therefore, we decided to inject the ipsilateral thalamus and in separate mice layer II/III of the contralateral cortex (in reference to the hemisphere of corpus callosum (CC) the myelin would be quantified). A pilot study was performed to first determine the best timepoint to study the lateral-to-medial myelination patterning. We performed CODEX on P7, P10, and P14 (P14; not included in manuscript) to verify that there was not a more optimal developmental time point other than P10 (please see the figure below). By P14 the myelination had already continued more medially past the cingulum bundle, so we ran the tracing experiment on P10 mice (n=3).

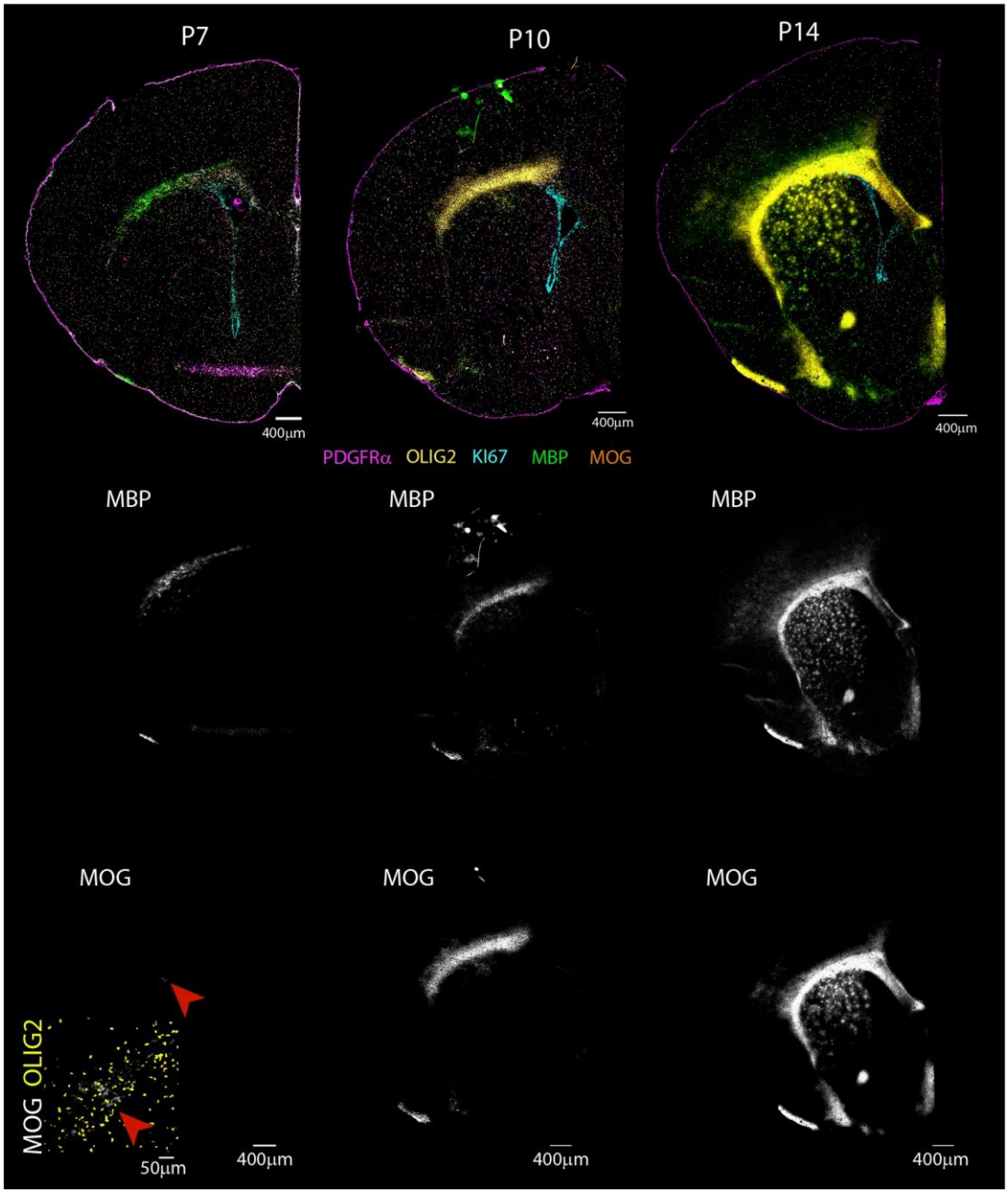

Retro-AAV-eGFP was injected at P1 to provide time for track labeling (P4 has less distal labeling of cortical thalamic neurons in CC; data not shown). Myelin was stained by performing IHC using an antibody against MBP followed by consecutive confocal imaging along the CC moving medial to lateral (Fig. 3i-k, please also see below). We first quantified the total myelin along the CC and found that around the cingulum bungle there was a shift and marked increase in MBP area within the defined CC area per image (Fig. 3l, please also see below). Total retro-AAV-eGFP was calculated as the percent area of the CC (Fig. 3m-n, please also see below). The cingulum bundle identified the track (CPN vs CThPN) CC occupation in which the labeled layer II/III CPN was medial and the CThPN was lateral. Of note the retro-AAV-eGFP did not occupy the entire area of the CC, which is expected as not the entire population of CPN (V/VI exclusion) and CThPNs were labeled, and the SCPN population was

experimentally excluded. Finally, we calculated the area of the CC that was double positive for MBP and retro-AAV-eGFP and found a similar trend that we observed with the eGFP only signal occupancy of the CC (Fig. 3n, please also see below). Taken together, these data support our findings of that the temporal and spatial patterning of myelination is likely linked to projection neuron subtype. One experimental approach that could further delineate this is to compare CThPN and SCPN that are closer to time in origin to one another and run along the lateral CC, however due to the distance of the SCPN terminus being farther away (midbrain, pontine or spinal cord), our concern is that the short labeling window of P1-P10 may not be long enough and the labeling too sparse.

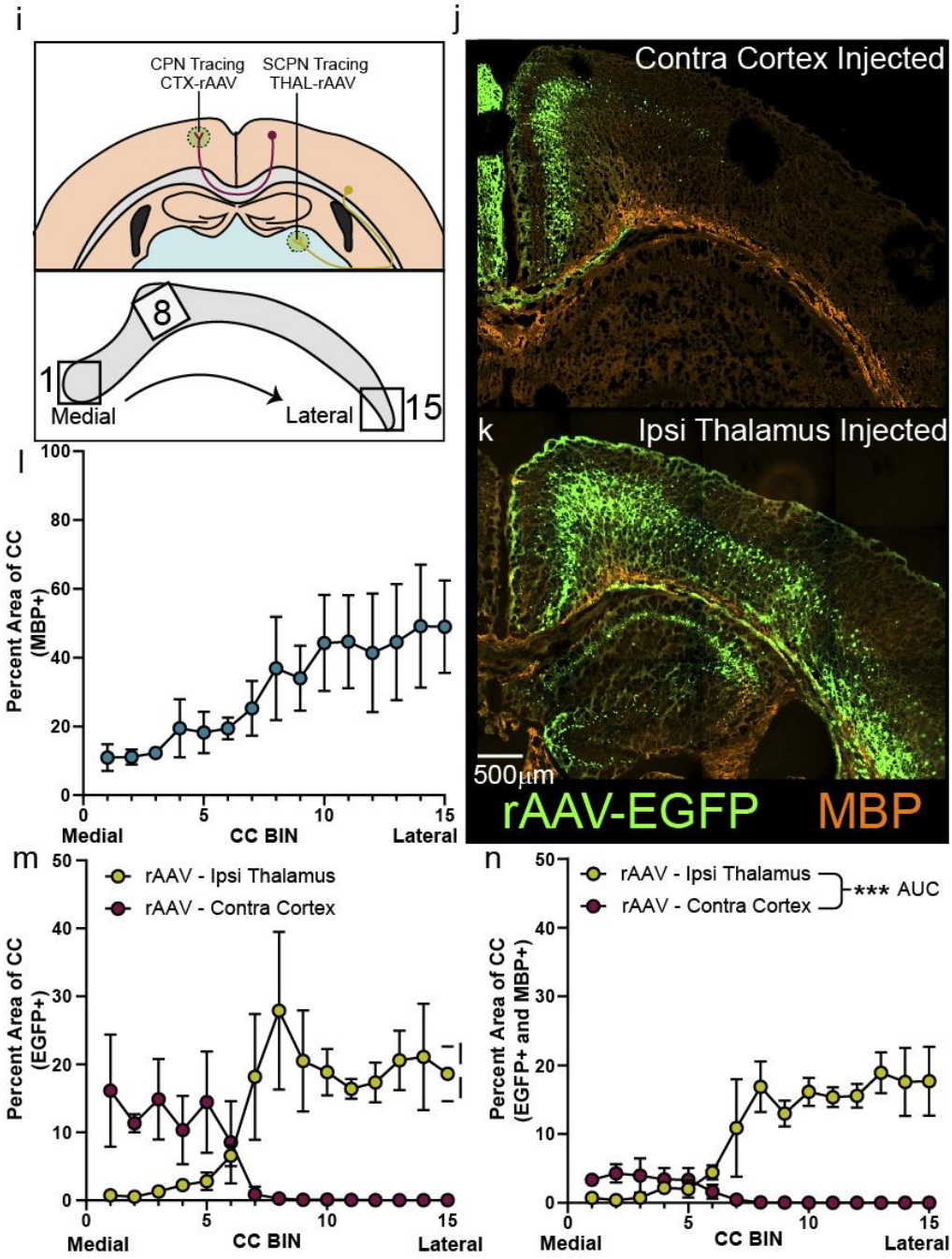

Fig. 3: i, Schematic illustration of the injection sites and tracing pathways for CPN and CThPN (top) using retro-AAV-eGFP at the terminal location for both tracts separately. Segmentation strategy using confocal imaging at high magnification (40x) for MBP staining and retro-AAV-eGFP labeling quantification throughout the corpus callosum (bottom). **j,** Confocal images (20x) stitched

together to capture the corpus callosum and overlying cortex of one hemisphere for CPN trancing in P10 mouse after retro-AAV-eGFP injection at P1. Representative retro-AAV-eGFP tracing from the contralateral cortical layer II/III injected terminal. **k,** Representative Retro-AAV-eGFP tracing from the ipsilateral thalamic injected terminal. **l,** Percent area of MBP staining per bin across the defined corpus callosum in each image moving medial to lateral (n=6; 3 CPN traced + 3 CThPN traced)**. m,** Percent area of retro-AAV-eGFP labeled axons of the area of corpus collosum defined per image**. n,** Percent area of co-labeled MBP and retro-AAV-eGFP labeled axons of the area of corpus collosum defined per image (n=3 CPN traced and n=3 CThPN traced). Significance was determined by calculating the area under the curve then running a two-tailed, unpaired t-test (P value = 0.0001) on the mean total area values (CTX: 18.79 and Thalamus: 143.2) with the standard error values (CTX: 2.770 and Thalamus: 7.942) that were derived from the area under the curve statistics. CTX: cortex, THAL: Thalamus.

- Overall a very nice resource paper

Response: We appreciate the reviewer for the positive comments.

Referee #2 (Remarks to the Author):

I appreciate the authors' comprehensive responses as well as the efforts in revising the manuscript. While the authors have strengthened the work by including additional data and time points, introducing new sample sets and performing a new AAV experiment, several key issues remain to be addressed. Additionally, I encourage the authors to compare their data with several recently published spatial technology studies such as SPACE-Seq (Huang et al., PNAS 2025) and ExIGS (Labade et al., Science 2025) to better highlight the advantages of their technology as the field moving forward.

Major:

Response: We agree with the reviewer that spatial omics is a rapidly evolving field and appreciate the suggestion to position our study within the context of recent technological advances. While our labs reported the first spatial epigenome sequencing methods back in 2022, we are equally excited to see the continued development in this field and, in particular, we enjoyed reading about SPACE-Seq and ExIGS. Each of these approaches has distinct characteristics, and we will discuss them in our revised manuscript. At the same time, we wish to emphasize that our work is primarily a developmental neuroscience data resource and biological discovery study, rather than being focused solely on technology development – although we note that the methods applied here remain best-in-class for generating comprehensive multi-modal spatial omics atlases.

- **SPACE-Seq** (Huang et al., PNAS 2025) represents an important step toward combining spatial epigenome (in the current form, ATAC only, and yet to be demonstrated for CUT&Tag), transcriptome, and lineage tracing. The "lineage tracing" capability of SPACE-seq was built upon post hoc inference from mitochondrial variants detectable in ATAC-seq reads, which is very interesting and different from other methods although further improvement is still needed. Currently, SPACE-Seq demonstrated relatively coarse spatial resolution (~55 μm pixels) and limited throughput (~3,800 spots per section), with per-spot data quality also remaining modest (typically ~2,500 UMIs and ~1,500 genes for RNA, less than 8000 fragments per spot for ATAC). In contrast, our DBiT-based spatial ARP-seq achieves 15–20 μm pixel resolution with dense sampling grids (100×100 and 220×220 spots, 10,000–48,400 spots per section) and delivers higher quality data (~6,000 UMIs, ~2,500 genes, >15,000 ATAC fragments, per spot), that might have contributed to our ability to identify more tissue features or clusters in the same brain region. For example, our data clearly resolved different cortical layers (See Figure below).

[REDACTED FIGURE]

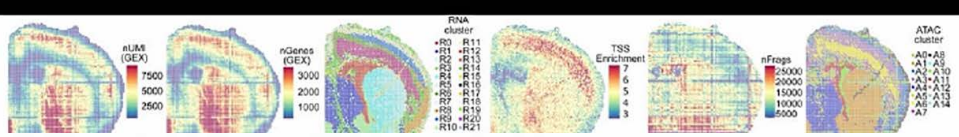

This combined advantage in resolution, throughput, and data quality is precisely what enables us to resolve biologically meaningful fine-scale features such as cortical laminar distinctions,

the precise sequence of myelination, and distal microglial activation along with-matter tracts—phenomena that would be obscured at coarser resolution or lower sensitivity.

- **ExIGS** (Labade et al., Science 2025) addresses a very different regime: by combining expansion microscopy with in situ genome sequencing, it resolves nanoscale subnuclear chromatin organization and links nuclear morphology to local chromatin regulation in single cells. This is highly valuable for mechanistic studies of nuclear architecture (e.g., lamin defects in progeria) but does not provide unbiased, tissue-scale RNA or ATAC maps across intact brain sections. In contrast, our spatial ARP-seq is designed for totally different purposes – to produce whole transcriptome and whole epigenome coverage simultaneously on the same tissue section, complemented by a protein layer and orthogonal CODEX imaging, thereby enabling systems-level analyses of cell states, regulatory networks, and spatially propagating pathology in the context of intact tissue architecture. We really appreciate the reviewer bringing this interesting work to our attention!

We thank the reviewer for this helpful suggestion. In response, we add a short discussion in the Discussions section citing SPACE-Seq and ExIGS, highlighting their differences and emphasizing their complementarity to our work. At the same time, we would like to reiterate that the main focus of our study is on the biological insights gained through applying high-resolution, unbiased multi-modal multi-omic mapping to postnatal brain development and demyelination models.

1. The robustness and reliability of their technology need to be further addressed. There are various instances within the manuscript that raise concerns about data quality:

Response: We thank the reviewer for raising this important point. We agree that robustness and data quality are critical for evaluating new spatial multi-omic technologies. In our datasets, per-pixel quality metrics are consistently high, across dense sampling grids of 10,000–48,000 pixels at 15–20 μm resolution. As mentioned above, these values for the ATAC modality substantially exceed those of existing Visium-based multiome approach (e.g., SPACE-seq, ~2,500 UMIs and ~1,500 genes per spot, with limited TSS enrichment at 55 μm resolution). Importantly, our datasets also robustly recapitulate well-established anatomical and developmental features, including cortical lamination, the precise temporal sequence of myelination, and distal microglial activation along white-matter tracts, providing independent biological validation of data quality. Together, these quantitative and biological validations demonstrate that our technology is robust and reliable, and that the data quality is sufficient to support the conclusions of this study.

a. The correlation of RNA and ATAC data across timepoints is similar or sometimes higher than the correlation across technical replicates within a time point, indicating the measurements somehow capture more sample-to-sample noise than robust developmental changes (rebuttal pg 4). For example, in the ATAC analysis, the majority of samples across different time points appear highly correlated. Additionally, the P2_S1 is more correlated with P0_S1 than P2_S2 in the RNA data. The authors should explain why their technology generates homogenous measurement but fails to capture meaningful developing signatures.

Response: We appreciate the reviewer's observation that cross–time-point correlations sometimes appear as high, or even higher, than correlations across technical replicates (Figure below).

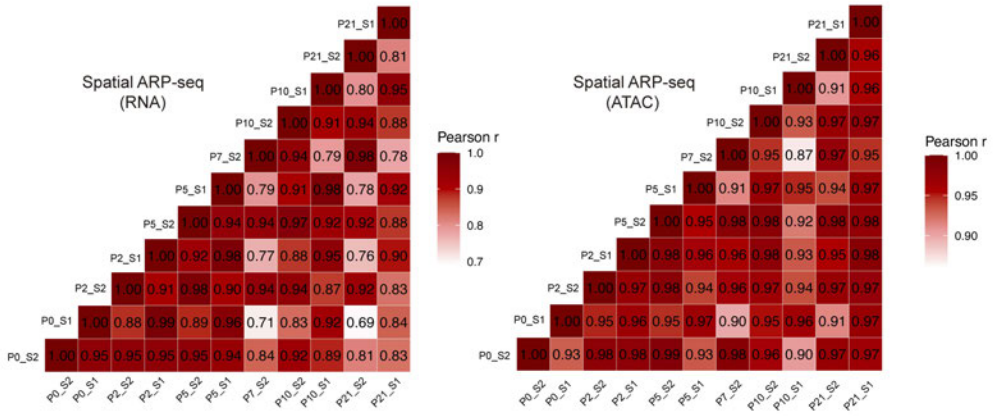

However, we would like to clarify why this pattern is expected and biologically consistent, and why it does not imply that our technology fails to capture developmental dynamics. There are two main considerations:

(i) Biological context: postnatal stability of cortical architecture

All of our datasets are derived from the *postnatal* period (P0–P21). By this stage, the fundamental laminar and regional architecture of the cortex is already established, in sharp contrast to the embryonic period when neurogenesis, migration, and differentiation drive massive global shifts in gene expression and chromatin state. Postnatally, the dominant biological processes are more gradual, such as myelination, synaptic maturation. Consequently, global transcriptome and epigenome profiles remain relatively stable between adjacent postnatal stages. High correlation between postnatal samples is therefore entirely consistent with biological expectations, and a strength rather than a weakness of our data. In fact, if we had observed drastic global divergence between P0, P2, and P7 samples, it would have been biologically implausible and inconsistent with well-established developmental neurobiology. Our clustering analyses further confirm that cortical lamination is preserved across samples, reflecting this expected global stability. We applied gene- and peak-level statistical modeling (e.g., GAM fitting, likelihood ratio testing) specifically designed to identify the smaller subset of features with significant temporal and spatial dynamics. These analyses reveal clear developmental trajectories and pathway enrichments, demonstrating that the technology captures meaningful dynamics even though global correlation appears high.

(ii) Compositional and technical factors in spot-based measurements

Our measurements are generated from 20 μm "spots", each capturing multiple cells. In the early postnatal period (P0–P2), when cell density is particularly high, each spot can contain mixtures of neurons, glia, and progenitors. This might explain how cases of differences in local tissue composition across sections (e.g., slight variation in layer representation or regional sampling) can introduce modest variability between technical replicates. With, for instance, a P2 section may appear more correlated with a P0 section than with its replicate P2 section. Importantly, such effects reflect the inherent multi-cell composition of each spot and biological

heterogeneity across slices, rather than a failure of the method. This phenomenon is well recognized in spatial omics datasets with spot-level resolution and is consistent with our observations.

Taken together, the high correlation across postnatal time points arises from (i) the biological reality of global stability during postnatal cortical maturation, (ii) modest technical and compositional variability inherent in spot-based measurements. These factors fully explain the reviewer's observation. Crucially, our downstream modeling robustly resolves hundreds of temporally regulated genes and chromatin peaks, together with enriched pathways, confirming that the technology faithfully captures meaningful developmental signatures within the expected globally stable background. We will add these points in the discussion.

b. Protein signal is occasionally not correlated with RNA and ATAC data, particularly with immune cell markers. Fig 5c protein data do not support the distal activation claim which was only observed in the ATAC and RNA data. The authors should explain why protein accumulation at the distal sites of Cd11b, CD11c, and Cd68 is not detected at the protein level, despite being observed at RNA and ATAC levels. Similar inconsistencies are observed in Fig 5h with CD45 and CD115. The authors should elaborate on why these discrepancies may exist.

Response: We acknowledge the reviewer's observation that the distal accumulation of immune markers appears less pronounced at the protein level in the ADT measurements (Fig. 5c, below).

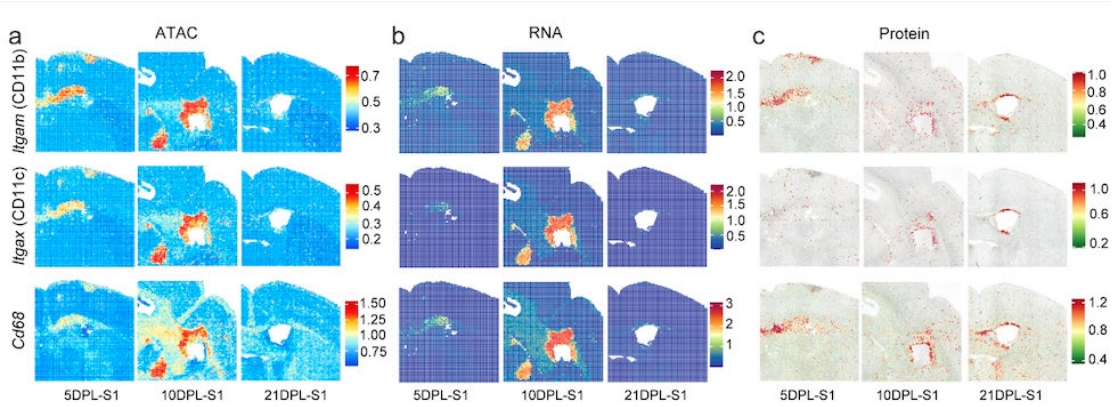

As CD45 and CD115 are not included in Fig. 5h, we interpret the reviewer's comment as likely referring to Fig. 4h. This discrepancy can be explained by both technical and biological factors. First, antibody-derived tag (ADT) profiling in spatial sequencing generally shows lower sensitivity than RNA/ATAC layers, particularly for membrane proteins such as CD11b, CD11c, CD68, CD45, and CD115, where epitope accessibility, antibody penetration, and capture efficiency can limit signal detection in low abundance regions. As a result, subtle distal signals may be underestimated. Second, RNA and ATAC changes represent early activation events (chromatin opening and transcriptional priming), whereas protein accumulation generally lags behind and requires higher abundance to be detected, especially by sequencing-based ADT. Consistent with this, we do observe weak but noticeable distal signals in the ADT data, and more importantly, high-resolution multiplexed protein imaging (CODEX) clearly reveals distal activation of these markers, fully consistent with the RNA and ATAC findings. Thus, the

discrepancy reflects sensitivity limits of ADT for low abundance signals, rather than a true biological absence of distal activation. We now comment on this aspect in the revised version of the manuscript.

c. Poor detection quality in the human sample should be discussed or repeated with higher quality replicates. Although working with human tissue is challenging, this issue will greatly limit the applicability of this technology in more relevant tissue types and therefore dampen enthusiasm for this technique. In Fig 2k, BCL11B and TBR1 show different expression patterns compared to Fig 1c. In Fig 2l, many key marker gene expressions in the human cortical layer appear undetected, as indicated by missing data in the heatmap. Additionally, Fig 1c data failed to detect layer makers (CUX1/2, CTIP2, and TBR1) and glia maker (PDGFRa), which should be abundantly expressed and been used as positive references (Qian et al., Nature 2025) The authors should include high-magnification images with clear cortical layer annotations to substantiate their claim that the technology can actually be used for human samples.
Additionally, the authors made several interpretations and statements that are not well supported by their data. For instance, they stated that high ATAC activity precedes RNA expression for all myelin-associated genes in human samples, but this is not true for MOBP and BCAS1 in Fig 2l.
Moreover, several conclusions are based on one single human sample, with no accompanying quality control and replicates. The authors should increase the number of sample sizes, replicates and provide quantification and statistics to strengthen these conclusions and findings.

Response: We appreciate the reviewer's concern about potential discrepancies, human tissue quality and sample size.

Regarding BCL11B/CTIP2, TBR1 and other cortical layer expression patterns, high-magnification images with clear cortical layer annotations were already included in the previous version of the manuscript in Extended Figs. 12-14, and in our previous *response to reviewer* on Page 44 (as we have already clarified previously, this is CODEX multiplexed immunofluorescence staining for protein, not RNA sequencing as shown in Qian et al). As can be seen below, BCL11B/CTIP2, TBR1 present at the RNA level similar expression patterns as at the protein level in CODEX, and thereby there are no discrepancies for these markers. We will include insets of the images in the Extended Figures in the Fig. 1c, so the CTIP2 staining becomes clearer.

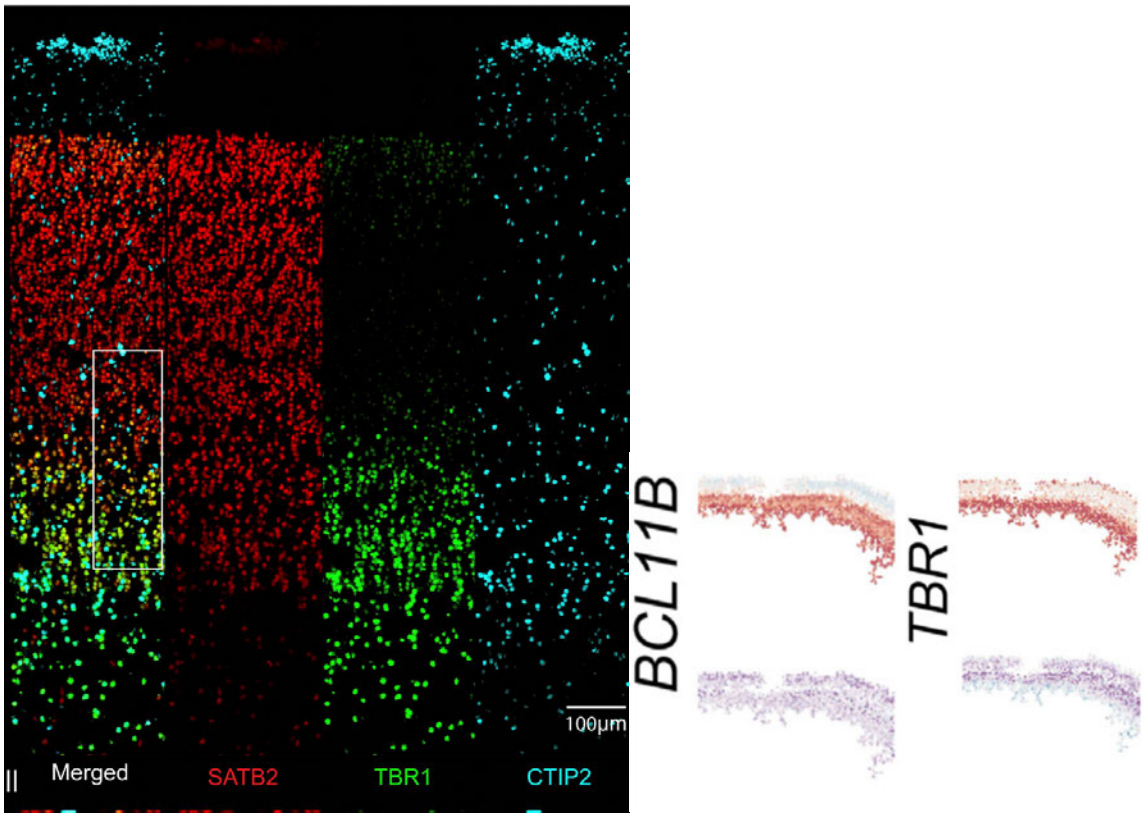

Regarding the statement that “high ATAC activity precedes RNA expression for all myelin-associated genes in human samples”, we agree with the reviewer and we will change the sentence to:

“In the genes associated with oligodendrogenesis, we saw higher incidents of ATAC gene activity in the genes associated with oligodendrogenesis, we saw higher incidents of ATAC gene activity genes (Fig. 2l and Extended Data Figs. 35 and 38), which was the case for ***a subset of myelin associated genes (MAG, MBP, MAL)****, and as observed in the mouse cortex”*

We would like to clarify that, unlike recent *Nature* studies that focused exclusively on the human cortex and analyzed 6–10 samples across multiple regions and ages, the human data in our study are not the primary focus but rather a small complementary section to demonstrate feasibility and translational relevance. In this context, we have already included three human cortical samples (prenatal and infant V1), which are exceptionally rare and difficult to obtain. As mentioned in the manuscript, these samples are from the same tissue blocks from the ones in Wang et al, Nature 2025 (https://www.nature.com/articles/s41586-024-08351-7), where they mapped the V1 regions at three developmental time points. In our study, we have analyzed all three corresponding V1 regions, and we show that our technology can recapitulate the transcriptomic findings by Wang et al. with an orthogonal technology, MER-FISH, with the advantage of adding additional omic layers. While the number is smaller than dedicated human-focused studies, it is substantial given the limited availability of such tissue and is sufficient to support the proof-of-principle demonstration. We will temper our claims accordingly, framing the human data as preliminary and consistent with the robust mouse findings.

Finally, we note that this manuscript represents part of the first phase BICCN effort, which has been more heavily focused on mouse datasets, with the human data included here only as an early exploratory demonstration. The ongoing BICAN program, in contrast, is dedicated to constructing a comprehensive human and non-human primate developmental brain atlas, encompassing nearly 12~15 human and ~20 non-human primate samples, and is expected to be completed in 2027.

2. Immunofluorescence or ISH validations are needed for several main statements.

a. In Fig 3c, the cell proportion analysis shows there is no OPC population at P10 and P21. Additionally, the Fig 3h shows a similar reduction of OPC maker along the development. As shown by many studies, OPCs populate the brain throughout life and continue to reside in the corpus callosum throughout (Dawson, 2003, Allen Atlas, 2011, Bergles and Richarson, 2016). This lack of OPC at juvenile brain is controversial and likely wrong – the authors should provide IF results of OPC markers throughout the development to validate their findings.

Response: We thank the reviewer for highlighting this point. In Fig. 3c the OPC population is subdivided into 3 sub-groups titled OPC, DivOPCs (OPCs in the cell cycle) and COPs (committed OPC). Since these subclusters express PDGFRa and NG2 (Marques et al. Science. 2016 and Falcao and van Bruggen et al. Nat Med. 2018 and) as it indicates that we indeed have OPC/COPs/DivOPCs present in the corpus callosum across all our developmental atlas (OPC subcluster between P0-P7 and the COPs between P2-P21). Therefore, our data is indeed consistent with the Dawson 2003, Allen Atlas 2011 and Bergles and Richardson 2016). We will clarify this point in the manuscript.

Regarding Fig. 3h, there is indeed expression of PDGFRa, however, due to the analysis being comparative between groups, it is much lower than earlier timepoints. Since spatial ARP-seq does not have single-cell resolution, it is not possible to isolate individual cell populations and determine expression maintenance of specific genes within a given cell type. As a result, gene expression profiles of cells in lower abundance are outcompeted by gene expression profiles of cells in greater abundance. This is seen in Fig. 3h when the predominent oligodendrocyte lineage cell population shifts from OPC/COP to mOLs at P7/P10 even though OPC/COPs are maintained throughout time. In Fig. 3b, we provide CODEX data of even higher magnification to show that the PDGFRa expressing OPC/COP is maintained in late development.

Data portal: All sequencing data and spatial maps are available at our public portal (https://spatial-omics.yale.edu/), where Pdgfra and Olig2 can be clearly visualized as persistently present across development. These markers are also shown throughout the Extended Data Figures. (e.g., Extended Figs. 2–9,19-21).

b. The author demonstrated that the lateral CC shows stronger MBP colocalization with AAV-labeled neuronal projections. However, the MBP signal in Fig 3j actually shows a flat distribution from lateral to medial CC – contradictory to the claim. The results in Fig 3m and 3n could just reflect the intensity differences of neuronal projections but not myelination itself. To validate this result quantitatively, authors may just stain a panel of well known myelination markers throughout the developmental ages and quantify the spatial distribution in lateral and

medial CC, which is a standard validation experiment.

Response: We thank the reviewer for this comment. To better show the MBP variation across the corpus callosum, we have included an additional panel showing MBP only staining with better quality images having less background signal (See the new figure panel below). In addition, we have drawn the borders around the corpus callosum, excluding the dorsal hippocampal commissure that lies ventral to the medial portion of the corpus callosum body. We excluded the dorsal hippocampal commissure white matter tract on the basis that it is not comprised of projection neuronal subtypes we have focused on in our study (Suárez, Gobius and Richards. 2014. and Bubb et al. 2020). In the MBP-only images, it is clear that the staining we quantified using the strategy depicted (panel i) is not due to bleed-through of channels. If we were experiencing channel bleed-through issues, it would clearly be visible in the contralateral cortex injection, where the GFP intensity is very strong; however, there is no staining observed in the MBP-only image.

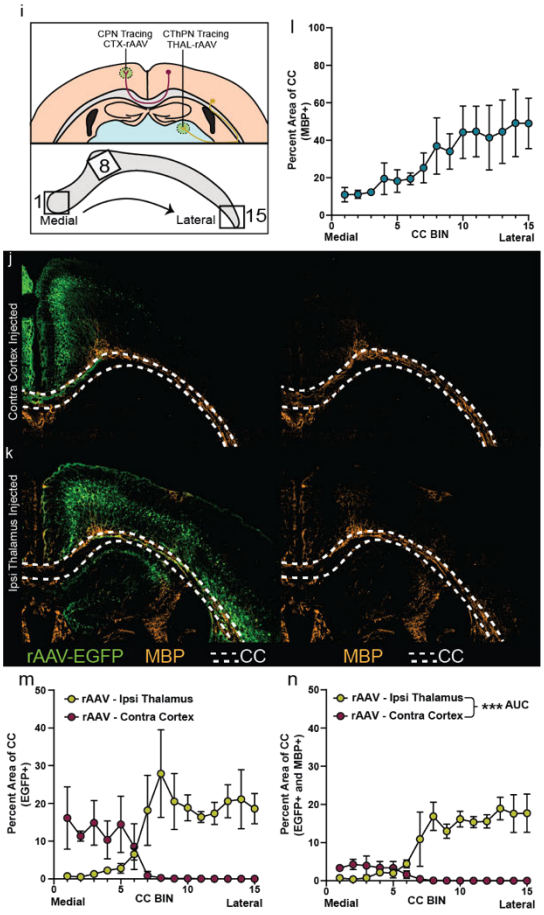

Based on reviewer concerns (first revision), we had expanded our developmental data set to include P7 to better depict the lateral to medial developmental myelination pattern. We had included two myelin proteins, MBP and MOG, in our CODEX imaging platform for P0, P2, P5, P7, P10, and P21. Now our developmental data more clearly shows lateral-to-medial myelination through the inclusion of the P7 timepoint (Fig. 3a and Extended Data Figs. 2-9). We would also like to highlight our addition of two previous studies, as we have referenced previously in our manuscript, that describe the lateral-to-medial myelination through multi-time point developmental analysis using histological methods, including MBP immunostaining,

Luxol Fast Blue myelin staining, and electron microscopy (Sturrock 1980 and Vincze et al., 2008).

c. The authors deduce in Fig 5 that there is distal activation of immune cells as an effect of LPC injection. The authors should provide IF/ISH staining alongside the CODEX images to validate their findings.

Response: We thank the reviewer for this comment. We would like to clarify that the CODEX data presented in Fig. 5 are based on antibody-driven immunofluorescence staining. Thus, CODEX inherently provides the IF validation of the spatial ARP-seq findings, while offering the additional advantage of multiplexing dozens of markers in the same tissue section. We have clarified in our previous response that CODEX is an antibody-based immunofluorescence technology (rebuttal Page 22-24); we reiterate this here to avoid any misunderstanding. The CODEX analysis independently confirms the induction of distal lesion–like immune activation, consistent with the spatial ARP-seq profiles. We therefore believe that additional single-channel IF or ISH experiments would not provide further validation beyond what has already been demonstrated with multiplex CODEX imaging.

3. A more rigorous and systematically controlled experimental design using the LPC mouse model is necessary to support the study's conclusions. The distal activation of microglia in white matter is an interesting finding but lack several critical controls and therefore cannot be interpreted. A bilateral sham injection should be used as a control. This control would validate that the distal microglial activation was a product of the lesion and not of mechanical damage to the brain by intracranial injection. Additionally, the LPC injections should be performed with a fluorescent marker so that they are able to show that leakage of the injection is not the cause of the distal activation.

Response: We appreciate the request for additional controls to exclude mechanical damage as an explanation for distal activation. However, multiple, convergent lines of evidence indicate that the tract-mediated distal responses we report are not due to injection trauma:

1) **Spatial-gradient principle (a first-order response to mechanical injury) and temporal separation: acute trauma vs. delayed demyelination.**

   If mechanical damage were the driver of immune activation, this should be maximal at the needle track/injection core and decay monotonically with distance. In contrast, our datasets show no distal activation at early time points (e.g., 5 DPL) and the emergence of robust distal activation along white-matter tracts at later stages (e.g., 10–21 DPL). A delayed, tract-localized response is incompatible with an acute mechanical-injury model and consistent with biology of demyelination-induced signaling and recruitment. Mechanical injury produces immediate local responses; by contrast, we observe temporal lag (no distal signal at 5 DPL; clear emergence at 10 DPL), matching expected kinetics for demyelination, debris handling, and microglial state transitions rather than needle-track effects.

2) **Independent PBS (sham) evidence at the core argues against trauma-driven activation.**

A recent preprint (Michael-John Dolan *et al.*, 2025) performed single-cell RNA-seq with spatial profiling across 3, 7, 12, and 18 dpi with PBS controls. Although their Slide-seqV2 spatial coverage focuses on regions immediately adjacent to the injection site, their PBS results indicate that immune responses at the core are not attributable to the mechanical injection itself. In other words, when trauma is isolated (PBS), core-proximal activation is minimal. This external control makes a trauma explanation for our far-distal effects even less plausible. Because the Dolan *et al.* PBS controls demonstrate minimal immune activation at the injection core, a far-distal activation cannot be a trauma artifact; it requires biological propagation (e.g., myelin damage–linked signaling) along white-matter tracts—precisely what our large-field (half/whole brain) maps capture but core-restricted assays are not powered to detect.

3) **Anatomical specificity: tract-aware patterning.**

Our spatial ARP-seq and CODEX cover half- to whole-brain sections, revealing activation that tracks along the callosal white matter and respects known axonal routes, with ipsilateral ≫ contralateral effects and minimal spillover into adjacent gray matter. A generic mechanical artifact would not reproduce this tract-constrained topology.

4) **Molecular concordance across modalities.**

Distal regions show matched signatures in RNA (transcriptional activation), ATAC (chromatin accessibility), and protein (CODEX IF) markers of microglial activation. Cross-modal agreement at distal ROIs is hard to attribute to an artifact of injection.

Taken together—**(a)** minimal activation under PBS at the injection core (external control), **(b)** delayed onset and tract-localized distal patterns, and **(c)** cross-modal molecular concordance—strongly support that the distal microglial activation we report is a bona fide consequence of LPC-induced demyelination rather than mechanical injury. To make this airtight in the revision, we will cite the PBS evidence from Dolan *et al.* in the Discussion to triangulate the argument.

a. The authors should define the criteria used for identifying “distal lesioned areas.” It would also strengthen the manuscript if they could provide quantitative data showing how the phenotype changes at varying distances from the lesion and at various temporal stages of the lesion.

Response: We appreciate the reviewer’s interest in a rigorous distance–time quantification across the brain. However, a true analysis of phenotype as a function of distance from the lesion is beyond the scope of this paper because it requires whole-brain, 3D tract-aware modeling (rather than 2D Euclidean measurements on single coronal sections), serial-section registration and reconstruction across animals and time points, and integration with tractography or cleared-brain imaging to follow white-matter routes faithfully. These tasks constitute a dedicated connectomic study that would require different data acquisition, substantially larger sample sizes, and specialized computational pipelines.

Our current work instead operationally defines distal lesioned areas based on consistent pathology extending along the white-matter tract, which suffices to establish the main spatial

biological findings. The focus of this study is on applying spatial ARP-seq and CODEX at the tissue scale to uncover key biological insights. We therefore defer a comprehensive tract-resolved, 3D distance–time quantification to future studies designed specifically for connectome-scale analysis.

b. The authors should include a control non-lesioned / mock injected animal in their analysis of cell proportion and microglial clusters in Fig 6.

Response: Please see answer to point 3.

c. The authors should compare their microglial subclusters to previous literature identifying activated microglial populations as an effect of demyelination of white matter areas. This would help confirm their findings and reliability of their technology.

Response: As requested by the reviewer and by other reviewers previously, we have included in the manuscript a comparison of our identified microglial subclusters, both in the core and distal lesions, with previous literature describing activated microglial populations in aging and in demyelination (Hammond *et al.* and Androvic *et al.*). These comparisons, presented in the new Fig. 6 of the previous version, confirmed our findings and the reliability of our technology.

Minor

1. In their rebuttal on page 29, the authors claimed to show P5 replicates next to each other to show consistency of the codex images. They did not provide this image.

Response: We respectfully note that this image was already included in our previous rebuttal on Page 29, and for clarity we have re-included the relevant excerpt and figure below.

- Fig 1b: the P5 brain seems to have overall diminished signals compared to others – is this biological or technical? ↵

Response: We thank the reviewer for the comment. The staining in Fig. 1b, including P5 mouse brain, was performed using the commercial CODEX platform (Akoya Biosciences), following the manufacturer's standard protocol. We have now increased the resolution of the image in Fig. 1b, which has improved the visualization of the P5 mouse brain. We have now also included a replicate for the P5 mouse brain in Fig. 1b, with two replicates presented side-by-side (please also see below). We did not observe a notable reduction in signal between the two replicates. To ease with visualization of CODEX images, we have provided higher magnification images in Extended Data Figs. 2-9.↵

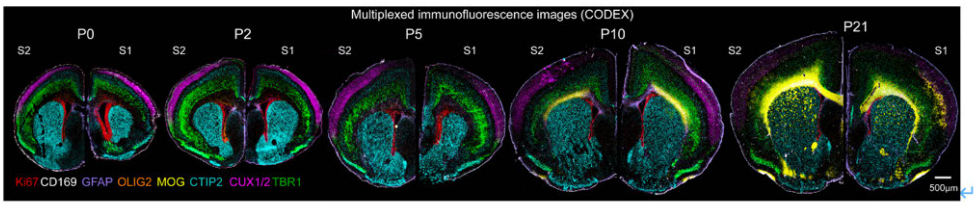

2. In Fig 4h, the authors should align the 10DPL-S1 images so they are not sideways.

Response: We thank the reviewer for the comment. We considered the best way to depict these images since the 10 DPL sample region of interest is angled, which was done in order to try to capture as much distal inflammatory area as possible to improve our analysis and

address the reviewer comment in our first revision. We could align the image so that there is alignment; however, we found it quite visually distracting to have a mix of square and diamond-shaped images. We purposefully included a rotated whole brightfield image (Fig. 4e) with the region of interest (integrated spatial data) to make it clear that the image was rotated in subsequent figures.

3. In Fig 5h, the slice chosen for 5DPL is posterior to the images in 10DPL and 21DPL. Authors should choose slices taken from the same region of the brain.

Response: We thank the reviewer for this comment. We have calculated the distance using a mouse brain atlas online resource (Paxinos, George, and Keith B.J. Franklin. *The mouse brain in stereotaxic coordinates: hard cover edition.* Access Online via Elsevier, 2001) and have found that our 5DPL sections are less than 0.1 mm posterior to those collected for 10 and 21 DPL (please also find the images below). The cryosectioning process alone involves proper alignment, lesion detection, and a priori sequential collection strategies to obtain tissue sections on two slide formats for downstream processing for spatial ARP-seq and CODEX.

[REDACTED FIGURES]

Referee #3 (Remarks to the Author):

The authors have adequately responded to previous concerns, by including additional references and new data convincingly showing the differential distribution of thalamo-cortical and cortico-cortical axons.

The only minor issue that remains for me is panel c in figure 3, is truly difficult to interpret and the figure legend is not very helpful.

Response: We sincerely thank the reviewer for the positive evaluation. We agree that Fig. 3c, which showed a pie chart representation of mixed cell types per 20 μm spot, may not be the clearest representation. In the revised version we have removed this panel and instead provide high-magnification CODEX images, which more clearly illustrate the cell types that may coexist. We believe this replacement improves clarity and better supports the conclusions.

We greatly appreciate the reviewers for all the constructive review comments, which contributed to a major improvement of our manuscript. We have fully addressed all the concerns from the reviewers. Please find below our point-by-point responses to all review comments. All revisions have been highlighted in yellow in the manuscript. Thank you so much!

Referees' comments:

Referee #1 (Remarks to the Author):

The authors have systematically addressed the raised concerns by substantial new experimental work, including the generation of new datasets and the addition of new experimental models. The revised manuscript exemplifies how an ideal resource and new method should be presented, as it not only introduces methodological advances but also uncovers new biological insights. Importantly, all of the reviewer's specific questions have been directly and convincingly addressed. We carefully checked each of our previously raised points (see below) and found that the authors have made a genuine effort to provide rigorous new analyses and meaningful biological new conclusions.
The authors convincingly demonstrate that the integration of spatial proteomics with transcriptomic and epigenomic profiling yields insights that could not be achieved with immunohistology together with single-cell omics alone.
I thank the authors for their thorough and thoughtful revisions and recommend publication of the manuscript in its current form.

Response: We sincerely thank the reviewer for the generous and encouraging comments. We deeply appreciate the recognition that our revisions systematically addressed the concerns through substantial new experiments, datasets, and models, and that the revised manuscript not only presents methodological advances but also uncovers new biological insights. We are especially grateful for the acknowledgement that integrating spatial proteomics with transcriptomic and epigenomic profiling yields insights beyond immunohistology and single-cell omics alone. The positive recommendation for publication is truly encouraging, and we are very thankful.

Point 1: Added Value of Protein Sequencing
- Initial Point: The manuscript needed to provide specific examples of how protein sequencing enhanced the tri-omic analysis.
- Author Response and Sufficiency: This point was addressed by adding a focused analysis of the lysolecithin (LPC) mouse model. The authors now utilize the spatial ARP-seq protein data to suggest differentially phased immune responses between primary and distal lesion compartments. They identify distinct protein expression patterns for markers such as the laminin receptor CD49f and the inhibitory receptor PD-1 (CD279) across different lesion clusters (LC1-LC5). This new analysis provides an example of how the proteomic data offers distinct biological insights into immune cell dynamics.

Response: We appreciate the reviewer's positive evaluation of our LPC-based analysis and the added value of proteomics.

Reviewer's Point 2: Reproducibility, Code Availability, and Data Consistency
- Initial Point: The code for the spatiotemporal regression model was not publicly available, and the

consistency of the findings across replicates was not demonstrated.
• Author Response and Sufficiency: This point has been fully addressed. The authors have made their negative binomial generalized additive model (NB-GAM) code publicly accessible on GitHub. They also generated a new, higher-resolution dataset (S2) using newly designed DBiT chips with 220x220 barcodes and a 15 μm pixel size. An additional developmental time point (P7) was also included. The provided correlation analysis shows high concordance between the original (S1) and new (S2) datasets for RNA (Pearson r > 0.95 for both corpus callosum and cortex genes) and moderate concordance for ATAC data (Pearson r ≈ 0.60). The inclusion of figures illustrating consistent spatiotemporal patterns across both datasets effectively demonstrates the reproducibility of their model and findings.

Response: We thank the reviewer for acknowledging that our code release and new datasets effectively demonstrate the reproducibility and consistency of our model and findings. We greatly appreciate the positive assessment.

Reviewer's Point 3: Mechanistic Insights into Microglial Dynamics
• Initial Point: A deeper investigation into the transcriptional and epigenetic differences between microglial populations at the lesion core versus distal sites was requested, including comparison with existing literature.
• Author Response and Sufficiency: The authors expanded this section by adding a new time point (10 DPL) to the LPC model. They performed sub-clustering on microglia-specific pixels and benchmarked their findings against published single-cell datasets from Androvic et al. and Hammond et al.. This analysis revealed that specific microglial states, such as disease-associated and injury-responsive microglia, are spatially organized between the primary lesion and distal white matter compartments. The investigation is further supported by protein analysis and CellChat modeling to explore cellular interactions.

Response: We thank the reviewer for recognizing our expanded analysis of microglial dynamics. We are glad that our additional time point and benchmarking with published datasets effectively addressed this point.

Reviewer's Point 4: Clarification on Tissue Sectioning and Alignment
• Initial Point: The methodology for cutting and aligning adjacent tissue sections for multi-modal analysis was not clearly described.
• Author Response and Sufficiency: The authors have clarified their procedure, stating that sections were cut at 10 μm thickness. They specified that sections for spatial ARP-seq and CODEX were either adjacent or from anatomically matched regions. Detailed sample information, including section-to-section distances, has been provided in new supplementary tables (Extended Data Tables 7-9). They also state that the sequencing and imaging data were analyzed independently for the purpose of cross-validation.

Response: We thank the reviewer for acknowledging our clarification of the tissue sectioning and alignment methodology.

Reviewer's Point 5: Potential Microfluidic Leakage

• Initial Point: The issue of potential microfluidic leakage was raised, based on observations of column and row artifacts in supplementary figures, along with questions about its cause and prevalence.
• Author Response and Sufficiency: The authors adequately address this point by clarifying that the observed effect is not leakage. They cite a previous publication (Cell, 2020, 183(6): 1665-1681) where they demonstrated that DNA diffusion is negligible. They explain that the row/column patterns are analogous to bead-to-bead variations common in single-cell sequencing, arising from slight differences in capture efficiency across microfluidic flow lanes. They state that these variations are correctable with standard normalization and do not affect downstream analyses, and that the phenomenon was not widespread in the current study.

Response: We thank the reviewer for acknowledging our clarification and appreciate the positive assessment.

Reviewer's Point 6: Analysis of Sparse CD169+ Immune Cells
• Initial Point: The need for a higher-resolution analysis of sparse CD169+ immune cells was identified, with a question as to whether the observed signal was biological or a technical artifact.
• Author Response and Sufficiency: This point has been thoroughly addressed. The authors provided new, high-resolution CODEX images for CD169 at single-cell resolution across all developmental time points (P0 to P21). To validate that the sparse signal is not an artifact, they compared their protein data with in situ hybridization (ISH) data for the corresponding gene (Siglec1) from the Allen Brain Atlas, which showed a similarly limited expression pattern. The response effectively demonstrates that the observation is biological.

Response: We thank the reviewer for acknowledging our higher-resolution analysis of CD169+ cells and the validation with ISH data, which confirms that the observation is biological. We greatly appreciate this positive assessment.

Reviewer's Point 7: Cross-Validation of Different Detection Methods
• Initial Point: The manuscript needed to clarify how the different detection approaches (CODEX, CITE-seq, RNA-seq) were used to validate one another and how any discrepancies were addressed.
• Author Response and Sufficiency: The authors acknowledge that a direct comparison is challenging due to technical differences and incomplete marker overlap between panels. However, they state that they observed good general concordance with no substantial discrepancies. They provide visual evidence showing consistent spatial patterns for several key markers (Mbp, Olig2, Itgam (CD11b), etc.) across RNA, ATAC, Protein (ADT), and CODEX, which sufficiently demonstrates the cross-platform consistency of their findings.

Response: We thank the reviewer for the positive feedback.

• Initial Point: The absence of sample sizes and statistic
• Author Response and Sufficiency: This point has been comprehensively addressed. The authors have revised figure legends to include sample sizes and added new Extended Data Tables (7, 8, 9) with detailed information for all samples. They also provide a clear and detailed explanation of the statistical framework underpinning their analysis, clarifying that it relies on model-derived statistics from negative

binomial generalized additive models (NB-GAMs) rather than traditional groupwise comparisons. They specify the use of likelihood ratio tests and stringent filtering criteria (FDR < 0.01, adjusted $R^2 > 0.025$) to identify significant spatiotemporal patterns.

Response: We thank the reviewer for recognizing and positively assessing our sample size and statistics updates.

Reviewer's Point 9: Limited Insights from Human Data

• Initial Point: The biological insights from the human data could be strengthened by a direct comparison with the mouse findings to provide better context.

• Author Response and Sufficiency: The authors responded directly to this by conducting a new comparative analysis between the human and mouse data to highlight conserved and divergent spatiotemporal dynamics in cortical development and oligodendrogenesis. This new analysis is presented in new figure panels (Fig. 2k,l) and a new manuscript section titled "Spatial dynamics of human visual cortical development," which sufficiently addresses the need for deeper contextualization.

Response: We thank the reviewer for acknowledging our comparative analysis and the new section, and we appreciate the positive assessment.

Minor Points: All minor points raised by the reviewer have been addressed, including corrections to typos, figure references, logical flow, terminology, and figure axes.

Response: We thank the reviewer for acknowledging that all minor points have been addressed.

Referee #2 (Remarks to the Author):

I appreciate the authors' comprehensive responses as well as the efforts in revising the manuscript. While the authors have strengthened the work by including additional data and time points, introducing new sample sets and performing a new AAV experiment, several key issues remain to be addressed. Additionally, I encourage the authors to compare their data with several recently published spatial technology studies such as SPACE-Seq (Huang et al., PNAS 2025) and ExIGS (Labade et al., Science 2025) to better highlight the advantages of their technology as the field moving forward.

Response: We greatly appreciate the reviewer's feedback. We are pleased to note that almost all of the reviewer's concerns were already addressed in our previous revision. Please find below our point-by-point response.

We agree with the reviewer that spatial omics is a rapidly evolving field and appreciate the suggestion to position our study within the context of recent technological advances. While our labs reported the first spatial epigenome sequencing methods back in 2022, we are equally excited to see the continued development in this field and, in particular, we enjoyed reading about SPACE-Seq and ExIGS. Each of these approaches has distinct characteristics, and we will discuss them in our revised manuscript. At the same time, we wish to emphasize that our work is primarily a developmental neuroscience data resource and biological discovery study, rather than being focused solely on technology development – although we note that the methods applied here remain best-in-class for generating comprehensive multi-modal spatial omics atlases.

- **SPACE-Seq** (Huang et al., PNAS 2025) represents an important step toward combining spatial epigenome (in the current form, ATAC only, and yet to be demonstrated for CUT&Tag), transcriptome, and lineage tracing. The "lineage tracing" capability of SPACE-seq was built upon post hoc inference from mitochondrial variants detectable in ATAC-seq reads, which is very interesting and different from other methods although further improvement is still needed. Currently, SPACE-Seq demonstrated relatively coarse spatial resolution (~55 μm pixels) and limited throughput (~3,800 spots per section), with per-spot data quality also remaining modest (typically ~2,500 UMIs and ~1,500 genes for RNA, less than 8000 fragments per spot for ATAC). In contrast, our DBiT-based spatial ARP-seq achieves 15–20 μm pixel resolution with dense sampling grids (100×100 and 220×220 spots, 10,000–48,400 spots per section) and delivers higher quality data (~6,000 UMIs, ~2,500 genes, >15,000 ATAC fragments, per spot), that might have contributed to our ability to identify more tissue features or clusters in the same brain region. For example, our data clearly resolved different cortical layers (See Figure below).

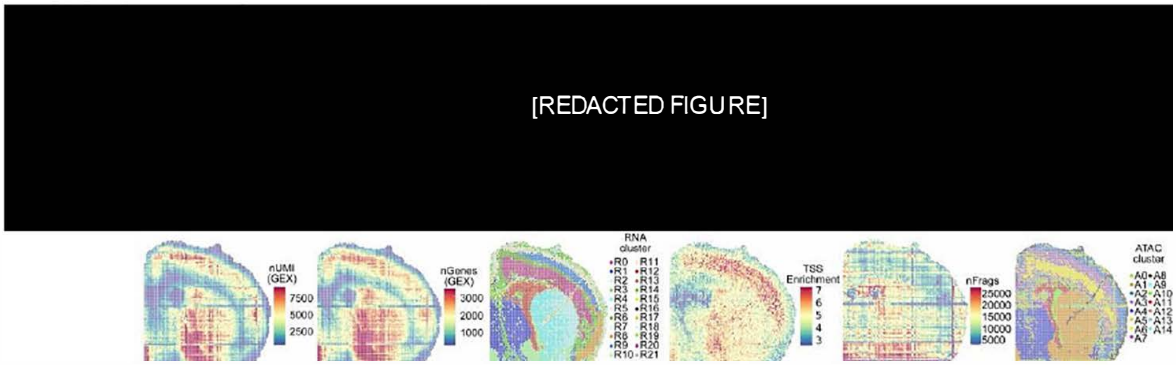

This combined advantage in resolution, throughput, and data quality is precisely what enables us to resolve biologically meaningful fine-scale features such as cortical laminar distinctions, the precise sequence of myelination, and distal microglial activation along with-matter tracts— phenomena that would be obscured at coarser resolution or lower sensitivity.

- **ExIGS** (Labade et al., Science 2025) addresses a very different regime: by combining expansion microscopy with in situ genome sequencing, it resolves nanoscale subnuclear chromatin organization and links nuclear morphology to local chromatin regulation in single cells. This is highly valuable for mechanistic studies of nuclear architecture (e.g., lamin defects in progeria) but does not provide unbiased, tissue-scale RNA or ATAC maps across intact brain sections. In contrast, our spatial ARP-seq is designed for totally different purposes – to produce whole transcriptome and whole epigenome coverage simultaneously on the same tissue section, complemented by a protein layer and orthogonal CODEX imaging, thereby enabling systems-level analyses of cell states, regulatory networks, and spatially propagating pathology in the context of intact tissue architecture. We really appreciate the reviewer bringing this interesting work to our attention!

We thank the reviewer for this helpful suggestion. In response, we have added a brief paragraph to the Discussion section citing SPACE-Seq and ExIGS, highlighting their differences and emphasizing their complementarity to our work (please also see below). At the same time, we would like to reiterate that the main focus of our study is on the biological insights gained through applying high-resolution, unbiased multi-modal multi-omic mapping to postnatal brain development and demyelination models.

Recent advances are expanding the suite of spatial omics approaches. SPACE-Seq (Huang et al., 2025) unifies tissue-scale chromatin accessibility and gene-expression profiling and enables post hoc lineage inference from mitochondrial variants. In a distinct regime, ExIGS (Labade et al., 2025) combines in-situ genome sequencing with expansion microscopy to map subnuclear DNA–protein organization at high resolution.

Major:

1. The robustness and reliability of their technology need to be further addressed. There are various instances within the manuscript that raise concerns about data quality:

Response: We thank the reviewer for the comment. We agree that robustness and data quality are critical for evaluating new spatial multi-omic technologies. In our datasets, per-pixel quality metrics are consistently high, across dense sampling grids of 10,000–48,000 pixels at 15–20 μm resolution. As mentioned above, the data quality for the ATAC and RNA modalities show better performance compared to the Visium-based multiomics approach. Importantly, our datasets also robustly recapitulate well-established anatomical and developmental features, including cortical lamination, the precise temporal sequence of myelination, and distal microglial activation along white-matter tracts, providing independent biological validation of data quality. Together, these quantitative and biological validations demonstrate that our technology is robust and reliable, and that the data quality is sufficient to support the conclusions of this study.

a. The correlation of RNA and ATAC data across timepoints is similar or sometimes higher than the

correlation across technical replicates within a time point, indicating the measurements somehow capture more sample-to-sample noise than robust developmental changes (rebuttal pg 4). For example, in the ATAC analysis, the majority of samples across different time points appear highly correlated. Additionally, the P2_S1 is more correlated with P0_S1 than P2_S2 in the RNA data. The authors should explain why their technology generates homogenous measurement but fails to capture meaningful developing signatures.

Response: We appreciate the reviewer's observation that cross–time-point correlations sometimes appear as high, or even higher, than correlations across technical replicates (Figure below).

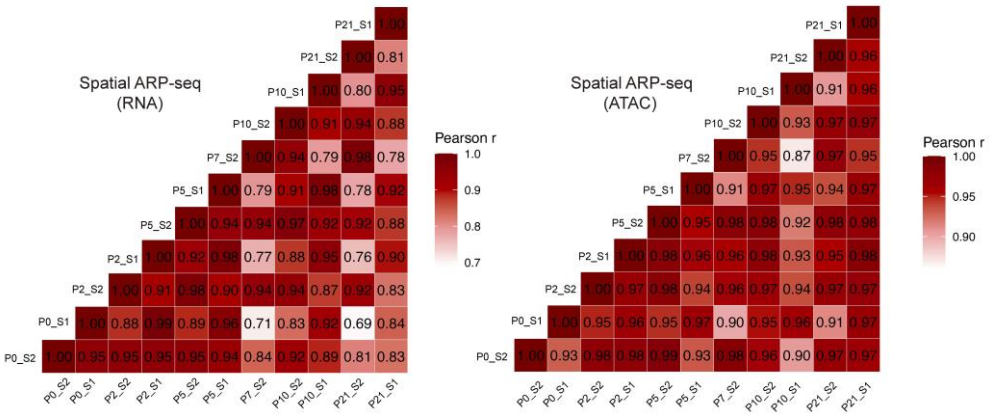

However, we would like to clarify why this pattern is expected and biologically consistent, and why it does not imply that our technology fails to capture developmental dynamics. There are two main considerations:

(i) Biological context: postnatal stability of cortical architecture

All of our datasets are derived from the *postnatal* period (P0–P21). By this stage, the fundamental laminar and regional architecture of the cortex is already established, in sharp contrast to the embryonic period when neurogenesis, migration, and differentiation drive massive global shifts in gene expression and chromatin state. Postnatally, the dominant biological processes are more gradual, such as myelination, synaptic maturation. Consequently, global transcriptome and epigenome profiles remain relatively stable between adjacent postnatal stages. High correlation between postnatal samples is therefore entirely consistent with biological expectations, and a strength rather than a weakness of our data. In fact, if we had observed drastic global divergence between P0, P2, and P7 samples, it would have been biologically implausible and inconsistent with well-established developmental neurobiology. Our clustering analyses further confirm that cortical lamination is preserved across samples, reflecting this expected global stability. We applied gene- and peak-level statistical modeling (e.g., GAM fitting, likelihood ratio testing) specifically designed to identify the smaller subset of features with significant temporal and spatial dynamics. These analyses reveal clear developmental trajectories and pathway enrichments, demonstrating that the technology captures meaningful dynamics even though global correlation appears high.

(ii) Compositional and technical factors in spot-based measurements

Our measurements are generated from “spots”, each capturing multiple cells. In the early postnatal period (P0–P2), when cell density is particularly high, each spot can contain mixtures of neurons, glia, and progenitors. This might explain how cases of differences in local tissue composition across sections (e.g., slight variation in layer representation or regional sampling) can introduce modest variability between technical replicates. With, for instance, a P2 section may appear more correlated with a P0 section than with its replicate P2 section. Importantly, such effects reflect the inherent multi-cell composition of each spot and biological heterogeneity across tissue sections, rather than a failure of the method. This phenomenon is well recognized in spatial omics datasets with spot-level resolution and is consistent with our observations.

Taken together, the high correlation across postnatal time points arises from (i) the biological reality of global stability during postnatal cortical maturation, (ii) modest technical and compositional variability inherent in spot-based measurements. These factors fully explain the reviewer’s observation. Crucially, our downstream modeling robustly resolves hundreds of temporally regulated genes and chromatin peaks, together with enriched pathways, confirming that the technology faithfully captures meaningful developmental signatures within the expected globally stable background.

b. Protein signal is occasionally not correlated with RNA and ATAC data, particularly with immune cell markers. Fig 5c protein data do not support the distal activation claim which was only observed in the ATAC and RNA data. The authors should explain why protein accumulation at the distal sites of Cd11b, CD11c, and Cd68 is not detected at the protein level, despite being observed at RNA and ATAC levels. Similar inconsistencies are observed in Fig 5h with CD45 and CD115. The authors should elaborate on why these discrepancies may exist.

Response: We acknowledge the reviewer’s observation that the distal accumulation of immune markers appears less pronounced at the protein level in the ADT measurements (Fig. 5c, below).

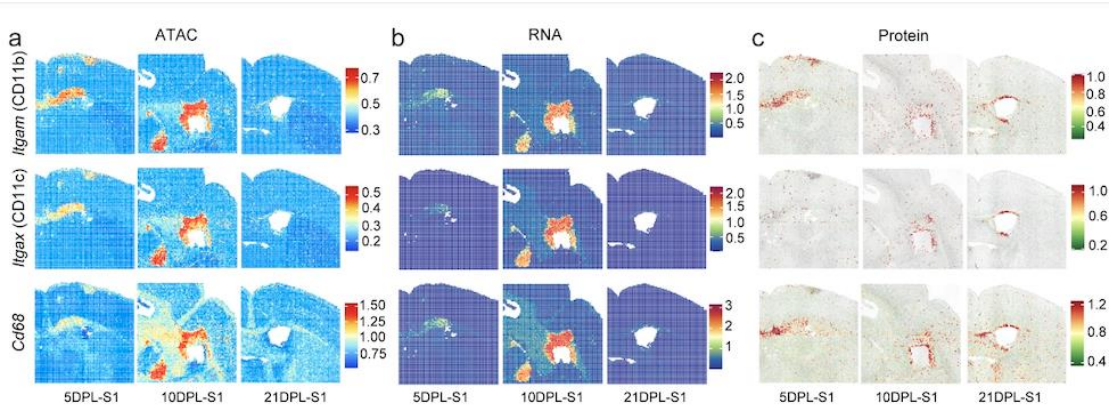

As CD45 and CD115 are not included in Fig. 5h, we interpret the reviewer’s comment as likely referring to Fig. 4h. This discrepancy can be explained by both technical and biological factors. First, antibody-derived tag (ADT) profiling in spatial sequencing generally shows lower sensitivity than RNA/ATAC layers, particularly for membrane proteins such as CD11b, CD11c, CD68, CD45, and CD115, where epitope accessibility, antibody penetration, and capture efficiency can limit signal detection in low abundance regions. As a result, subtle distal signals may be underestimated. Second, RNA and ATAC changes represent early activation events (chromatin opening and transcriptional priming), whereas

protein accumulation generally lags behind and requires higher abundance to be detected, especially by sequencing-based ADT. Consistent with this, we do observe weak but noticeable distal signals in the ADT data, and more importantly, high-resolution multiplexed protein imaging (CODEX) clearly reveals distal activation of the corresponding markers, fully consistent with the RNA and ATAC findings. Thus, the discrepancy reflects sensitivity limits of ADT for low abundance signals, rather than a biological absence of distal activation. We have now commented on this aspect in the “Microglia dynamics in focal de/remyelination” section of our revised manuscript.

A similar pattern was observed with spatial ARP-seq for both RNA and ATAC signal, as well as at the protein level, although the latter showed weaker but consistent signals, likely due to limited capture efficiency.

c. Poor detection quality in the human sample should be discussed or repeated with higher quality replicates. Although working with human tissue is challenging, this issue will greatly limit the applicability of this technology in more relevant tissue types and therefore dampen enthusiasm for this technique. In Fig 2k, BCL11B and TBR1 show different expression patterns compared to Fig 1c. In Fig 2l, many key marker gene expressions in the human cortical layer appear undetected, as indicated by missing data in the heatmap. Additionally, Fig 1c data failed to detect layer makers (CUX1/2, CTIP2, and TBR1) and glia maker (PDGFRa), which should be abundantly expressed and been used as positive references (Qian et al., Nature 2025) The authors should include high-magnification images with clear cortical layer annotations to substantiate their claim that the technology can actually be used for human samples.
Additionally, the authors made several interpretations and statements that are not well supported by their data. For instance, they stated that high ATAC activity precedes RNA expression for all myelin-associated genes in human samples, but this is not true for MOBP and BCAS1 in Fig 2l.
Moreover, several conclusions are based on one single human sample, with no accompanying quality control and replicates. The authors should increase the number of sample sizes, replicates and provide quantification and statistics to strengthen these conclusions and findings.

Response: We thank the reviewer for the comments. Regarding BCL11B/CTIP2, TBR1 and other cortical layer expression patterns, high-magnification images with clear cortical layer annotations were already included in the previous version of the manuscript in Extended Figs. 12-14, and stated in our previous *response to referees letter* on Page 44 (as we have already clarified previously, this is CODEX multiplexed immunofluorescence staining for protein, not RNA sequencing as shown in Qian et al). As can be seen below, BCL11B/CTIP2, TBR1 present at the RNA level similar expression patterns as at the protein level in CODEX, and thereby there are no discrepancies for these markers.

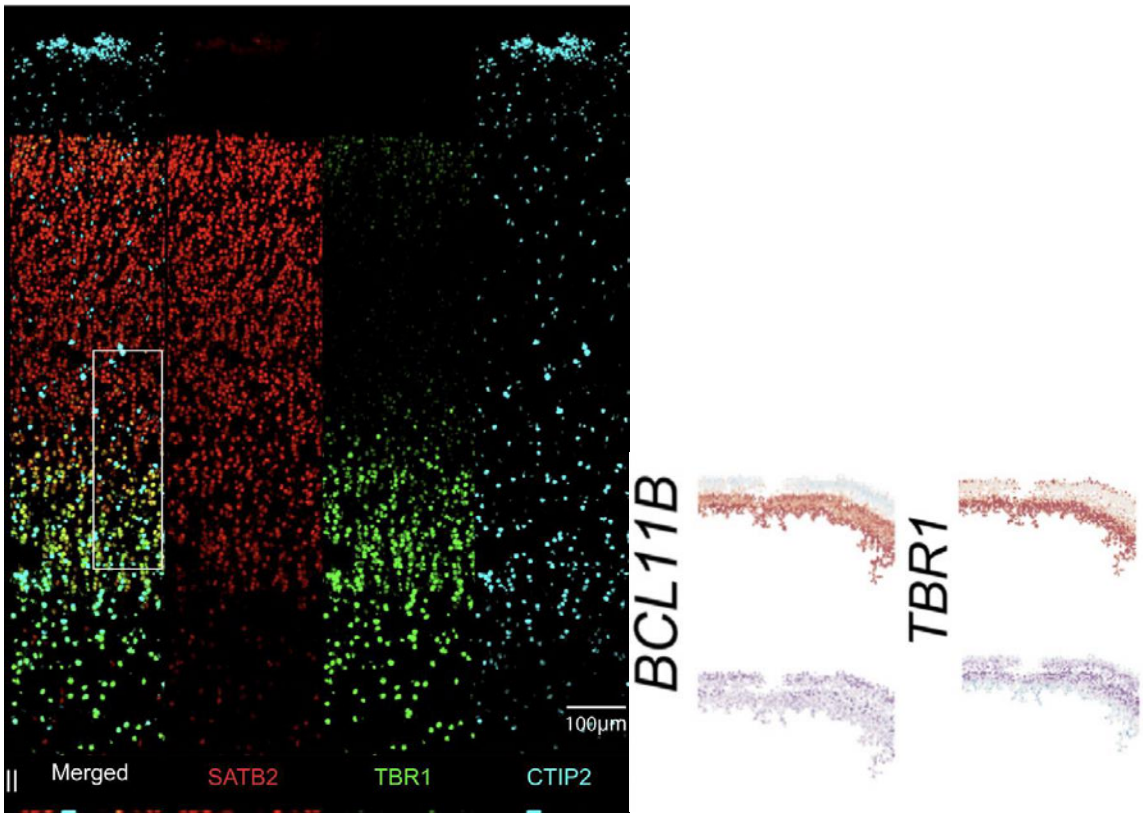

Regarding the statement that "high ATAC activity precedes RNA expression for all myelin-associated genes in human samples", we agree with the reviewer and we will change the sentence to:

"In the genes associated with oligodendrogenesis, we saw higher incidents of ATAC gene activity that preceded the RNA expression compared to what was observed in the neurogenesis associated genes (Fig. 2l, Extended Data Fig. 7 and Supplementary Fig. 31), which was the case for ***a subset of myelin associated genes (MAG, MBP,*** **and** ***MAL)****, and as observed in the mouse cortex."*

We would like to clarify that, unlike recent *Nature* studies that focused exclusively on the human cortex and analyzed 6–10 samples across multiple regions and ages, the human data in our study are not the primary focus but rather a small complementary section to demonstrate feasibility and translational relevance. In this context, we have already included three human cortical samples (prenatal and infant V1 regions), which are exceptionally rare and difficult to obtain. As mentioned in the manuscript, these samples are from the same tissue blocks from the ones in Wang et al, *Nature* 2025 (https://www.nature.com/articles/s41586-024-08351-7), where they mapped the V1 regions at three developmental time points. In our study, we have analyzed all three corresponding V1 regions, and we show that our technology can recapitulate the transcriptomic findings by Wang et al. with an orthogonal technology, MERFISH, with the advantage of adding additional omic layers. While the number is smaller than dedicated human-focused studies, it is substantial given the limited availability of such tissue and is sufficient to support the proof-of-principle demonstration. We have tempered our claims accordingly, framing the human data as preliminary and consistent with the robust mouse findings:

"We used our human V1 cortical maps as a small scale benchmark for the observations we made in our murine cortical dataset."

Finally, we would like to note that this manuscript represents part of the first phase BICCN effort, which has been more heavily focused on mouse datasets, with the human data included here only as an early exploratory demonstration. The ongoing BICAN program, in contrast, is dedicated to constructing a comprehensive human and non-human primate developmental brain atlas, encompassing nearly 12~15 human and ~20 non-human primate samples, and is expected to be completed in 2027.

2. Immunofluorescence or ISH validations are needed for several main statements.
a. In Fig 3c, the cell proportion analysis shows there is no OPC population at P10 and P21. Additionally, the Fig 3h shows a similar reduction of OPC maker along the development. As shown by many studies, OPCs populate the brain throughout life and continue to reside in the corpus callosum throughout (Dawson, 2003, Allen Atlas, 2011, Bergles and Richarson, 2016). This lack of OPC at juvenile brain is controversial and likely wrong – the authors should provide IF results of OPC markers throughout the development to validate their findings.

Response: We thank the reviewer for highlighting this point. In Fig. 3c (now Extended Data Fig. 9a) the OPC population is subdivided into 3 sub-groups titled OPC, DivOPCs (OPCs in the cell cycle) and COPs (committed OPC). Since these subclusters express *Pdgfra* and *Cspg4*/NG2 (Marques et al. Science. 2016 and Falcao and van Bruggen et al. Nat Med. 2018). It indicates that we indeed have OPC/COPs/DivOPCs present in the corpus callosum across all our developmental atlas (OPC subcluster between P0-P7 and the COPs between P2-P21). Therefore, our data is indeed consistent with the Dawson 2003, Allen Atlas 2011 and Bergles and Richardson 2016. We have clarified this point in the “Chromatin priming of CC myelin genes” section:

“Our data is consistent with previous reports (refs 50-52) that OPCs populate the adult brain since there are cellular constituents of Pdgfra+ OPCs (including COPs and DivOPCs) throughout development, moreover we observe PDGFRα+ cells throughout development (Fig. 3b and Extended Data Figs. 8a-c and 9a).”

Regarding Fig. 3h (now Fig. 3g), there is indeed expression of *Pdgfra*, however, due to the analysis being comparative between groups, it is much lower than earlier timepoints. Since spatial ARP-seq does not have single-cell resolution, it is not possible to isolate individual cell populations and determine expression maintenance of specific genes within a given cell type. As a result, gene expression profiles of cells in lower abundance are outcompeted by gene expression profiles of cells in greater abundance. This is seen in Fig. 3h when the predominent oligodendrocyte lineage cell population shifts from OPC/COP to MOLs at P7/P10 even though OPC/COPs are maintained throughout time. In Fig. 3b and Extended Data Figs. 2–9 (now Supplementary Figs. 2–9), we have already provided CODEX data of even higher magnification to show that the PDGFR*α* expressing OPC/COP is maintained in late development.

Data portal: All sequencing data and spatial maps are available at our public portal (https://spatial-omics.yale.edu/), where *Pdgfra* and *Olig2* can be clearly visualized as persistently present across development. These markers have also been shown throughout the Supplementary Figures (e.g., Extended Data Fig. 2 and Supplementary Figs. 2–9,18).

b. The author demonstrated that the lateral CC shows stronger MBP colocalization with AAV-labeled neuronal projections. However, the MBP signal in Fig 3j actually shows a flat distribution from lateral to medial CC – contradictory to the claim. The results in Fig 3m and 3n could just reflect the intensity differences of neuronal projections but not myelination itself. To validate this result quantitatively, authors may just stain a panel of well known myelination markers throughout the developmental ages and quantify the spatial distribution in lateral and medial CC, which is a standard validation experiment.

Response: We thank the reviewer for this comment. To better show the MBP variation across the corpus callosum, we have included an additional panel showing MBP only staining with better quality images having less background signal (See the new figure panel below, updated now in Figure 3). In addition, we have drawn the borders around the corpus callosum, excluding the dorsal hippocampal commissure that lies ventral to the medial portion of the corpus callosum body. We excluded the dorsal hippocampal commissure white matter tract on the basis that it is not comprised of projection neuronal subtypes we have focused on in our study (Suárez, Gobius and Richards. 2014. and Bubb et al. 2020). In the MBP-only images, it is clear that the staining we quantified using the strategy depicted (panel h) is not due to bleed-through of channels. If we were experiencing channel bleed-through issues, it would clearly be visible in the contralateral cortex injection, where the GFP intensity is very strong; however, there is no staining observed in the MBP-only image.

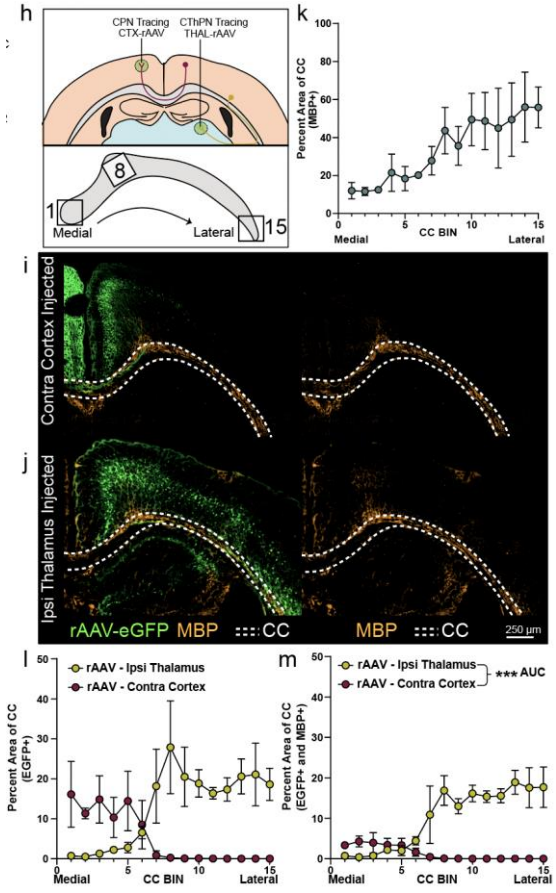

Based on reviewer concerns in the previous revision, we had expanded our developmental dataset to include P7 to better depict the lateral to medial developmental myelination pattern. We had included two myelin proteins, MBP and MOG, in our CODEX imaging platform for P0, P2, P5, P7, P10, and P21. Now our developmental data more clearly shows lateral-to-medial myelination through the inclusion of

the P7 timepoint (see Fig. 3a and Supplementary Figs. 2-9). We would also like to highlight our addition of two previous studies, as we have referenced previously in our manuscript, that describe the lateral-to-medial myelination through multi-time point developmental analysis using histological methods, including MBP immunostaining, Luxol Fast Blue myelin staining, and electron microscopy (Sturrock 1980 and Vincze et al., 2008).

c. The authors deduce in Fig 5 that there is distal activation of immune cells as an effect of LPC injection. The authors should provide IF/ISH staining alongside the CODEX images to validate their findings.

Response: We thank the reviewer for this comment. We would like to clarify that the CODEX data presented in Fig. 5 are based on antibody-driven immunofluorescence staining. Thus, CODEX inherently provides the IF validation of the spatial ARP-seq findings, while offering the additional advantage of multiplexing dozens of markers in the same tissue section. We have clarified in our previous response that CODEX is an antibody-based immunofluorescence technology (rebuttal Page 22-24); we would like to restate this here for clarity and to avoid any possible misunderstanding. The CODEX analysis independently confirms the induction of distal lesion–like immune activation, consistent with the spatial ARP-seq profiles. We therefore believe that additional single-channel IF or ISH experiments would not provide further validation beyond what has already been demonstrated with multiplex CODEX imaging.

3. A more rigorous and systematically controlled experimental design using the LPC mouse model is necessary to support the study's conclusions. The distal activation of microglia in white matter is an interesting finding but lack several critical controls and therefore cannot be interpreted. A bilateral sham injection should be used as a control. This control would validate that the distal microglial activation was a product of the lesion and not of mechanical damage to the brain by intracranial injection. Additionally, the LPC injections should be performed with a fluorescent marker so that they are able to show that leakage of the injection is not the cause of the distal activation.

Response: We appreciate the request for additional controls to exclude mechanical damage as an explanation for distal activation. However, multiple, convergent lines of evidence indicate that the tract-mediated distal responses we report are not due to injection trauma:

1) **Spatial-gradient principle (a first-order response to mechanical injury) and temporal separation: acute trauma vs. delayed demyelination.**
   If mechanical damage were the driver of immune activation, this should be maximal at the needle track/injection core and decay monotonically with distance. In contrast, our datasets show no distal activation at early time points (e.g., 5 DPL) and the emergence of robust distal activation along white-matter tracts at later stages (e.g., 10–21 DPL). A delayed, tract-localized response is incompatible with an acute mechanical-injury model and consistent with biology of demyelination-induced signaling and recruitment. Mechanical injury produces immediate local responses; by contrast, we observe temporal lag (no distal signal at 5 DPL; clear emergence at 10 DPL), matching expected kinetics for demyelination, debris handling, and microglial state transitions rather than needle-track effects.

2) **Independent PBS (sham) evidence at the core argues against trauma-driven activation.** A recent preprint (Michael-John Dolan *et al.*, 2025, doi.org/10.1101/2025.04.22.649486) performed single-cell RNA-seq with spatial profiling across 3, 7, 12, and 18 dpi with PBS controls. Although their Slide-seqV2 spatial coverage focuses on regions immediately adjacent to the injection site, their PBS results indicate that immune responses at the core are not attributable to the mechanical injection itself. In other words, when trauma is isolated (PBS), core-proximal activation is minimal. This external control makes a trauma explanation for our far-distal effects even less plausible. Because the Dolan *et al.* PBS controls demonstrate minimal immune activation at the injection core, a far-distal activation cannot be a trauma artifact; it requires biological propagation (e.g., myelin damage–linked signaling) along white-matter tracts—precisely what our large-field (half/whole brain) maps capture but core-restricted assays are not powered to detect.

3) **Anatomical specificity: tract-aware patterning.** Our spatial ARP-seq and CODEX cover half- to whole-brain sections, revealing activation that tracks along the callosal white matter and respects known axonal routes, with stronger ipsilateral than contralateral effects and minimal spillover into adjacent gray matter. A generic mechanical artifact would not reproduce this tract-constrained topology.

4) **Molecular concordance across modalities.** Distal regions show matched signatures in RNA (transcriptional activation), ATAC (chromatin accessibility), and protein (CODEX IF) markers of microglial activation. Cross-modal agreement at distal ROIs is hard to attribute to an artifact of injection.

Taken together—**(a)** minimal activation under PBS at the injection core (external control), **(b)** delayed onset and tract-localized distal patterns, and **(c)** cross-modal molecular concordance—strongly support that the distal microglial activation we report is a bona fide consequence of LPC-induced demyelination rather than mechanical injury. To make this airtight in the revision, we have cited the PBS injection evidence from Dolan *et al.*, 2025 and Lloyd *et al.*, 2019 (*Nat Neurosci* 22, 1046–1052 (2019)). in the Discussion to triangulate the argument. Please also see below.

Also, our observations are most likely not a consequence of mechanical injury resulting from injection induced injury, since the inflammation is only observed at the primary lesion site and at the entry point of the needle at 5 DPL, with the distal compartment occurring only at 10 DPL. Furthermore, monocyte-derived macrophage infiltration and microglia cellular augmentation are found exclusively within lesion area in mice with white matter demyelination caused by LPC injection[90,91]*.*

a. The authors should define the criteria used for identifying “distal lesioned areas.” It would also strengthen the manuscript if they could provide quantitative data showing how the phenotype changes at varying distances from the lesion and at various temporal stages of the lesion.

Response: We appreciate the reviewer’s interest in a rigorous distance–time quantification across the brain. However, a true analysis of phenotype as a function of distance from the lesion is beyond the scope of this paper because it requires whole-brain, 3D tract-aware modeling (rather than 2D Euclidean

measurements on single coronal sections), serial-section registration and reconstruction across animals and time points, and integration with tractography or cleared-brain imaging to follow white-matter routes faithfully. These tasks constitute a dedicated connectomic study that would require different data acquisition, substantially larger sample sizes, and specialized computational pipelines.

Our current work instead operationally defines distal lesioned areas based on consistent pathology extending along the white-matter tract, which suffices to establish the main spatial biological findings. The focus of this study is on applying spatial ARP-seq and CODEX at the tissue scale to uncover key biological insights. We therefore defer a comprehensive tract-resolved, 3D distance–time quantification to future studies designed specifically for connectome-scale analysis.

b. The authors should include a control non-lesioned / mock injected animal in their analysis of cell proportion and microglial clusters in Fig 6.

Response: Please see answer to point 3.

c. The authors should compare their microglial subclusters to previous literature identifying activated microglial populations as an effect of demyelination of white matter areas. This would help confirm their findings and reliability of their technology.

Response: We thank the reviewer for the comment. As requested by the reviewer and by other reviewers previously, we have included in the manuscript a comparison of our identified microglial subclusters, both in the core and distal lesions, with previous literature describing activated microglial populations in aging and in demyelination (Hammond *et al.* and Androvic *et al.*). These comparisons, presented in the new Fig. 6 of the previous version, confirmed our findings and the reliability of our technology.

Minor

1. In their rebuttal on page 29, the authors claimed to show P5 replicates next to each other to show consistency of the codex images. They did not provide this image.

Response: We respectfully note that this image was already included in our previous rebuttal on Page 29, and for clarity we have re-included the relevant excerpt and figure below.

- Fig 1b: the P5 brain seems to have overall diminished signals compared to others – is this biological or technical?

Response: We thank the reviewer for the comment. The staining in Fig. 1b, including P5 mouse brain, was performed using the commercial CODEX platform (Akoya Biosciences), following the manufacturer's standard protocol. We have now increased the resolution of the image in Fig. 1b, which has improved the visualization of the P5 mouse brain. We have now also included a replicate for the P5 mouse brain in Fig. 1b, with two replicates presented side-by-side (please also see below). We did not observe a notable reduction in signal between the two replicates. To ease with visualization of CODEX images, we have provided higher magnification images in Extended Data Figs. 2-9.

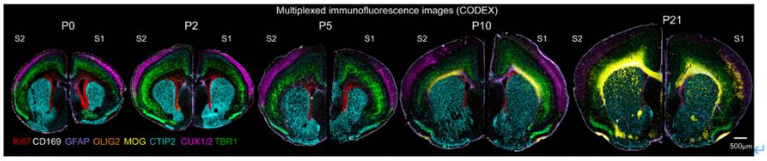

2. In Fig 4h, the authors should align the 10DPL-S1 images so they are not sideways.

Response: We thank the reviewer for the comment. We considered the best way to depict these images since the 10 DPL sample region of interest is angled, which was done in order to try to capture as much distal inflammatory area as possible to improve our analysis and address the reviewer comment in our first revision. We could align the image so that there is alignment; however, we found it quite visually distracting to have a mix of square and diamond-shaped images. We purposefully included a rotated whole brightfield image (Fig. 4e) with the region of interest (integrated spatial data) to make it clear that the image was rotated in subsequent figures.

3. In Fig 5h, the slice chosen for 5DPL is posterior to the images in 10DPL and 21DPL. Authors should choose slices taken from the same region of the brain.

Response: We thank the reviewer for this comment. We have calculated the distance using a mouse brain atlas online resource (Paxinos, George, and Keith B.J. Franklin. *The mouse brain in stereotaxic coordinates: hard cover edition.* Access Online via Elsevier, 2001) and have found that our 5DPL sections are less than 0.1 mm posterior to those collected for 10 and 21 DPL (please also find the images below). The cryosectioning process alone involves proper alignment, lesion detection, and a priori sequential collection strategies to obtain tissue sections on two slide formats for downstream processing for spatial ARP-seq and CODEX.

[REDACTED FIGURE]

[REDACTED FIGURE]

Referee #3 (Remarks to the Author):

The authors have adequately responded to previous concerns, by including additional references and new data convincingly showing the differential distribution of thalamo-cortical and cortico-cortical axons.

Response: We sincerely thank the reviewer for the positive evaluation and thoughtful comments.

The only minor issue that remains for me is panel c in figure 3, is truly difficult to interpret and the figure legend is not very helpful.

Response: We thank the reviewer for the comment and apologize that Fig. 3c was difficult to interpret. In this panel, we show per-spot pie charts depicting cell-type composition across the corpus callosum. The individual wedges are small due to space constraints. To improve clarity and better support the conclusions, we have reorganized this content as Extended Data Fig. 9a, presented alongside the spatial patterns from RNA–ATAC joint clustering derived with our NB-GAM framework.

We greatly appreciate the reviewers for all the constructive review comments, which contributed to a major improvement of our manuscript. We have fully addressed all the concerns from the reviewers. Please find below our point-by-point responses to all review comments. Thank you so much!

Referees' comments:

Referee #1 (Remarks to the Author):

Overall, the authors' responses are acceptable. Only the reviewer2's concern about the human data is still valid. Authors should limit human comparisons and add the following clarification: "These human data serve as exploratory benchmarks to demonstrate human-tissue applicability of DBiT-based spatial ARP-seq. Analyses establish technical feasibility and cross-species consistency of epigenome-transcriptome-protein mapping in situ, rather than delivering definitive biological conclusions." With these revisions, the primary concern of that reviewer would be addressed. I think rest of the issues are well addressed and can be published.

Response: We sincerely thank the reviewer for the positive and encouraging feedback! In accordance with the reviewer's suggestions, we have limited human–mouse comparisons and incorporated the suggested clarification in the "Human cortical development benchmarking" section.